UNIVERSITY OF SOUTHAMPTON

HIGH FREQUENCY SONAR: APPLICATION INTO OCEANOGRAPHY WITH REFERENCE TO OIL SLICK MONITORING

By

M. B. E. BELLOUL

M.Phil Thesis

Department of Oceanography

August, 1990

A la mémoire de

Mohand Akli Belloul

un père, un exemple...

Acknowledgments

Many thanks to all those who helped me through this research, and without whom none of this work would have been achieved.

First and above all, Steve Thorpe, my research supervisor who gave many of his precious time to guide me through the hazards of the research. His insight, his ideas and his encouragements were the main driving force all the way through the work.

I am also very grateful to Alan Hall (IOSDL) who was always there when I needed his help and whose expertise in operating the equipment made it all seem so simple.

I would also like to mention Neil Hurford (WSL) who made it possible for us to join his team for the North Sea cruises, and David Wallace (WSL) for supplying me with additional data from the oil slick experiment, and especially the airborne imagery.

I am also thankful to Jeremy Nedwell and Jerry Stanley (ISVR) for allowing me to use their equipment.

To my wife Nacima who had the patience and the courage to endure those difficult moments while I was completing this work, and to our newly born daughter Dahlia, I dedicate this work with all my love.

This work was carried out while in receipt of a research studentship from the Algerian Ministry of Higher Education. I would also wish to thank the AET for their financial support during the final stages.

UNIVERSITY OF SOUTHAMPTON

ABSTRACT

FACULTY OF SCIENCE

OCEANOGRAPHY

Master of Philosophy

HIGH FREQUENCY SONAR: APPLICATION INTO OCEANOGRAPHY WITH REFERENCE TO OIL SLICK MONITORING

By Mohamed Bachir El-Kamal BELLOUL

The use of sonar as a practical remote sensing technique of potential commercial interest has previously been given little attention. Two novel experiments involving the use of a side scan sonar in a towed mode and in a fixed mode, under unique conditions are described and analyzed.

The first of these experiments, conducted in the very shallow waters of a river revealed very promising results about the possibilities of using high frequency sonars as oceanographic remote sensing tools for monitoring weak and variable surface currents in environments where conventional measuring equipment are difficult to deploy. The sonar clearly identified moving targets on the surface which are thought to be clouds of bubbles formed by the breaking of the surface waves and other dynamical processes. The analysis of the evolution and the redistribution of these bubble clouds formed the basis for the measurement of the surface current.

In a second experiment, which formed the major part of this work, the same side scan sonar was towed from a ship in the North Sea. It was used to investigate the feasibility of detecting and monitoring oil slicks by sonar. Artificial oil slicks were scanned by towing a high frequency sonar (248kHz) looking at the sea surface, and the backscatter signal analyzed. It revealed a reduction in backscatter within the oil slick at incidence angles greater than 20° from the horizontal, and that the differential backscatter was about 5db lower under the slick. The differential backscatter gradually decreased as wind speed decreased and as the slicks got older. The analysis of the backscatter also revealed information about the frequency of wave breaking in the slick, which showed no significant difference with that in water free of oil under the same conditions. These observations are consistent with the hypothesis that at small incident angles, where no noticeable reduction in backscatter was observed under the slick, scattering is mainly due to breaking waves. Comparisons with radar reflection from an oil covered surface is presented. It is concluded that differential scattering of radar from oil slicks may exceed that of sonar. Radar has also some advantages for rapid scanning. Sonar however has better resolution which, in some circumstances, may make it of value in surveying oil slicks.

TABLE OF CONTENTS page n°

Abbreviations

A/DC	Analog to Digital Converter
Asdic	Anti-Submarine Detection science
BBS	bottom backscatter strength
CW	Carrier wave
dB	decibels
DSP	Digital Signal Processor
EM	Electro-magnetic
GLORIA	Geological Long Range Inclined Asdic
IOS	Institute of Oceanographique Sciences, Deacon Laboratory
IR	Infra-red
ISVR	Institute of Sound and Vibration Research, Southampton University
NIO	National Institute of Oceanography (presently IOS)
PC	Personal Computer
ppb	part per billion
SAR	Synthetic Aperture Radar
SLAR	Side Looking Airborne Radar
SNR	Signal to Noise Ratio
SONAR	Sound Navigation and Ranging
SSS	Side Scan Sonar
UV (LS)	Ultra-violet (Line Scan)
VDU	Video Display Unit
WSL	Warren Spring Laboratory

Chapter 1

INTRODUCTION

In the past twenty years, the many advantages of using radar as a remote sensing tool have become widely recognized. These advantages include surveying large areas in short time (airborne and satellite SAR), and obtaining measurements where conventional instruments are difficult to deploy or maintain.

Here however, we shall be considering active sonar as a means of measurement. Like radar, it can be used for 'sensing at a distance' in a non-interfering way. The principal advantage of a sonar system over radar for remotely sensing the air-sea interface is that it can be placed on the sea bed for continuous long term monitoring, especially in regions far from shore. This option is easier and less expensive to implement than using a geosynchronous satellite for monitoring a given spot in the ocean. The fact that the instrument is operated underwater opens up the possibilities of gathering information about the layer adjacent to the surface where measurements are often difficult to perform.

Unfortunately, underwater acoustics has not received as much attention as radar in regard to its use as an alternative method of remotely sensing the upper ocean boundary layer. Sonars could play a key role in the field of oceanography by making qualitative as well as quantitative measurements. Only recently

have parameters such as wind speed and surface stress (Shaw et al,1978) been determined from ambient noise measurements, and breaking waves and bubbles density from high frequency backscatter measurements (Thorpe,1982; Thorpe and Hall,1983; Thorpe et al,1985).

The present work looks at the possibilities of developing and exploiting such a system as an underwater tool to collect information about the sea surface and the subsurface layer.

We will be looking at two different situations where a high frequency side scan sonar (248kHz) was used for the first time

i/ to determine the direction of propagation and the magnitude of the surface current in very shallow waters by measuring the variations in the range of bubble plumes drifting near the surface,

ii/to detect the presence of an oil slick floating on the surface by analyzing the acoustic backscatter from the surface.

The emphasis will be on the second of these where most of the work was concentrated.

In the following chapter, we will discuss those elements of sound propagation in water which are important to the research we have undertaken, in particular to describe the different processes involved in the absorption mechanisms. The chapter first draws a historical review of how sound became to be used in the century, and some of the applications that we know of today in the oceanographic field. It also briefly describes the similarities that are to be found between electromagnetic and acoustic-ocean waves interactions and which enables subsequent comparisons between the two types of interactions to be made.

The next chapter reports some observations made in

Southampton waters in the spring of 1987 when a high frequency (248kHz) side scan sonar system was used. In very shallow waters (5m depth), the sonar clearly identified targets moving on the surface and thought to be clouds of bubbles being advected by the surface water flows. This result could be very interesting as it could provide a way of measuring the surface currents in shallow regions where deployment of a conventional current meter is made difficult by the density of the shipping traffic.

The next three chapters mainly deal with the effect of oil slicks on the sea surface and on radar and sonar backscatter signal. In the first of the three, we review the spreading properties of oil, its effect on the sea surface wave spectrum and the consequent changes in the sea surface backscatter. We also report some experimental results obtained by electromagnetic sensing. The discussion is focused on the processes involved in the scattering of microwave and acoustic radiation at the sea surface, and its angular variation in particular. The second chapter describes the experiment carried in the North sea in 1987. The experiment, carried out in collaboration with the *Institute of Oceanographic Sciences* and the *Warren Spring Laboratory*, was aimed at observing an artificially produced oil slick using the previous side scan sonar in a towed mode. The practical objective was to establish the feasibility of oil slick monitoring by sonar. The results, promising in many ways, show that the slick could be observed through its effects on the small scale sea surface roughness. These results can be found in chapter 6.

Chapter 2

REVIEW OF UNDERWATER ACOUSTICS AND SONAR DEVELOPMENT FOR OCEANOGRAPHIC USE

2.1. HISTORICAL SURVEY : early developments

Electromagnetic waves are very rapidly attenuated in the sea. Apart from the blue light which can penetrate the first tens of meters, and the low frequency radar waves which can go down to a few tens of meters, all other forms of radiant energy are reflected or absorbed within the first few centimetres of the surface. The need to explore the vast areas covered by the oceans and the seas for strategic, economic and scientific purposes calls for an alternative form of energy that can be transmitted out to useful ranges underwater to be found. Sound has so far proved to be the only known source of energy that can fulfil this task.

Underwater acoustics, which is the study of underwater sound propagation, might be said to have begun as early as 1826, when Colladon and Sturm (cf. Wood,1941) set an experiment in the fresh waters of Lake Geneva, aimed at measuring the speed of sound in freshwater. They obtained measurements within 0.2% of the currently accepted value of 1438 m/s.

Though determination of the speed of sound was a considerable advance in underwater research, little further progress was made in that respect for the remaining years of the nineteenth

century, mainly due to technical difficulties faced at that time. Nevertheless, by the end of the 1890's, the development of the telephone gave a new impetus to underwater acoustics. The new advances in telephone design led to developments in underwater communications, which resulted in applications such as sonic warning systems for coastal shipping and waterproofed telephones and microphones.

The sinking of the Titanic in 1912 gave rise to proposals for ultrasonic echo ranging as a means of detecting obstacles such as icebergs. The efforts culminated in the development of an oscillator which produced a series of undamped acoustic waves, suitable for modulation into morse by means of simple telegraph transmission techniques. The first echo from an iceberg was received from a range of about 2 miles, by a device developed by Fessenden (1914) operating at a frequency of about 1100Hz.

At the onset of World War I, passive sonar (**so**und **na**vigation **r**anging) systems became widely used in underwater military defence. To counter this development, noise levels of submarines were soon reduced to such an extent that simple passive sonars became totally inadequate and more sophisticated underwater sound devices were needed. In the late 1915, two physicists Langevin and Chilowsky developed an underwater source that transmitted sound across the Seine in Paris. Their original sound projector enabled them to obtain echoes from experimental targets distant by 200m from the source. The introduction of piezoelectric material and electronic components in the sound projector enabled the same team to improve the maximum attainable range by a factor of 7.5, and by 1918 the first echo from a submarine was received (cf. Urick, 1975). The same results were obtained almost simultaneously by Boyle in England. This time the military demands resulted in the development of the first active sonar for accurate location of underwater targets.

During the 25 year period between the two wars, echo sounding became widely used both in military and in civilian shipping. It appeared that echo ranging to the sea floor was a useful way of determining the depth of the water column. This subsequently led to the development of the depth-sounder, which is nowadays an integral part of almost any ship. The fishery industry also benefited a great deal from the development of underwater acoustics which made detection and location of fish schools possible. More details about other achievements during the interwar period are described by Klein (1967).

Further effort was directed towards the advance of transducer technology (converters of electric to acoustic energy) to improve the performances of underwater acoustic instruments so that range, resolution, scanning angle and other parameters can be improved.

With the Second World War, a new impulse was given to underwater acoustics, again for the purpose of solving military problems such as detecting and tracking enemy submarines, and the development of acoustic homing torpedoes. The speed of sound in sea water had to be measured with a higher accuracy since the knowledge of sound propagation in the sea, in particular the problems of refraction, surface and bottom reflections, scattering and attenuation, became essential. Although the primary objective of any new development during this period was purely military, a great part of the research programmes was dealing with the technology itself and the design of various instruments useful for other applications. It was observed that low frequency sound waves, useful for long range tracking during the war, had the property of penetrating the sea bed. This property of acoustic waves had a direct application into sub-bottom geological mapping of the ocean floor and led to the development of the first sub-bottom profilers (Ewing and Worzel,

1948). On the other hand, high frequency sound reflections from the sea floor appeared to reproduce a consistent correlation between the acoustic backscatter and the sea bed topography.

2.2. CHARACTERISTICS OF UNDERWATER SOUND PROPAGATION

Sound consists of a regular motion of the molecules of an elastic substance. The regular motion of the particles initiated for instance by a sound projector or an explosion, is transferred to the adjacent particles owing to the continuity of the medium and its elastic properties. A sound wave is thereby propagated outward from the source at a velocity equal to the velocity of sound. In a fluid, or in any other medium, this sound wave generates pressure changes which can be detected, and therefore measured, by acoustic devices such as hydrophones and transducers.

2.2.1. The speed of sound

The speed of sound remains the most important parameter in determining the characteristics of sound propagation in the ocean. Sound velocity is a function of temperature, salinity and pressure. As these quantities vary considerably in time and from one location to an other, significant fluctuations can take place, and these in turn can have a dramatic effect on the sound propagation pattern. Sound speed is therefore usually represented as a profile derived from temperature and salinity profiles, rather than having an assumed constant value.

Since we are concerned with sound propagation in the upper ocean (top 50-100m) where the water column is quite uniform owing to strong vertical mixing processes sustained by the surface turbulence, changes in temperature and salinity are insignificant. Contribution from pressure changes are also insignificant as they amount to only $1.6\ 10^{-2}$ m/s per metre of

water. We can therefore suppose that sound propagates uniformly in that part of the ocean, except when propagation takes place in regions where large compressibility gradients exist such as through bands or clouds of bubbles. Our main concern is the attenuation of the acoustic energy by viscous effects, chemical absorption, geometrical spreading or transmission loss across the boundaries.

2.2.2. Transmission Loss

Operational range limits of transducers are largely dictated by transmission losses due to attenuation of the acoustic energy during propagation. The maximum effective range that can be achieved by sonar systems is a function of transmission losses relative to the peak acoustic output of the transducer. The general form for attenuation is

$$A = \int_S \alpha \, ds \qquad (2.1)$$

where α is the attenuation coefficient expressing the different processes involved in sound absorption and is expressed in dB/m, ds is an element of length of the sound ray.

1. Reflection at the air/sea interface

In the upper ocean, it is important to know how much of the energy directed towards the sea surface will "escape" through the interface. According to Clay and Medwin (1977), the reflection coefficient of a sound wave incident on an air-water interface at an angle θ from normal is given by:

$$R = \frac{m\cos\theta - (n^2-\sin^2\theta)^{1/2}}{m\cos\theta + (n^2-\sin^2\theta)^{1/2}} \qquad (2.2)$$

where $m = \rho_{air}/\rho_{wat}$, ρ being the density,

and $n = c_{wat}/c_{air}$ is the refraction index.

In the situation where the interface is the sea surface, the quantity m«n so that |R| becomes very close to unity. At normal incidence, |R| differs from unity by the quantity $5.7\ 10^{-4}$ which represents the ratio of the transmitted to the incident energy. Under these conditions, it can be assumed that all the energy arriving at the air-sea interface will be reflected into the water and that losses through the interface are negligible.

2. Attenuation due to absorption

The most important processes involved in sound absorption in sea water are viscous dissipation and chemical absorption. The absorption coefficient α_a, expressing the loss of acoustic energy to the medium from these processes, can be written as a sum of the contribution from each of these processes as

$$\alpha_a = \alpha_v + \alpha_c \qquad (2.3)$$

where α_v is the viscous dissipation coefficient and α_c is the chemical absorption coefficient.

Attenuation due to viscosity has been calculated by Rayleigh (1945) and was found to be

$$\alpha_v = \frac{16\,\pi^2}{3\,\rho\,c^3}\left(\mu_s + \frac{3}{4}\mu_v\right) f^2 \qquad (2.4)$$

where μ_s and μ_v are the shear and volume viscosity coefficients of the water and f is the frequency of the sound wave.

Chemical absorption is caused by ionic relaxation due to the presence of magnesium sulphate (Leonard, Combs and Skidmore,1949) and boric acid in sea water. A large amount of laboratory and field results, collected for frequencies between 2 and 25kHz, have been fitted by Shulkin and Marsh (1962) into an empirical equation expressing α_c in terms of frequency, salinity and the relaxation frequency. This relaxation frequency is the reciprocal of the relaxation time needed by the molecules to return to equilibrium. Later, Clay and Medwin (1977) added a

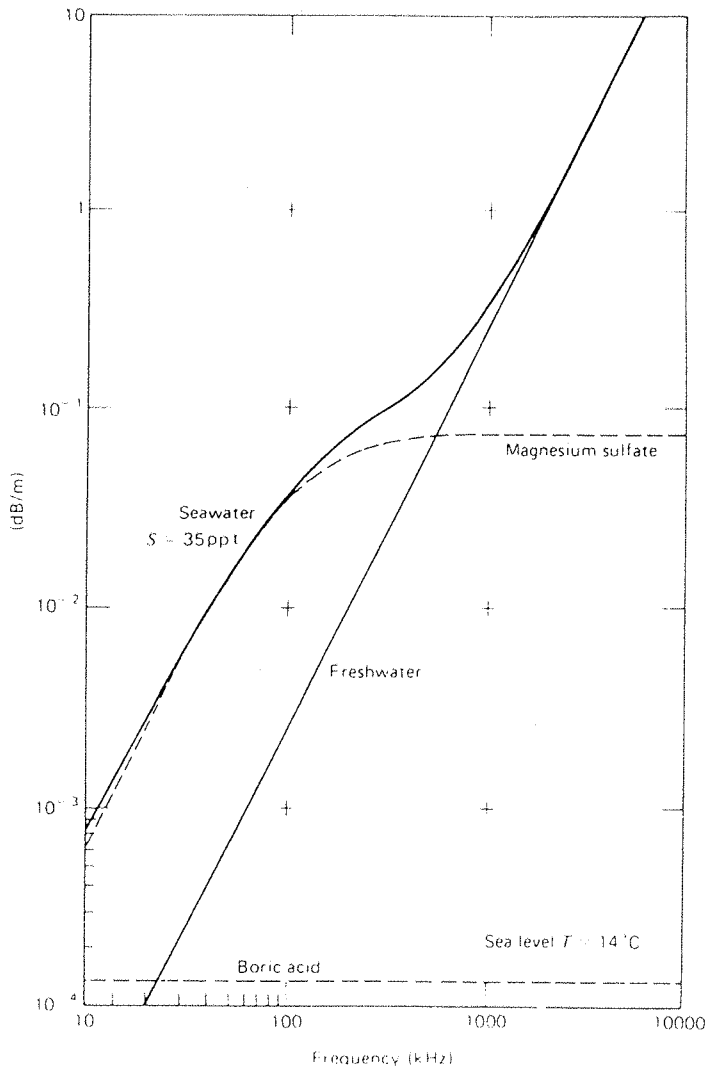

Fig 2.1 Attenuation coefficient α due to absorption in seawater and freshwater at high frequency (from Clay & Medwin, 1977).

pressure factor to the formulae to take into account the depth dependence. The expression (in dB/m) is given by

$$\alpha_c = \alpha_m + \alpha_b \quad \text{with} \quad \alpha_m = A\ S\ \frac{f_m\ f^2}{f_m^{\ 2} + f^2}\ (1 - 1.23\ 10^{-3}\ P_A)$$

$$\text{and} \quad \alpha_b = B\ \frac{f^2\ f_b}{f^2 + f_b^{\ 2}} \qquad (2.5)$$

where $A = 2.03\ 10^{-5}$,

$B = 1.2\ 10^{-4}$ dB/(m.kHz),

S is salinity in ppt, f is frequency in kHz and P_A is ambient pressure in atm. f_m and f_b are respectively the relaxation frequencies for the magnesium sulphate and the boric acid molecules. They are both temperature dependant (Clay and Medwin,1977).

Figure 2.1 shows a plot of α_a (eq 2.3) at high frequency. For frequencies in the range 100 - 1,000Hz, between 4 and 40dB are lost, every 100m, through chemical absorption in sea water.

3. Refraction of sound rays

Considering that the top 100m is well mixed, the speed of sound will have a quasi-linear dependence with depth. Under the influence of pressure, sound rays will be subjected to bending as sound travels through the water column. According to Snell's law these sound rays will be shaped as arcs of circles with a radius of curvature given by

$$\mathcal{R}^{-1} = q\ \left|\frac{dc(z)}{dz}\right| \qquad (2.6)$$

where q is the ray constant and is given by $q = \cos\theta_s/c_s$, θ_s being the angle of incidence (from the horizontal) and c_s the speed of sound at the source. In the situation where sound speed varies

linearly with depth with the constant described above ($dc(z)/dz$ = constant $\approx 1.6\ 10^{-2}$ $m.s^{-1}/m$), the radius of curvature for rays leaving the source at angles varying between vertical (90°) and grazing incidence (10°) will vary between infinity and around 95km. Since this is very large compared to the distance travelled by the sound rays, we can consider the rays to be straight lines.

The only time sound velocity changes in the ocean will be so important that sound rays are submitted to considerable bending, and therefore leading to larger transmission losses, is through propagation in layers of air bubbles (Hall,1989). For instance, a volume fraction of air in water of about 0.001 will create a change to the sound speed from about 1500 ms^{-1} to 320 ms^{-1}.

4. Outward spreading of acoustic energy

A sound wave propagating outwards from its source will be subjected to signal spreading in all directions resulting from geometrical effects. This signal spreading is characterised by a weakening of the signal without, however, involving any direct loss of energy. Spherical spreading for instance occurs when energy is spread from a point source and equally radiated in all directions so as to be equally distributed over the surface of a sphere of radius r surrounding the source. In this case the intensity decreases proportionally to the square of the range, so that transmission loss increases at the same rate.
Spherical spreading can be expressed as

$$\alpha_g = 10\ \mathrm{Log}_{10}\ r^2 = 20\ \mathrm{Log}\ r \qquad (2.7)$$

For side scan sonars, the spreading pattern is greatly modified due to the directionality of the sound beam and the focusing of the acoustic energy. In this case the weakening of

the acoustic signal is considerably less than in the spherical spreading case as sound is only transmitted in a finite angle rather than isotropically.

2.3. SIDE SCAN SONAR

Since the Second World War, underwater acoustics has developed into a science. Observation of the spatial and temporal distribution of scatterers on the surface and within the water column have provided a convenient means for the study of various processes (internal waves, surface currents, air-sea gas exchanges). Gathering of underwater information was made possible owing to the various applications into underwater instrumentation. We focus attention here on the side scan sonar.

2.3.1. Fundamentals of sonar systems

The principle of echo sounding is basically to transmit a pulsed sound wave in the water column, directed towards the area of interest by means of a directional transducer. Part of the acoustic energy will be scattered by any obstacle (object, fish, bottom feature, etc) located within the beam. A portion of this energy will be scattered back to the receiver following the same path, or by way of multiple reflection. The time delay T associated with the received signal gives the distance r between the target and the sonar (Eq2.8) whilst the intensity gives some information about the scattering properties of the target.

$$r = cT/2 \quad , \tag{2.8}$$

where c is the speed of sound.

The technical basis of a side scan sonar is the same in principle as that of a simple echo-sounder. It is particularly

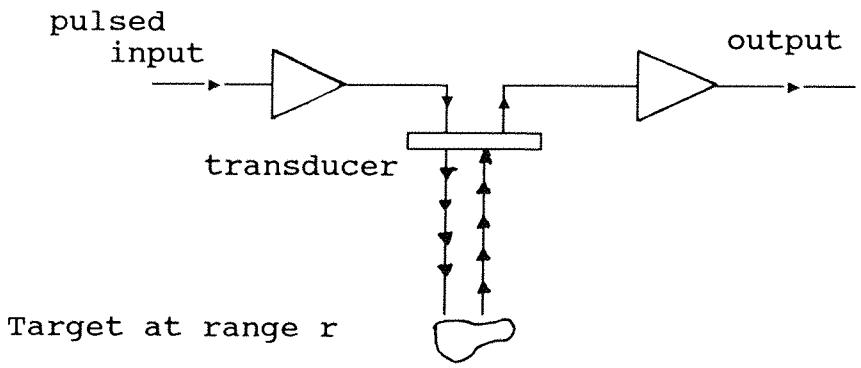

Figure 2.2 Principle of echo-sounding.

useful when surveying large areas of the ocean or when a two dimensional picture of a particular area is needed (bottom features, ship wreck, etc). Figure 2.2 is a basic illustration of this principal.

Sonar systems usually consist of a single beam (and sometimes double) transducer mounted on a towed body or fixed to the side of the ship. The beam is wide in the vertical direction and narrow in the horizontal (see Figure 5.6). Scanning takes place in two directions: along the survey track, and perpendicular to it. The cross-track scanning is achieved by the passage of the sound wave through the water, the reception of echoes from successively greater ranges occurring at successively later arrival times. Along-track scanning is achieved by physical translation of the transducer. In this direction scanning is not continuous, but governed by the repetition rate of the transmitted pulse.

2.3.2. Choice of transducer parameters

To resolve the wide spectrum of spatial scales encountered in the ocean, ranging from tens of microns for microscopic air

bubbles, to hundreds of meters in the case of internal waves, large current and eddy flows, the choice of the various parameters of the transmitting and receiving sonar have to be carefully selected according to the particular phenomena to be observed, and to the range at which it is to be observed. These parameters include the frequency of the carrier wave (CW), the pulse repetition rate, the beam pattern and the source's power. There are however some practical limitations that make the optimum choice for the different sonar parameters generally difficult to meet, so that a compromise is unavoidable. The main areas of concern that govern the design parameters may be summarized as follows:

i/ In order to resolve small scale phenomena, high frequency needs to be used. This is to the detriment of the range, as chemical absorption and loss to the medium increase with increasing frequency (§ 2.2.2).

ii/ The beam pattern depends upon the ratio of the linear dimensions of the transducer to the acoustic wavelength and that means for long range observations (low frequency) the size, and consequently the cost rises steeply, and handling problems may arise.

iii/ Larger transducers transmit more power at greater cost, but for a given size of transducer there is an upper limit to the transmission power at which cavitation occurs, that is when bubbles form at the surface of the vibrating membrane due to negative pressure, causing loss of acoustic power in absorption and scattering, and deterioration in the beam pattern (Urick,1975; p70). The onset of cavitation is determined by the sound pressure and the face area of the projector.

iv/ The ability to detect a target at a large distance from the transmitter depends ultimately upon the signal to noise ratio (SNR) of the system. The greater the transmitted power the higher

the SNR. However, this is not true for close range targets where reverberation (volume scattering) dominates the noise due to concentration of the acoustic energy.

2.3.3. Resolution

Resolution is particularly important in that it will define how accurate a representation of the observed phenomenon can be achieved. The resolution can be improved either by changing the parameters of the acoustic instrument such as its beam width, the repetition rate of transmission, the towing speed (if applicable), but generally it is the characteristics of the transmitted pulse (frequency, bandwidth, length) that will define the degree of the resolution.

1. Resolution along the beam

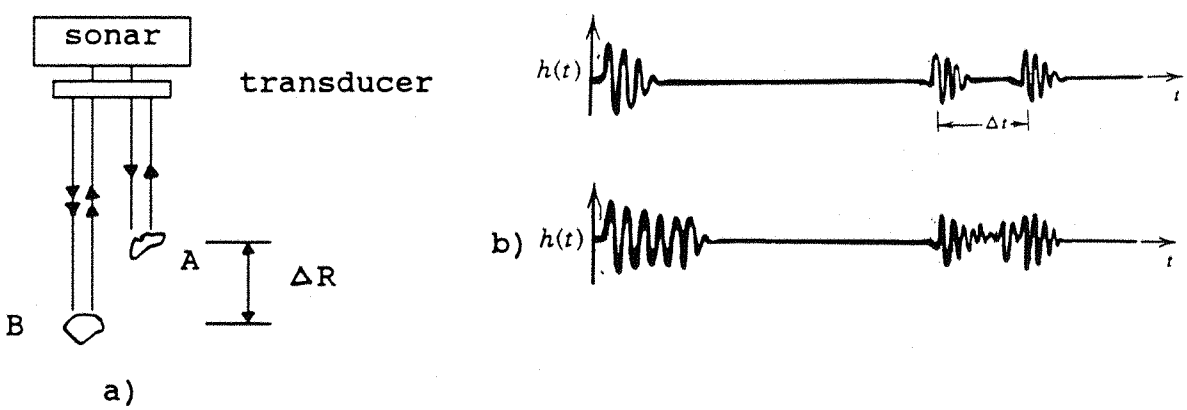

Fig 2.3 a) Returns from closely spaced objects A & B
b) Depending on the pulse length, the returns from A and B are well resolved (top) or poorly resolved (bottom).

To enable the signals scattered or reflected from two closely spaced objects to be resolved, the length of the transmitted pulse should be as short as possible to prevent the return signals from overlapping (Figure 2.3).

The output signal from transient sonars can be ideally represented by the expression

$$s(t) = \exp[-t^2/(\tau/2)^2] \exp[\, i2\pi f_c t \,] \qquad (2.9)$$

Here, $\exp[-t^2/(\tau/2)^2]$ is a Gaussian function representing the envelop of the pulse, τ is the time length of the pulse and f_c is the frequency of the carrier.

By applying the Fourier Transformation to eq 2.9, we obtain

$$S(f) = \int s(t) \exp[-i2\pi ft]\, dt$$
$$= \int \exp[-t^2/(\tau/2)^2] \exp[i2\pi(f_c-f)t]\, dt$$

which yields to

$$S(f) \approx \exp[-\pi^2 (f-f_c)^2 \tau^2/4] \qquad (2.10)$$

The spectrum of the transmitted pulse can also be expressed in terms of the bandwidth of the signal B. The bandwidth of a

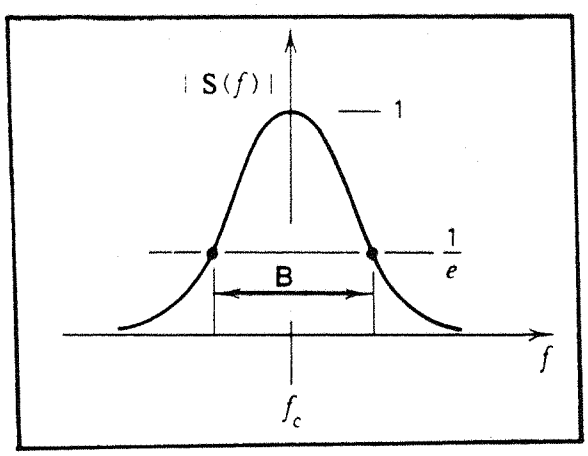

Fig 2.4 Spectrum of a single transmitted pulse with a carrier frequency f_c.

sonar system has an arbitrary definition, but in general it is the 1/e to 1/e specification that is most commonly used (Figure 2.4). In this case, the spectrum will have the form

$$S(f) = \exp[-(f-f_c)^2/(B/2)^2] \qquad (2.11)$$

By equating eqs 2.10 and 2.11, we obtain

$$\tau B = 4/\pi \qquad (2.12)$$

The ability of a sonar to distinguish between two objects will depend on the minimum distance ΔR separating the two objects. In practice, this distance can be set as equal to the spacial length of the pulse, so that objects A and B will be resolved only when

$$\Delta t = \tau = 2\Delta R/c$$

It results that the minimum distance that can be resolved should be at least

$$4c/2\pi B. \qquad (2.13)$$

From these results we can draw the following conclusions:

i/ The resolution along the beam does not depend on the frequency of the carrier.

ii/ The shorter the pulse length the better will the scattering field be resolved. But the longer the pulse the more energy can be transmitted in order to achieve a better signal to noise ratio.

2. Resolution across the beam

Resolution across the beam is affected both by the shape of the transmitting and receiving beam, and by the repetition rate of the transmitted pulse.

a. Directionality of the transducer

The configuration in which we intend to use the sonar in our experiments is with the beam axis directed obliquely towards the sea surface (Figure 2.5). This way, the trace of the beam (in the vertical plane parallel to the beam axis) will extend along

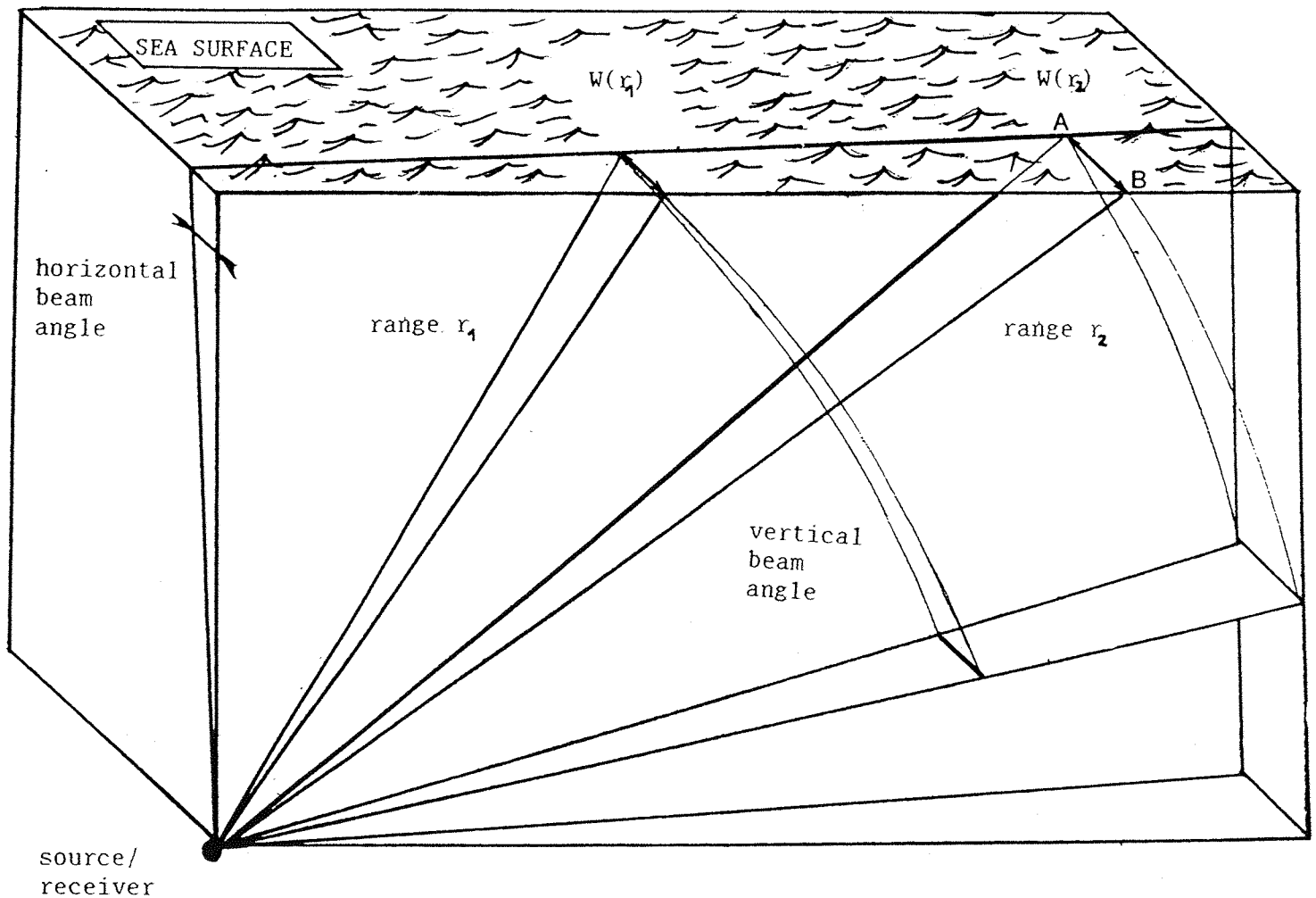

Fig 2.5 Schematic diagram illustrating the volume of water covered by the main sound beam, and particularly the section of the sea surface.

the sea surface and the time of arrival of the echo can be expressed into a horizontal distance along the sea surface in the direction of the beam (eq 5.1), or into an angular position (eq 6.2). The horizontal beam angle (Figure 2.5) will determine how accurately the sonar can discriminate two separate, closely spaced, objects on the sea surface situated at the same range from the source. The signal received at the transducer is integrated o ver the width W(r) of the sound beam at each range increment, and therefore the smaller the beam width, the better the sonar can resolve separate objects.

To illustrate this, let us consider two objects A and B (Figure 2.5) located at range r_2 and separated by the distance $W(r_2)$=AB, normally oriented to the beam axis. The echoes from A and B will be integrated over the distance $W(r_2)$ and the operator interpreting the return signal from range r_2 will be unable to discriminate A from B. If, on the other hand, A and B (still separated by the same distance $W(r_2)$ were located at range r_1, the echoes from each of them will be received separately as only one of A or B will be present on the beam at any one time.

Assuming θ_h (the horizontal beam angle) is small, the area of the sea surface (at range r) over which the received signal is integrated will have a width W(r) given by

$$W(r) = \theta_h r \qquad (2.14)$$

For a transducer with a horizontal beam of 1° operating at a depth of 25m,

W(25m) = 0.4m and W(180m) = 3.1m,

which means the further the sound travels the larger is the averaging surface and the poorer is the resolution.

b. Rate of transmission

In a stationary mode (mounted on the sea bed, or on a platform), the ability of the sonar to detect the movement of an object by receiving as many echoes as possible from the moving target (so that a more realistic image of the scattering field can be obtained) will depend on the rate at which the transmitted pulse is being sent out. This rate is governed by the maximum range the sonar can get to so that the next pulse can only be transmitted when the echo from the furthest point out has been received. The frequency of the carrier will be the determining parameter in that regard. High frequency sound is strongly attenuated. Consequently the full operational range becomes shorter as frequency increases and therefore the period between two succeeding transmissions can be shortened.

In the situation where the sonar is operated in a towed mode, the survey ship's speed V_s will determine the spatial separation between two consecutive echoes. By reducing V_s the spacing can be reduced, and consequently the spatial resolution improved. This is however at the cost of taking longer for the ship to complete a run and of possibly greater changes in the observed features.

2.3.4. Applications

1. Geological side scan

The side scan sonar (SSS) was developed in the wake of the anti- submarine warfare efforts of World War II and the subsequent defence research. However, it was 1957-58 before the first operational SSS was developed at the National Institute of Oceanography (NIO) (Kunze,1957; Chesterman et al,1958). By using a simple echo-sounder with the main beam pointing at right angle to the path of the survey ship, and directed slightly below

the horizontal, Chesterman and his colleagues showed that acoustic images of large areas (500 yards range) of the sea floor could be obtained in relatively short periods of time. They used a narrow beam transducer (2°X 10°-20°) mounted on the side of the ship. The survey area had a depth of 25-35m. He clearly identified bottom features such as bands of sand waves and piles of rocks.

SSS can also be towed from a ship for deep sea geological surveying. The stability of the sonar is improved by keeping the transducers away from the turbulent surface. The effects of the air bubbles generated around the ship on sound propagation are also eliminated.

Example : GLORIA

Following the success of the technique used by Chesterman et. al. in mapping the sea floor, the NIO developed a new system in 1969 (Rusby,1970) called GLORIA (Geological LOng Range Inclined Asdic) for the purpose of looking at larger scale features of the ocean floor. The system would be capable of scanning at depths of up to 8000m with a dual beam giving a total swath width of up to 30Km on each side. The system was designed primarily to look at features of the ocean basin. The beam dimension is 30° X 2.5° (10°X 2.5° on MkI) inclined by 20° below the horizontal. Its operating frequency is within range 6.2-6.8kHz. With regard to the relatively long duration of the travel time between the transmission of the pulse CW and reception of the echo (40s for a round trip of 60km), yaw of the transducer array would cause a serious problem in matching the listening beam with the insonified area at the bottom. A way of overcoming this situation was to place the transducer array in a specially designed naturally buoyant vehicle, towed at a depth of 50m using 400m of cable to insure a significant decoupling from the towing ship (Rusby,1970). The GLORIA system proved so successful that

by 1982 it had surveyed an area equivalent to 1% of the total ocean surface (Laughton,1981).

2. Acoustic tomography

Sonar has now been developed as a tool for studying the water column. For example, acoustic tomography has been used to monitor a variety of ocean features such as mesoscale eddies, currents and internal waves. The basic measurements involved in tomography are the acoustic signal travel time perturbations due to sound speed variations and travel time differences of reciprocally transmitted signals due to current caused by oceanographic phenomena (eg internal waves, fronts) along the acoustic multipaths. Inverse techniques are applied to these measurements to reconstruct the sound speed profile and flow fields. Large areas of the ocean can be monitored by using this procedure without the need for ships to be continually at sea.

3. Upward looking sonars

By the mid-seventies, a new dimension was given to underwater acoustics. This time, sound was looked at as a possible way of investigating physical processes taking place in the upper ocean boundary layer and particularly at the surface where deployment and maintenance of conventional instruments is made difficult by the hostility of the region. Because the surface reflects sound better than the sea bed, this means less energy would be lost through transmission and absorption at the interface.

First to have used this approach are two Russian scientists, Aleksandrov and Vaindruk (1974), who used an inverted narrow (about 2.5°) beam ultrasonic sounder (9kHz) mounted on the sea bed in 20m of water (Figure 2.6). They recorded the echoes from

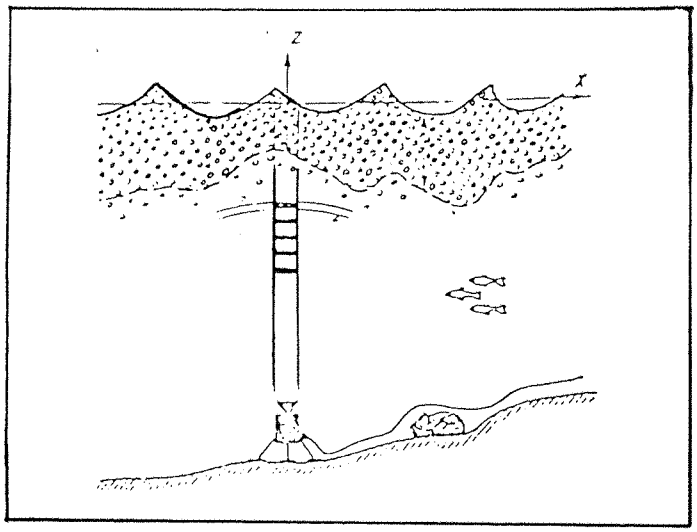

Fig 2.6 Experimental arrangement for pulse sounding of the surface bubble layer with a 9kHz inverted ultrasounder (From Aleksandrov & Vaindruk).

successive transmissions, and by measuring the time differences between the echoes from the volume reverberation caused by the presence of a layer of gas bubbles beneath the surface and the reflection from the surface itself, they derived the extent of the bubble layer. Modulation of the thickness relative to the surface wave motion provided a method of investigating the near surface vertical turbulence.

Prior to Aleksandrov & Vaindruk's paper, Kanwisher (1963) mentions how recordings from an echo sounder floating at a depth of 30m and looking up, showed, under violent wind conditions, bubbles being carried down to 20m when a breaking wave happened to travel above the instrument. It was however Thorpe who established the use of inverted echo-sounders and upward-looking side scan sonars as a remote sensing tool. His work on air bubbles behaviour (Thorpe,1982), breaking waves, fronts and surface currents(Thorpe & Hall,1983; Thorpe et al,1985), internal waves (Thorpe et al,1987) and temperature stratification (Thorpe and Brubaker,1983) was a pioneer in its kind.

a. Stationary mode

The sea surface, as opposed to the sea bed, is constantly in movement owing to winds and current. A way of monitoring changes

occurring at the surface, for long periods of time, can be achieved by fixing the transducer on the sea bed or to a floating mooring away from the turbulent surface.

ARIES (Automatically Recording Inverted Echo Sounder) (Thorpe,1986) is an example of sonar operated in a stationary mode, mounted on a buoy floating at mid-depth. The system consists of an inverted echo sounder made of two transducers mounted at right angle on the top of a vertically positioned buoyant metal tube. Extra buoyancy is provided by metal buoys mounted around the main tube. The structure is maintained in the same position by means of a heavy mooring and is allowed to float at mid-depth. The sound beams are directed vertically upwards. The extent of the area covered by the beams depends on the depth of the transducers.

Aleksandrov and Vaindruk adopted a different setting. They had their transducer fixed to the sea bed and had a 1m section spot of the surface irradiated with their echo sounder (Figure 2.6). Early work by Thorpe was also relying on the same arrangement but using a side scan sonar (35° beam in the vertical) having the main sound axis tilted from the vertical. The sound beam covered a total surface of 150m while operated at 34m depth. In an other setting, Thorpe had two different sound beams pointing at right angle from each other. Assuming that the scattering region is located at the surface, an acoustic image consistent with the features appearing on the surface can be obtained by combining the information gathered by the two beams.

b. Towed mode

Just like Side Looking Airborne Radar systems can produce "images" of the sea surface by combining the motion of the aircraft over the illuminated surface with the repeated transmissions/receptions of the signal, an upward-looking side

scan sonar towed across the sea can also produce two dimensional acoustic "pictures" of the sea surface.

The sonar can be towed from a long cable to ensure a maximum decoupling from the ship' movement (Thorpe et al,1985) or from a submerged vehicle (e.g. submarine) at some distance from the sea surface, as with Crawford and Farmer (1987).

Each of the two modes has some advantages and disadvantages on the other but the final choice is generally more a matter of convenience and will usually depend on the nature of the phenomenon to be observed. If for instance the horizontal velocity of the phenomenon is more important than the towing body's speed the stationary mode is more appropriate in that the sonar will be able to capture the evolution and movement of the event in more detail. If on the other hand the event is slower, such as an oil slick drifting, the towed mode could provide a 2-D image of the area similar to those obtained by radar scans. In this mode however the area of the surface located within the ship's wake (if a surface ship is used) will be artificially disturbed and any signal returning from that area will be useless. The cost is also more important in this configuration. In the stationary mode the sound beam will always be pointing towards the same area and could be missing regions of interest outside that area, whereas in the towed mode the sonar can be deployed whenever the need arises.

2.4. SIMILARITIES BETWEEN EM- AND ACOUSTIC - SEA SURFACE INTERACTIONS

Before we start using some of the results obtained in the em-ocean waves studies, it is necessary to see what are the fundamental similarities between the two types of interactions with the sea surface.

Sound waves are analytically simpler to analyze than electromagnetic waves because the field of the latter is the solution of a vector wave equation, and is given by the electromagnetic field (E,B), where E is the electric field vector and B is the magnetic field vector, whilst the acoustic field is given by the solution of a scalar wave equation.

In both situations, the problem consists of solving the Helmholtz equation

$$\nabla^2 \psi + k^2 \psi = 0 \qquad (2.15)$$

where ∇^2 is the laplacian sum of the second derivatives with respect to the three cartesian coordinates, k is the wave number and ψ represents the velocity potential in the acoustic case and a component of any of the field vectors or their electromagnetic (em) potential in the other case.

For the study of the reflection and scattering of em or acoustic waves at the sea surface, eq 2.15 must be solved with boundary conditions imposed by the rough surface S. These boundary conditions generally determine the value of ψ and its normal derivatives at that surface.

There are two cases where the acoustic and the em boundary conditions are in exact analogy, namely

$$\psi_s(0) = 0 \qquad (2.16)$$

which for acoustic waves corresponds to the case of a free surface, and in em problems to a perfectly conducting surface with ψ representing the tangential component of the electric field strength, and

$$\left.\frac{\partial \psi}{\partial n}\right)_s = 0 \qquad (2.17)$$

which corresponds to a rigid surface in the acoustic case, and to a perfectly conducting surface in the em case with ψ representing the strength of the magnetic field and n a unit vector normal to the surface.

In these cases, the solutions will be similar, differing only in the form of waves generated at the radar or sonar, and the backscatter should be identical for a given wavelength. However, given the differences in the physical properties of the mediums in which these two forms of energy propagate and the asymmetry of the air-sea interface, these will have significant effects depending mainly on the frequency range of the radiant waves and the angle of incidence. For instance, very high frequency acoustic waves (millimetric wavelengths) will be significantly scattered and attenuated by a layer of bubbles. On the other hand, spray and rain can alter the properties of the medium in which the radar signal propagates and might have a significant effect on the propagation of em waves. However, this effect is not expected to be as strong as that of the bubbles for acoustic waves.

Chapter 3

PRELIMINARY RESULTS :
Shallow water experiments

3.1. INTRODUCTION

Near surface currents are time and space varying phenomena which are dependant on a multitude of environmental conditions (wind stress, tidal stream, internal waves etc). The current velocity fluctuations can have a wide range of frequencies and can assume directions at any conceivable angle to the measurement platform. These conditions make accurate measurements of the near-surface current difficult to perform. Conventional measuring devices are not easy to deploy owing to the surface activity of the waves. These instruments can also introduce intrinsic errors as they might alter the water flow around them. Acoustic remote sensing devices which generally rely on the Doppler shift induced by particles moving near the surface have been widely used to gather surface current measurements, and have generally proved to be reliable instruments (Appell et al,1985).

In this chapter we propose and test a method of remotely sensing this parameter in the shallow waters of an estuary using a side-scan sonar. The method consists of correlating the time delays of successive returns from individually distinct clouds of bubbles and of estimating the rate of change of their range with time. This method has already been used by Thorpe et al (1983;1987) in deeper waters.

This method avoids the complexity of Doppler sonars but presently relies on sonograph interpretation. The method also avoids the hazards to instruments from being exposed to shipping movement in a river or channel.

3.2.THE METHOD

3.2.1.Scattering from a single gas bubble

When a gas bubble is struck by a sound wave, it will react to that wave according to its size and to the incident frequency. At a given frequency, the bubble will enter into resonance and a maximum amount of energy will be extracted from the incident sound wave by the bubble. A portion of this energy is scattered around the pulsating bubble, and the remainder is converted into heat. The acoustic scattering cross-section of a bubble at resonance is about 400 times its geometrical cross section (Figure 3.1), and about 10^{10} times the acoustic scattering cross-section of a particle of the same size.

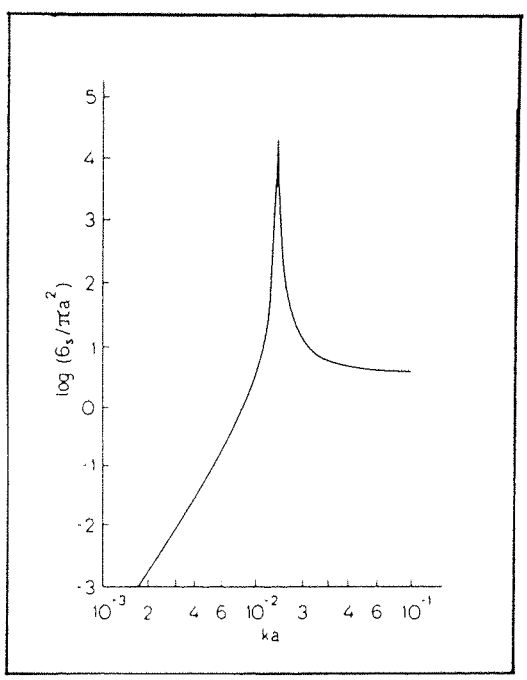

Fig 3.1 Ratio of the acoustic to the geometric cross- section of an ideal air bubble. k is the wave number of the incident wave, a is the radius of the bubble and σ_s is the acoustic scattering cross-section (from Brekhovskikh & Lysanov,1982).

The radius of resonance is calculated from the sound frequency to which it is inversely proportional (Clay and Medwin,1977). For an ideal bubble, i.e. a bubble which does not dissipate acoustic energy into heat, a_r is given by

$$a_r = (1/2\pi f)\sqrt{3\gamma P/\rho} \qquad (3.1)$$

where f is the incident frequency, γ is the ratio of specific heat (C_p/C_v), P is the hydrostatic pressure and ρ is the water density.

For example, for an incident frequency of 250kHz the radius of the resonant bubbles located at the surface is about 13 microns.

3.2.2.Scattering from a cloud of bubbles

When the bubble is no longer a single target but part of a cluster of gas bubbles or a bubble cloud, it has a different behaviour. Bubbles clouds, usually formed by, and remaining in the wake of, a breaker, consist of a large population of air bubbles having a wide size spectrum and undergoing all kinds of physical and chemical processes and interactions. Considering that the majority of these bubbles are made of air trapped underneath the crest of the breaking wave, and could therefore contain alien particles such as sand and dust, these bubbles are not always clean and will not as a consequence behave like ideal bubbles. In addition, the "skin" of bubbles is not necessarilly clean as it is assumed for an ideal bubble, and the bubble will therefore be inclined to lose more energy through heat conduction. All of these observations will tend to reduce the strength of the scattering cross-section of a bubble at resonance.

The scattering cross-section of a bubble cloud M_V depends on the bubbles' size distribution and population. M_V is given by

$$M_V(z,t) = \int N(a,z,t)\ \sigma(a,z)\ da \qquad (3.2)$$

where $N(a,z,t)$ is the number of bubbles per unit volume, and $\sigma(a,z)$ is the scattering cross-section of a bubble of radius a located at depth z at time t.

The detection of the bubble cloud by the sonar results from the contribution of the scattering cross-sections from the total amount of bubbles present in the cloud, although bubbles with radii much smaller than a_r will not be contributing so much.

Experimental values of M_V published by Thorpe in 1983 showed a good analogy with those derived from the bubble size distribution and population measurements of Johnson and Cooke (1979) obtained using an optical technique.

3.2.3.Measurement of the horizontal component of the surface current in the direction of the sound beam

Given that small bubbles (but not necessarily smaller than a_r) persist for a time in the water (the rising speed is proportional to the square of the radius), and if we assume that their rising speed is negligible compared to the mean surface currents, these bubbles when exposed to the surface turbulent flow will act as Lagrangian tracers of the water mass motion. This motion can be detected as the apparent path of the bubble plumes observed on the sonographs and can provide a measure of the magnitude of the horizontal component of the mean surface current along the sound beam by estimating the rate of change of their range with time. The apparent drift of the bubbles relative to the beam direction will also indicate the direction of propagation of the water flow.

We must emphasize at this point that we are only interested in those bubble plumes produced by individual breaking waves and that interest is focused on those bubbles left behind after the breaking event and which persist for a while in the water column. How long this period is will be seen later (section 3.3).

3.2.3.Error sources in the measurement of the horizontal component of the surface current

The velocity u_* measured by the sonar transducer is the sum of the component of the real horizontal current in the direction of the beam $u_{//}$, and the contribution from the various error sources which might produce an apparent displacement of the bubbles relative to the transducer.

One source of error is introduced by the additional component induced by the vertical motion of the buoyant bubbles. This vertical motion will mainly affect large bubbles (the rising speed is proportional to the square of the radius of the bubble) which can have rising speeds comparable in magnitude to the horizontal surface current. For small bubbles however, this contribution will be negligible. Only a fraction of the movement induced by this speed will be apparent as a horizontal displacement.

To quantify this contribution, let us assume that a bubble is located near the surface at heigth h from the sonar, and that it is moving vertically at a speed w. If the transducer is at a depth $d \approx h$ and the bubble at range r from the transducer (Figure 3.2), the vertical motion of the bubble will contribute with a quantity (w sin) to the apparent horizontal speed of the bubble, where is the grazing angle of incidence. At near vertical incidence, contribution from the vertical displacement w to the measured velocity u_* will be at a maximum ($u_* = u_{//} + w$

+ errors). As a precaution, only bubble plumes detected at low incidence will be considered in the analysis.

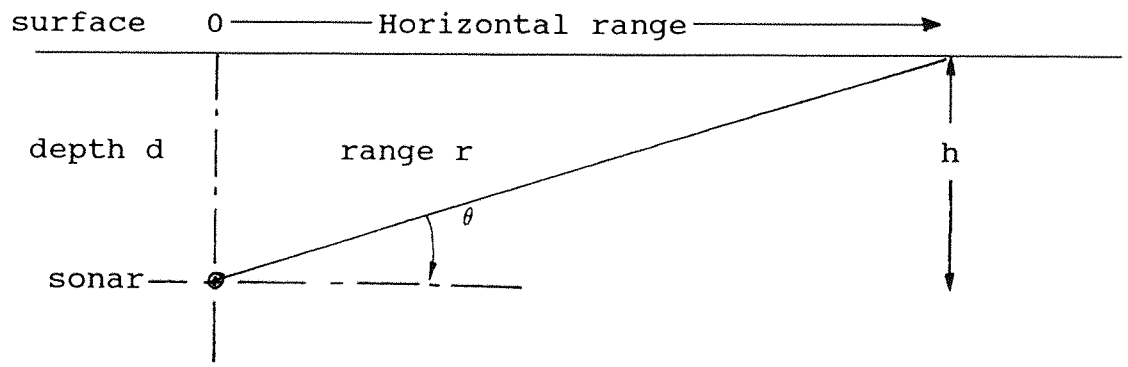

Fig 3.2 Geometrical configuration.

Other local dynamical processes such as Langmuir circulation, which sometimes generate quite important vertical velocities, can also introduce an additional source of error.

3.3. EXPERIMENTAL WORK

3.3.1.Description

A field experiment aimed at assessing the use of a high frequency side scan sonar system in very shallow waters was carried out in Southampton estuary. A site, located at the mouth of the river Hamble (Figure 3.3) was chosen for a period of three days between April 9th and 11th 1987. The water depth at the location was about 4m with a tidal range of about 1m during the observation period.

The sonar (described in more details in Chapter 5) was fixed at 50cm above the river bed and had its main beam pointing at the surface either downstream (210°T) or across the river (300°T). No wind speed and direction measurements were made during the

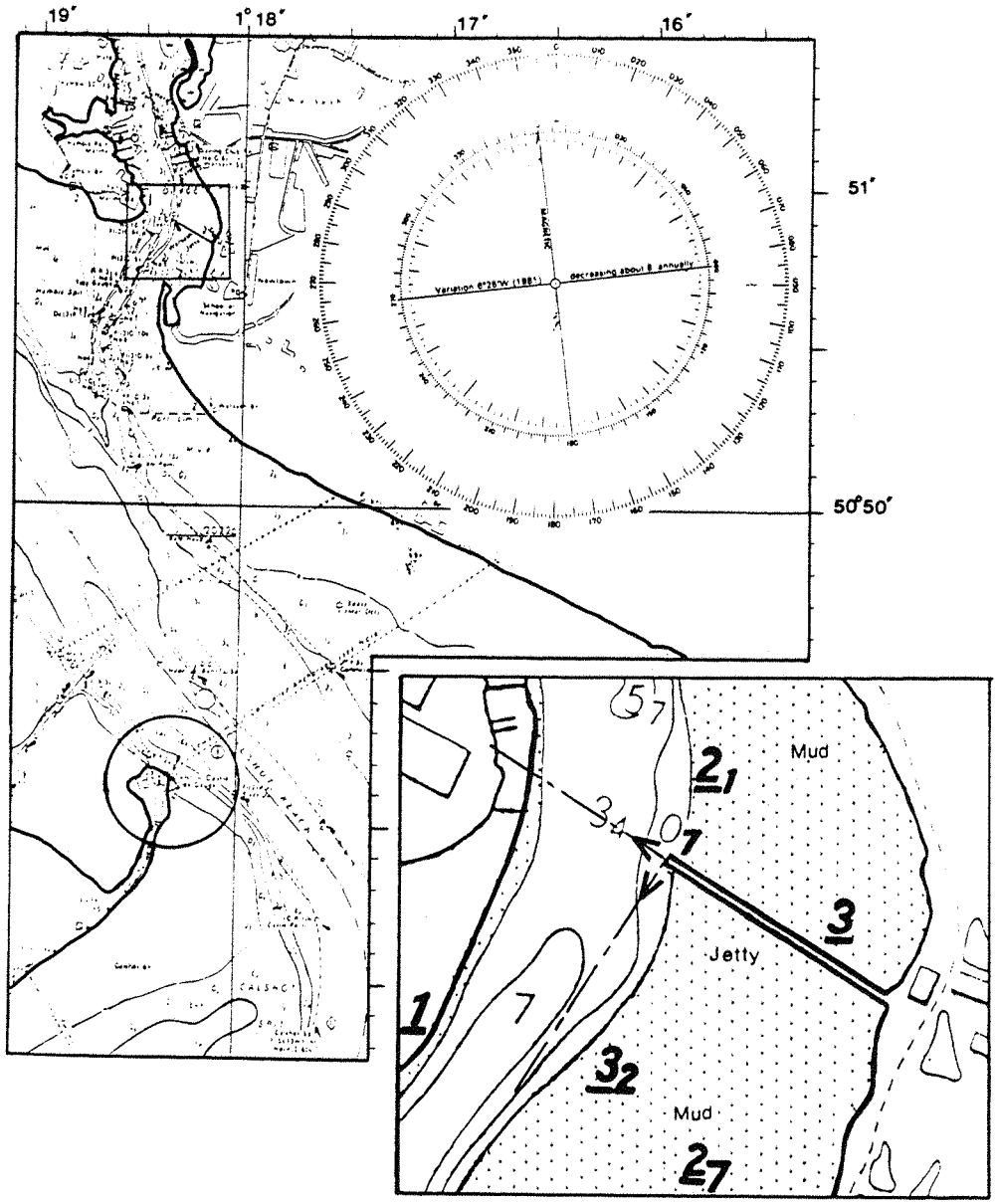

Fig 3.3 Site of the experimental area at the mouth of the river Hamble in Southampton waters (area in square).The enlarged area shows the directions the sonar was pointing at during the experiment and water depths at lowest astronomical tide. Underlined figures are heights above mean level,in metres, at spring tide.
The circled area (bottom left) is the station where tidal elevation was measured.

trials.

3.3.2.Operating difficulties

The main problems of operating a sonar in very shallow depths and particularly in rivers or shallow tidal estuaries can be summarized as follow

i/ The proximity of the surface to the bottom leads to multiple reflections between the two boundaries and may considerably affect the backscatter, especially at close range,

ii/ The substantial amount of suspended particles present in estuarine waters considerably affects sound propagation by increasing the volume reverberation level which depends on the nature and density of the particles. This translates into a reduction of the maximum operational range compared to propagation in water free of suspended matter (see 3.4.2).

iii/ In some areas, long term monitoring would need more frequent supervision and maintenance than would a system deployed in coastal areas, as aquatic life tends to be more active in a river and can grow on the sound projector face causing distortion of the sound beam.

3.4. OBSERVATIONS AND RESULTS

3.4.1.Introduction

The data is represented in the form of sonographs which consist of images reproducing the strength of the acoustic backscatter. The process by which sonographs are produced is explained in paragraph 5.3.2. Basically, each vertical line (eg Figure 3.4) represents the echo received after the transmission of a short pulse. By combining the returns with a slight displacement of the chart prior to each transmission, an image of the scattering field is obtained. The display of the scattered field helps to visualise and extract some useful

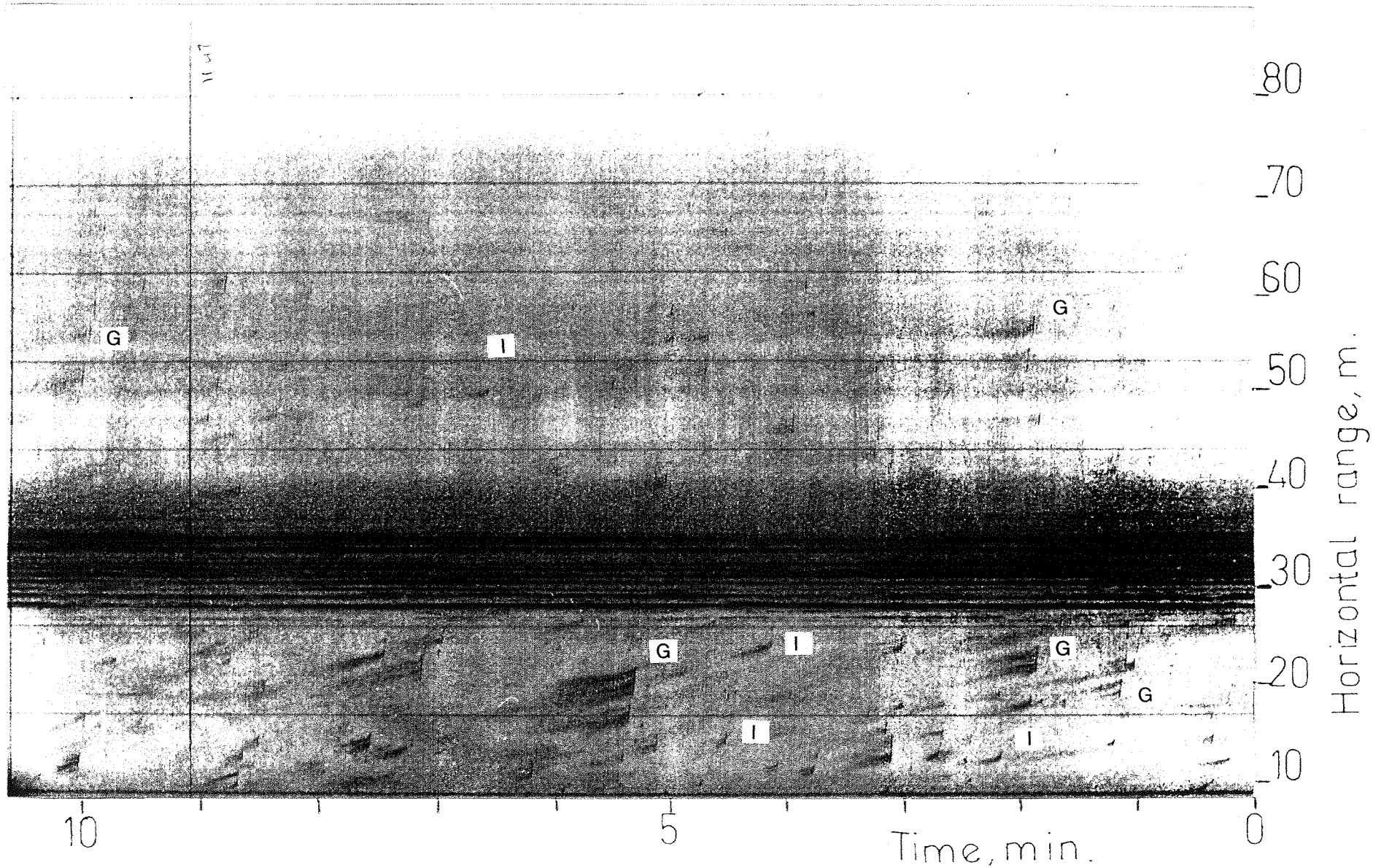

Fig 3.4 a) Sonograph of the sea surface obtained with the sonar pointing down the channel. Echoes from range 25-40m are from a fixed pole.

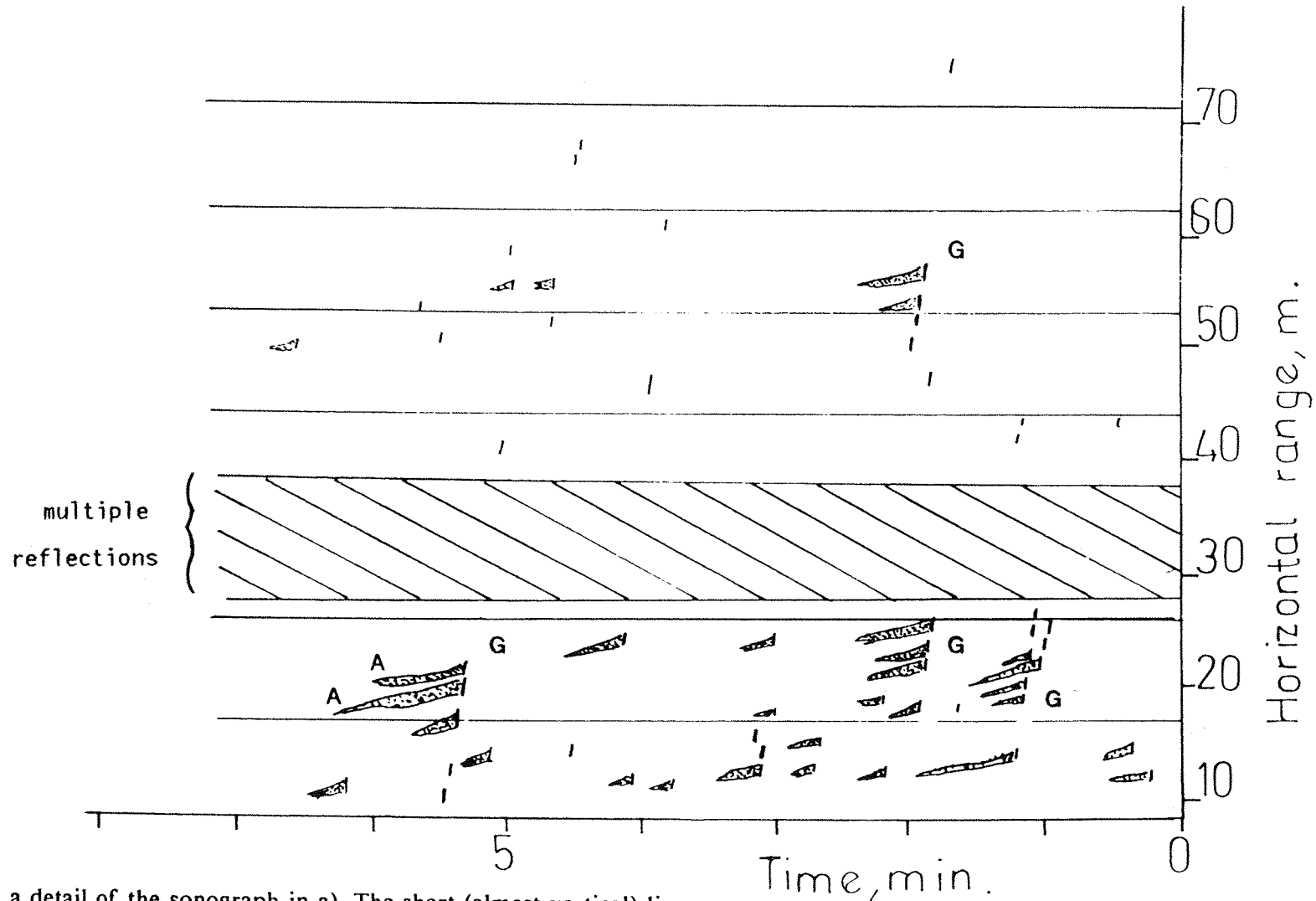

Fig 3.4 b) Sketch showing a detail of the sonograph in a). The short (almost vertical) lines are echoes of waves breaking individually and in groups (G). Bubble plumes (A) can be seen to be generated by the breaking waves.

information about some physical events or moving objects. The delay time between transmission and reception of the echo provides a measure of the range of the observed phenomena from the transmitting platform given the speed of sound in the area. Given the depth of the sonar, this distance can also be expressed in terms of horizontal distance from a point on the surface vertically above the sonar.

3.4.2.Description of the sonographs

Figure 3.4a shows a sonograph with the sonar pointing down the channel at 210°.

The scale at the right of the sonographs shows the effective range along the surface of targets which are on the surface or close to it. Owing to the various transmission loss processes discussed in chapter 2.2 and to the strong volume reverberation level, the maximum operational range attained by the 248kHz sonar used was in the region of 120m. The horizontal scale is time, running to the left. The regularly spaced horizontal lines divide the total width of the chart into ten equal sections each equal to one tenth of the repetition time (=0.125s (8Hz) in this particular record).

The vertical lines (eg. at about 9min from origin in Figure 3.4) are automatically printed by the recorder at time intervals which are pre-set by the operator.

Due to the shallowness of the water, multiple surface and bottom reflections were present over the first ten meters or so from the transducer. The presence of fixed buoys, poles and other river traffic beacons in and around the experimental area also led to strong multiple reflections from these fixed objects. These multiple reflections usually occupy an extended portion of the sonographs considering the multitude of possible paths (via the surface and bottom) from the object to the receiver.

The strong echoes seen at range 25-40m are due to a wooden pole (delimiting the dredged channel) located on the beam's way. Once a sound pulse is transmitted, any surface or object with compressibility properties different to that of the water will reflect and/or scatter the sound. In the case of the wooden pole, some of the possible paths followed by the sound rays are illustrated in Figure 3.5.

The direct path (1), and the specular reflections from the sea bed (2) and the sea surface (3) (if these surfaces were smooth) are shown. However, due to the irregularity of the boundaries, other routes are also possible. This explains the multiplicity of lines at constant range visible

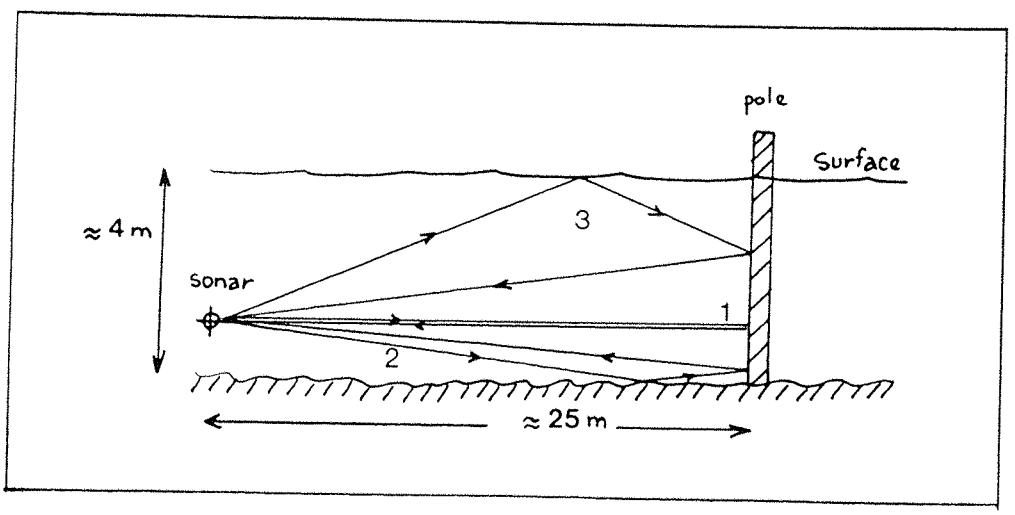

Fig 3.5 Multiple reflections from a vertical pole.
(1) is the direct path, (2) and (3) are respectively the specular reflections paths via the sea bed and the surface.

in the echo seen at 25 - 40m in Figure 3.4a.

In order to clarify the displays, the sections containing multiple reflections and where no useful information could be observed (like the first ten meters from transmission) have been removed.

3.4.3. Experimental results

In this section, we will report some of the features observed on the sonograph records during the experiment.

a.Breaking waves : Figure 3.4

At range 10 to 25m, we can notice wide patches of darker shade (A in Figure 3.4b) which are quite distinct from the background. These are seen to persist from a few seconds to a minute. Their range from the sonar is seen to be gently decreasing.

At the origin of these patches, echoes having the shape of a short inclined line can be seen. The lines are generally directed towards the sonar, are more intense and have a higher slope than the echoes from the large patches, and they generally last for less than 1 sec.

These short lived echoes are thought to be the reflection from individual breaking waves, from where most of the less intense echoes (A in Figure 3.4b) have their origin. It is believed that these longer lasting eches are from the bubble plumes produced during the breaking and leftin the wake of the breakers. As it prepares to break, the wave gains amplitude and its surface slope becomes steeper. The substantial inclination of the sea surface, as a breaking wave passes by, suggests that in some situations, sound rays incident on the flanks of the breaking wave are more likely to be locally subject to specular reflection than if they were incident on a flat surface (Figure 3.6b). Additionally, the densely populated bubbles formed in the area around the crest during the breaking process will also scatter sound and will therefore enhance the backscatter from the region around the breaking point.

For the type of breakers commonly encountered in deep water, i.e. plunging and spilling breakers, the chances for specular

reflection to take place at the front of the wave (as the wave travels away from the sonar, along the direction of the beam) are very remote. As a matter of fact, the curved surface at the front of a plunging breaker makes it difficult for sound to be locally reflected by a wave facet perpendicularly oriented to the ray. And in the case of spilling breakers, the front of the wave is disturbed by the formation of bubbles and will therefore act as a sound scatterer rather than a reflector. Observations, on the other hand, have shown that the surface at the back of a breaking wave is usually slick and smooth. The assumption that sound is specularly reflected at a breaking wave would therefore imply that such a mechanism will be mostly confined to the "back side" of the wave (i.e. the side that faces the sound source as the wave propagates towards the source).

For waves with their crests oriented along the sound beam direction, the echoes from the tilted surface of the breaking wave will be very short as the surface is exposed to the beam only for a short period of time, and will tend to reflect sound forwards rather than backwards in the direction of the sound source. However, the echo from the scattering bubbles will be

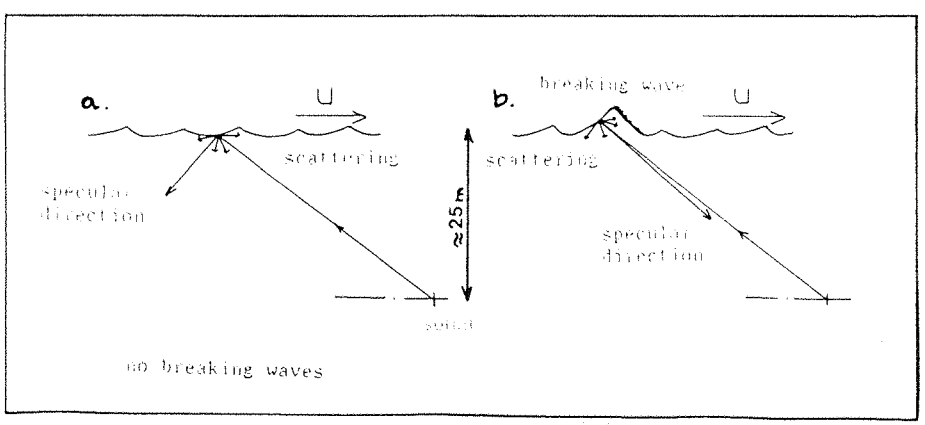

Fig 3.6 Reflection and scattering from a "flat" surface (a), and from a breaking wave (b).

apparent for the time it takes the wave to travel across the sound beam whilst continuing to break.

The sonographs of the sea surface presented by Thorpe and Hall (1983) seem to agree with this. Indeed, in all of those showing surface waves breaking in groups, the direction of propagation of the groups is always seen to be towards the sonar, regardless of the direction of observation.

Figure 3.4 also illustrates a phenomena featuring groups of waves breaking in succession. As each individual wave advances through the group it grows in amplitude, breaks and then passes forward towards the leading edge of the group, thus leaving a trace on the sonographs which appears to be in line with the one from the group immediately preceding it, and so on. The phenomena was discussed and visually observed in deep water by Donelan, Longuet Higgins and Turner (1972) and was later observed by Thorpe and Hall (1983) in deep water also using a side scan sonar.

As a consequence of this property and as long as a group remains within the sonar beam each of the breaking waves in the group will leave an echo trace. In figure 3.4, taken in much shallower waters, occasional patterns of lines made of succesive echoes from breaking waves can be seen on the record (marked G). In each pattern made out of 2 or more short lines, we can see that each line terminates before the succeeding one begins.

Whenever they are visible on the sonographs, these patterns can provide some indications about the propagation of the surface waves in the area. Both the waves' group and the phase velocities in the sonar direction can be derived from the records. The phase velocity c is determined from the slope of the surface waves patterns (long and inclined parallel stripes) whilst the group velocity c_g is estimated from the slopes of the lines joining each individual breaking wave (the intense short

lived echoes) that are part of a group. It should be noted that the values of these measured velocities will include a measure of the surface current, and that it is only when this surface current is small compared to c and c_g that the values of the slopes can be identified as those of c or c_g. This condition can be verified by estimating the surface current from the velocity of the drifting bubble plumes (see next two sections). Under the effect of a substantial surface current (say u), the slopes of the surface waves features will be those of c+u and c_g+u. In Figure 3.4a, the surface current along the sonar beam was estimated and found to be 2.5 ± 0.2 cm/s. The slopes of the wave patterns and the wave groups (which in this case can be considered as those of c and c_g) were respectively 2.1 ± 0.15 m/s and 1.25 ± 0.05 m/s. The frequency of the waves can also be measured from the sonographs by estimating the period between two successive wave patterns.

Using the relationship between group and phase velocity

$$\frac{c_g}{c} = \frac{1}{2}\left[1 + \frac{2kh}{\sinh 2kh}\right] \qquad (3.3)$$

to find kh, and the dispersion relation

$$\sigma^2 = gk \tanh kh \qquad (3.4)$$

to find k, since σ is known from the sonograph image, we deduce that the waves have a 2.8m wavelength and propagate in waters 0.8m deep. Although this latter figure was not experimentally determined, it lies within the range of water depths in the area.

There is also the possibility of estimating the direction of propagation of the waves (in relation to the sonar direction) by comparing the wavelength derived from eq 3.4, and the wavelength in the direction of the sonar beam estimated from the sonograph image and which is given by the distance between two successive wave stripes. In Figure 3.4a, the two wavelengths are

comparable, which suggests that the waves are travelling along the sonar beam.

b.Bubble plumes: Figures 3.7 and 3.9

Breaking is usually followed by the formation of bubble clouds trapped by the overturning wave and dispersed into the water column by the turbulent energy of the surface waves. These bubbles generally persist for some tens of seconds in the water before dissolving or rising to the surface where they burst. For the time they are present in the water, the sonar will detect these clouds of air bubbles which are visible on the sonographs in the form of long dark patches immediately following the short intense echoes from the breaking waves described above. These can be seen on Figure 3.4a where some of the strong echoes associated with a breaking wave are at the origin of longer lasting weaker echoes (marked A) from the bubbles left in the water.

Air bubbles present in the water can have other origins. Figure 3.7 for instance shows a sonograph with the beam pointing across the river at 300°. The echo seen at about 24m is from a swinging dinghy moored close to the sonar.

A speed boat advancing upstream was passing across the beam at range 50 to 55m. A bubble plume lasting about 4min can be seen at this range. At the origin of the plume, there is a short lived echo of slope 1.6 ± 0.1m/s. There are two distinct sources of bubbles, separated by about 2.5m. As time increases, and for the first minute or less from their origin, the furthest plume is seen to be expanding away from the sonar while the nearest plume expands towards the sonar. At one stage (≈ 5min from the start of the record), the two plumes merge before they eventually disappear.

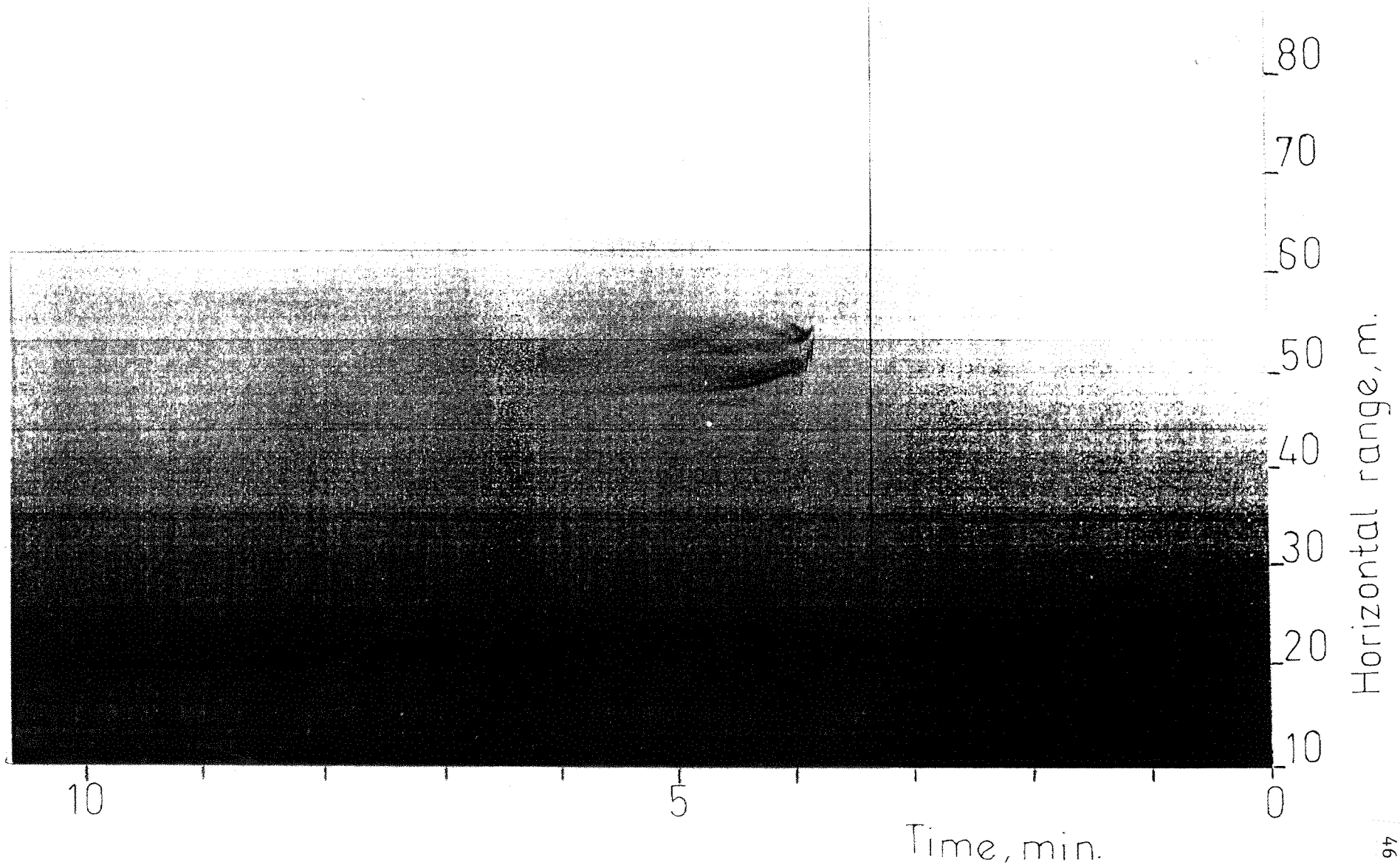

Fig 3.7 Sonograph of a bubble plume left behind a speed boat.

In this particular situation, we are confronted with two different sources of air bubbles: one is the rotating blades of the propellers, and the other is the breaking of the wake in the vicinity of the boat. The plumes observed on the sonograph appear more likely to have been formed by the second of these mechanisms.

To illustrate this, we have drawn a sketch of the speed boat with its wake insonified at t_1, t_2, and t_3 (Figure 3.8). At t_1,

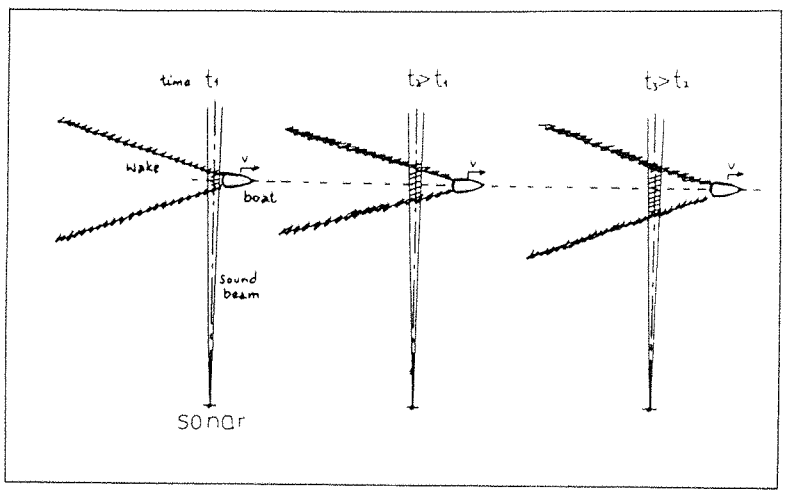

Fig 3.8 Sketch showing a sequence of pictures featuring a speed boat passing across the sound beam.

the wakes are generated on both edges of the boat and should be approximately separated by the width of the boat ($\approx$ 2.5m). At time t_2, the persistence of some bubbles in the water in addition to the newly formed bubbles generated by the moving wake make the plume seem to expand in both directions. At time t_3, the intensity of breaking in the wake is reduced. Surface currents and turbulence have merged the two plumes, but as time increases the bubbles tend to disappear by rising to the surface or dissolving in the water.

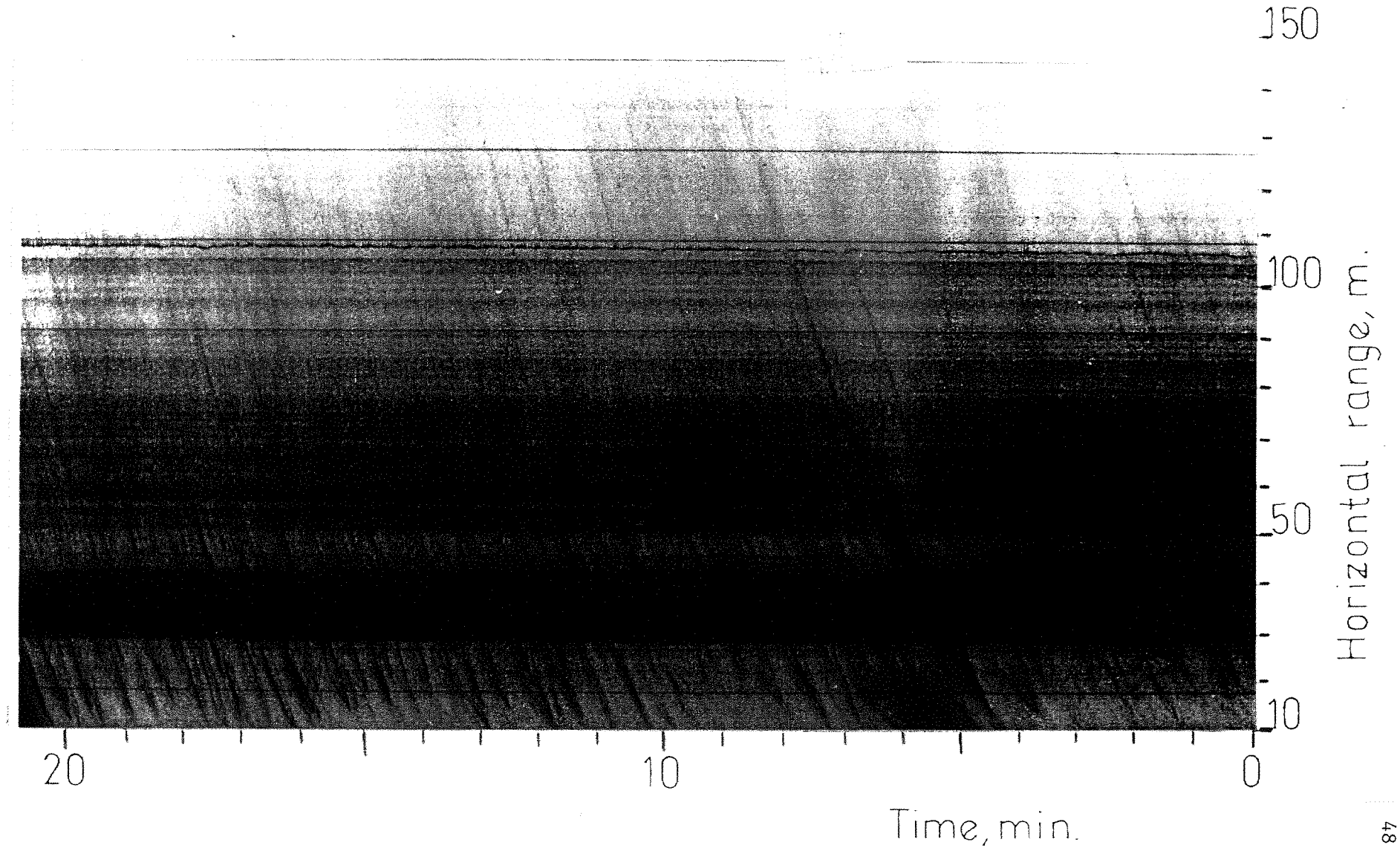

Fig 3.9 Sonograph of a bubble plumes generated by the water flow around the structure supporting the sonar. The plumes are being adverted away from the sonar.

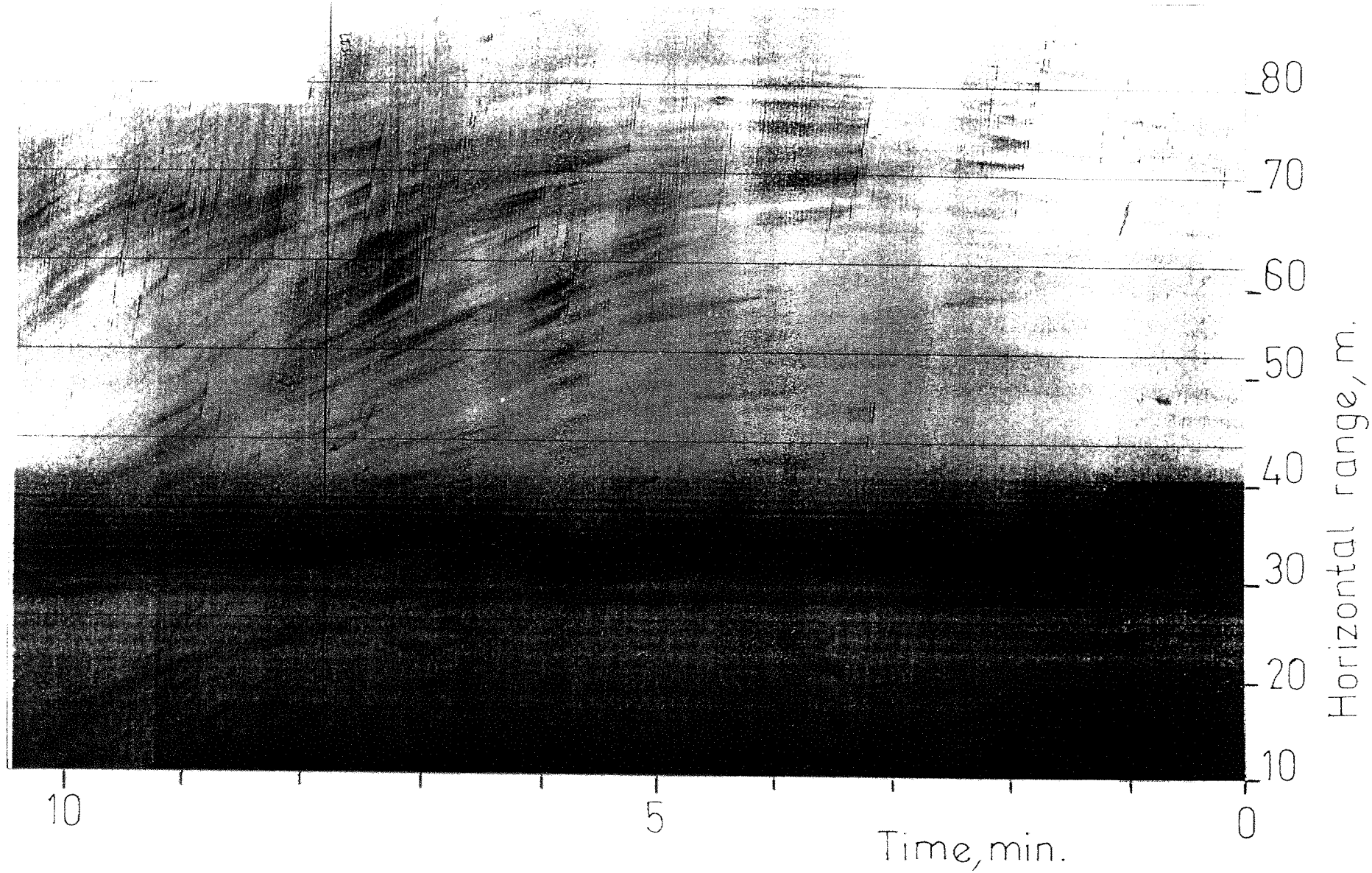

Fig 3.10 Sonograph showing a change in the direction and the slope of the drifting bubble plumes associated with fluctuations of the magnitude and direction of the surface current around low water.

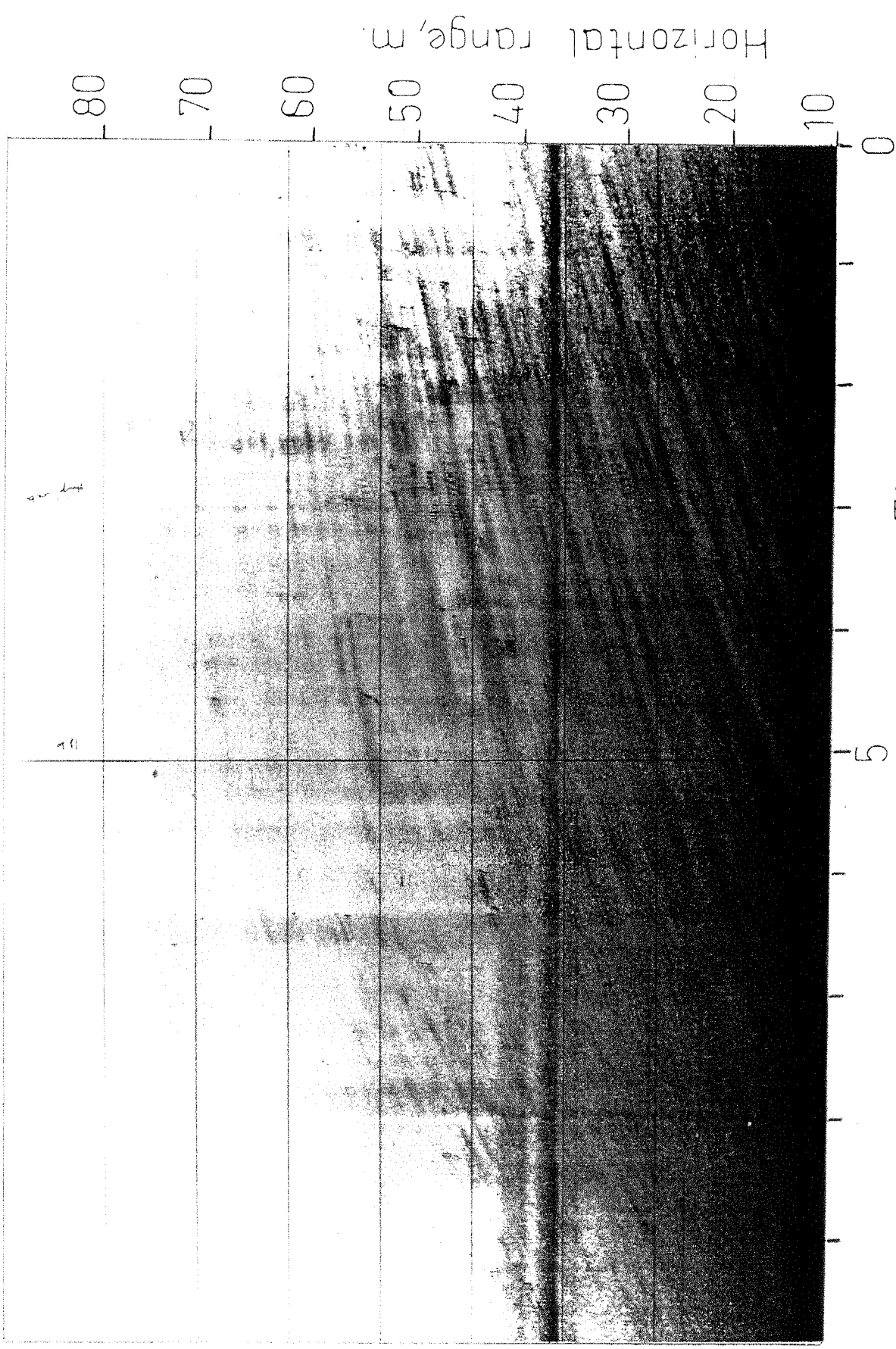

Fig 3.11 Sonograph showing a change in the slope of the drifting bubbles without observed directional changes.

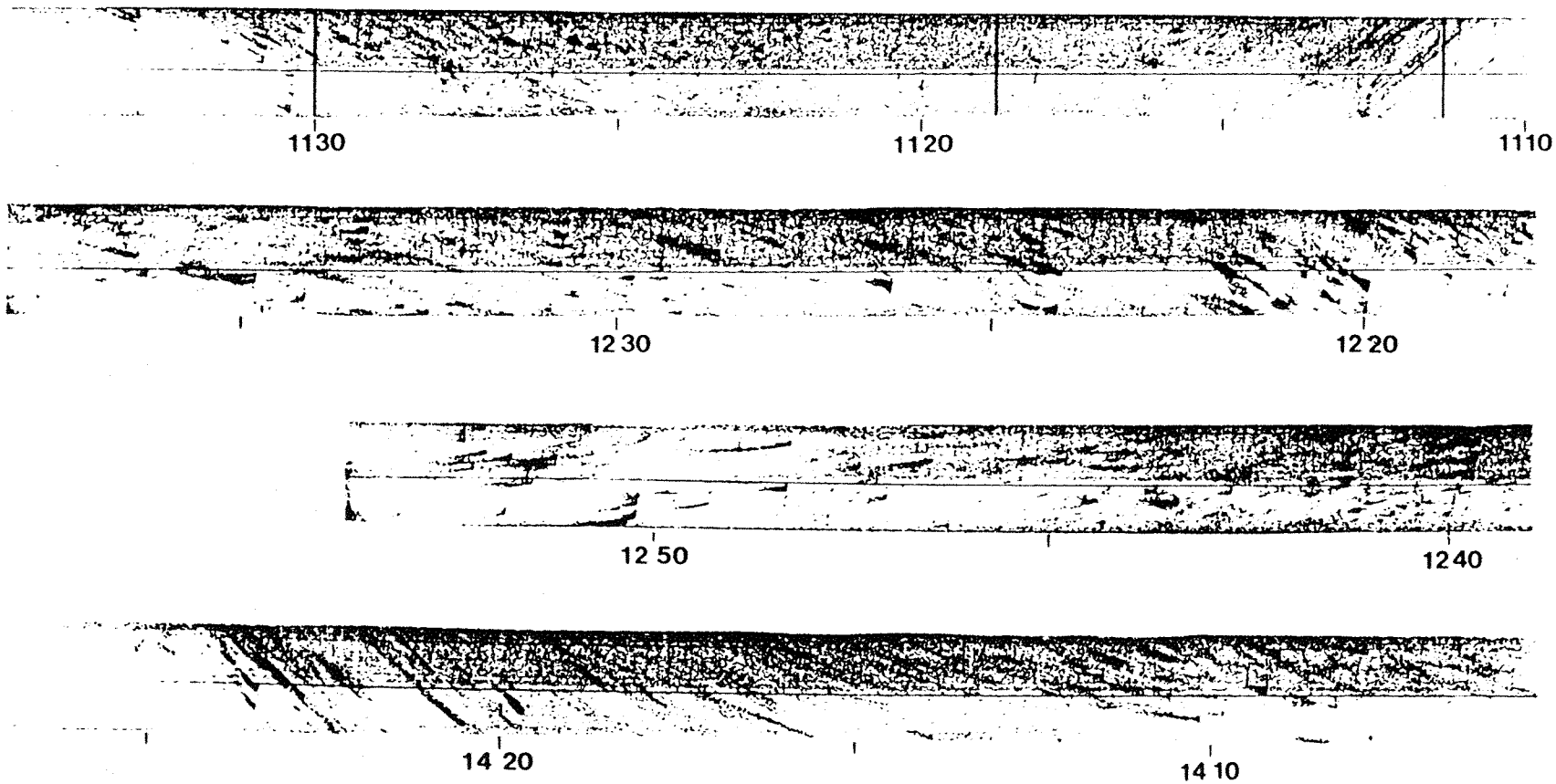

Fig 3.12 Sequence of sonographs showing bubble clouds formed after wave breaking. Vertical scale is horizontal distance extending between 10 and 25m along the surface,from a point vertically above the sonar. The direction these bubble clouds are being advected is seen to be fluctuating.

The presence of the short lived echoes at the origin of the nearest plume which are most probably the reflections from the waves generated by the wake propagating towards the sonar (the lines are approaching the receiver as time increases) seem to be in agreement with this suggestion. Reflections from the wake propagating away from the sonar are "masked" by shadowing effects.

Figure 3.9 is another example of bubble plumes. The sonograph was taken with the beam pointing down the channel. This time the plumes appear to have been generated by the water flow around the wooden poles supporting the sonar as the tide ebbed and the flow was propagating downstream. No breaking is visible at the origin of each plume and most of the plumes are generated close to the sonar (at range 10 to 20m). A measure of the slope of the drifting plumes indicates that the surface currents along the direction of observation were of the order of 0.6 ± 0.1m/s.

c.Surface currents Figures 3.10 to 3.12

Figures 3.10 and 3.11 are two typical examples of sonographs obtained during low frequency variations of the magnitude and direction of the horizontal component of the surface current. These sonographs were obtained with the sonar pointing downstream. The sloping angle of the bubble plumes is seen to be varying with time. These changes, caused by variations in the surface current, were almost certainly associated with the high and low cycles of the tide. The orientation of the plumes with respect to the sound beam indicates the direction of propagation of the tidal stream.

In Figure 3.10, the current changes from a downstream flow to an upstream flow, at the time of low water. The velocities estimated from the apparent slopes of the bubble plumes vary from

-2.5cm/s to 6.0cm/s. We can still notice waves breaking in groups and from which most of the bubble plumes originate. Figure 3.11 on the other hand only shows a change in the surface current magnitude without any apparent change in the direction of the river flow.

One of the most interesting observations made during the trials was a sequence of multiple changes in the current's magnitude and direction which lasted for about two hours. Figure 3.12 shows a succession of sonographs from one of these observations. The sonographs have been cleared from the parts affected by the irrelevant multiple reflections. The bubble plumes show that the surface current changes from an upstream to a downstream flow. In Figure 3.13 are plotted the magnitudes of the horizontal surface current component in the direction of the sound beam, derived from Figure 3.12. We also plotted the tidal elevation above the mean sea level at Calshot castle (circled in Figure 3.3), which is located some 1 1/2 mile downstream of the

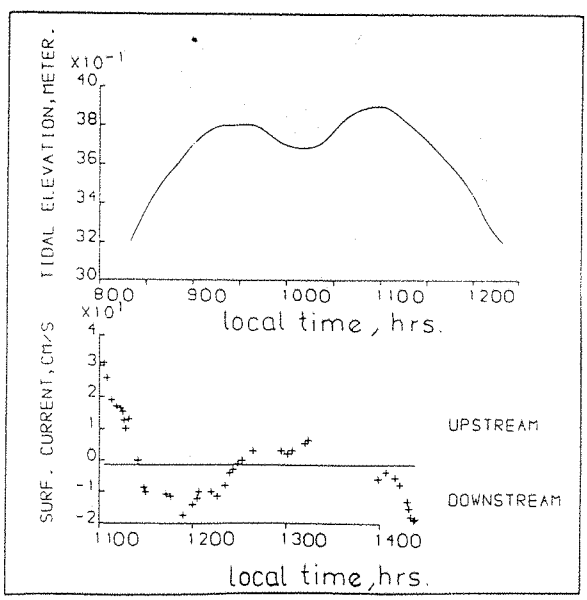

Fig 3.13 Plot of the horizontal component of the surface current in the sonar direction derived from the slopes of the bubble plumes in Fig 3.12. Tidal elevation for the same period at a different location (see Fig 3.3) is also shown.

experimental area. The data was extracted from the *Associated British Ports'* tide tables. The period of the (double) high water recorded in the estuary is of the same temporal scale as the phenomenon observed. Considering the distance between the two stations and the complexity of the boundaries, there is a substantial phase difference (≈ 2hrs) between the two events. By taking into account this phase difference, the current is seen to be propagating upstream whenever the tide floods, and downstream whenever it ebbs. We conclude that these current changes are related to the double water inflow at high tide in this particular arrangement.

3.4.4.EXPERIMENTAL IMPROVEMENTS

Following the 1987 experiment, a second trial was conducted in June 1989 at a location further upstream on the estuary, about 1 mile up from the Itchen bridge in Southampton (Figure 3.14). It was spring tide at the time of the experiment and the water depth was varying between 3.5 and 6m.

This time a set of two transducers (90 and 248kHz) was mounted on specially designed frames clamped to wooden poles situated at the extremities of a floating platform, 1m above the river bed. The axes of the two beams were pointing towards the river at 45° from the line joining the two transducers (Figure 3.15). The sound beams crossed at 90° to each other and were viewing the same body of water. It was possible to change the horizontal inclination of the beam (and therefore moving the spot where the two sound beams intercept) by adjusting the supporting frames. It was intended that backscatter from the two transducers would be combined to estimate the horizontal surface current grid at the crossing point between the two beams.

Fig 3.14 Experimental area on Itchen river.

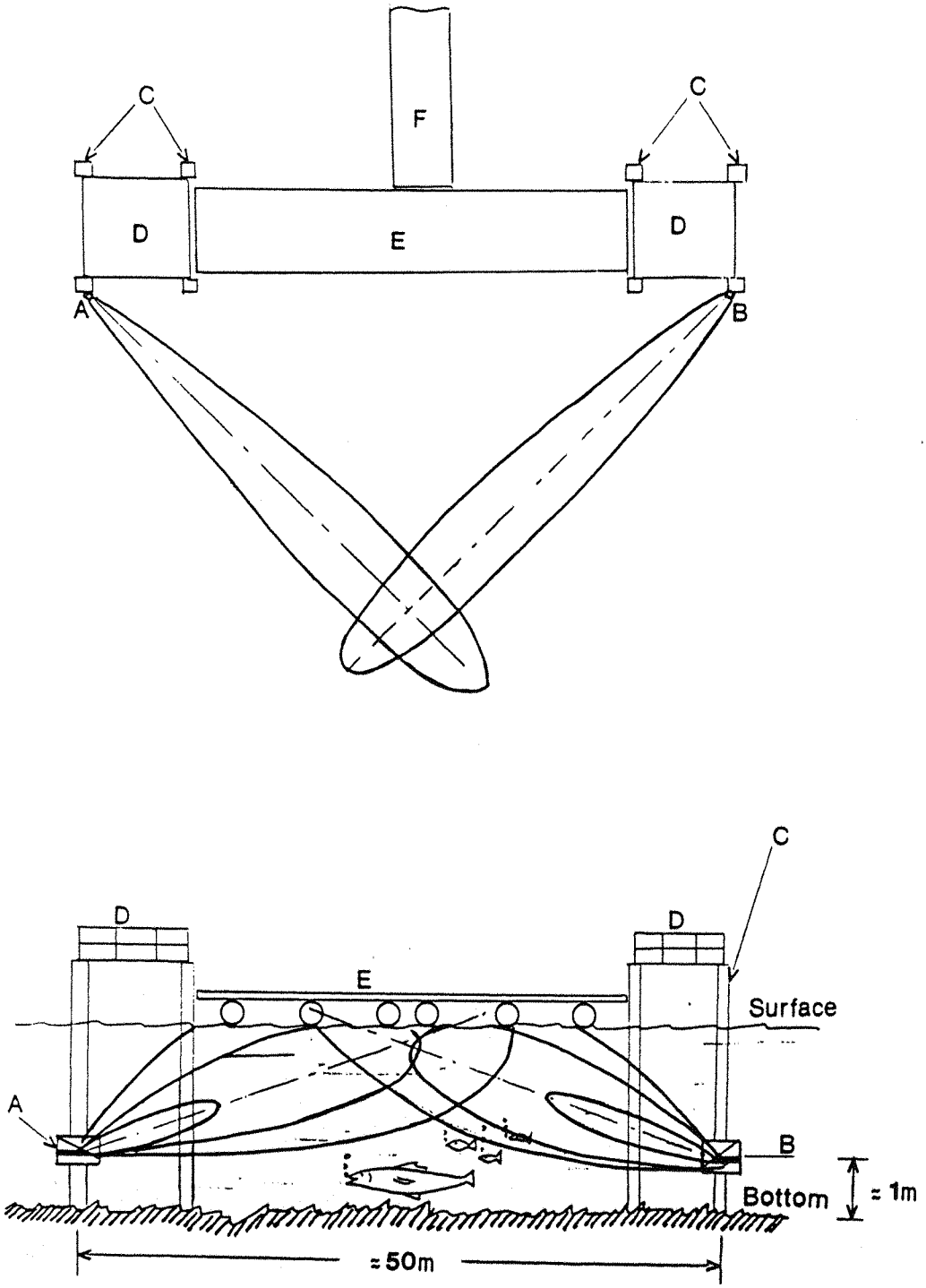

Fig 3.15 Sketch showing an aerial and front view of the experimental area.
A: 248kHz transducer with frame.
B: 90kHz transducer with frame.
C: supporting wooden poles.
D: concrete platform.
E: floating platform.
F: jetty.

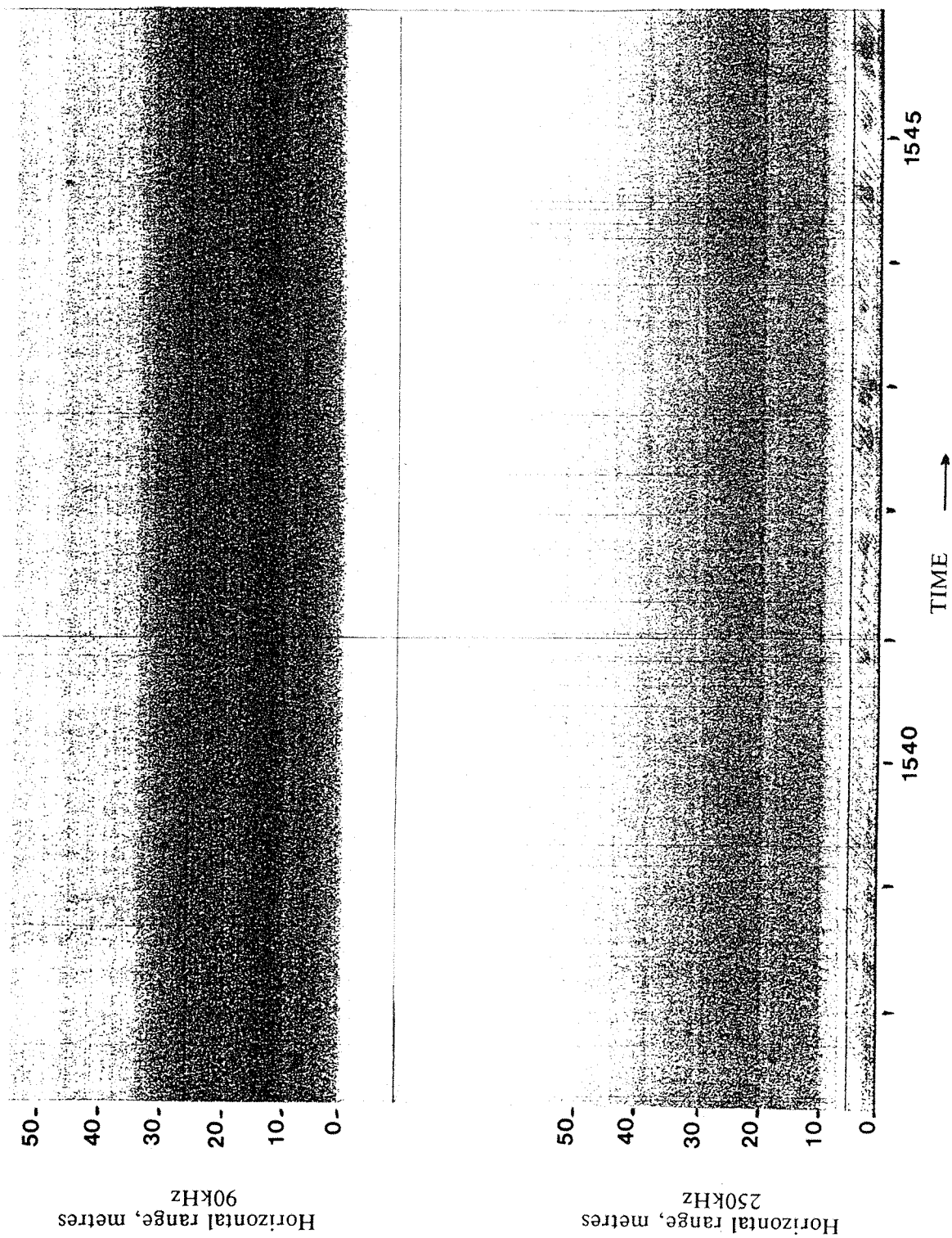

Fig 3.16 Sonograph record from June 90 Itchen river experiment. The top sonograph is from the 90kHz, and the bottom sonograph is from the 250kHz transducer. Some wave patterns and stripes from drifting bubble plumes can be seen at close range on the 250kHz beam, but the 90kHz is failing to reproduce any of these.

Some adjustments were made in order to reduce bottom and side reflections. The frames were fitted with absorbing plates made of 1/8" thick steel covered with a 1/2" thick mat of enclosed foam to act as a sound absorber. As a consequence, the effects of multiple surface and bottom reflections like those seen in the first ten meters from the sonar in the previous configuration were considerably reduced. The possibility of recording the return signal on magnetic tapes for subsequent digital analysis was also available. Wind speed and direction were monitored by a meteorological station at a shore site near the experimental area. The wind speed generally varied between 0 to 6m/s with occasional peaks at 13m/s. Surface current measurements proved unfeasible by conventional moored instruments due to a heavy shipping traffic along Itchen river. Instead, the use of a time lapse video camera (pointing at the area of interest) was suggested. Surface tracers would be provided by paper cards released from the measuring platform. However, this option was to be used only if the experiment progressed satisfactorily.

Unfortunately, the results from this experiment were very poor. Figure 3.16 is an example of sonograph obtained during these trials. It shows the return from the 250kHz (bottom) and the 90kHz (top) transducers under very low winds. The 90kHz transducer showed some operating difficulties and failed to reproduce any signal consistent with the 250kHz transducer. Winds were also very low during most of the experimental period. In addition, the location (which was the only one available at the time) offered a very short fetch and was protected from the Southerly winds by a river bend (Figure 3.14). This prevented the surface waves from fully developing into breakers. The inability of the transducers to detect the bubble clouds shows one of the weaknesses of this method in sheltered situations where no significant breaking takes places.

One of the objectives of June 89's experiment was to evaluate the difference in the return signals between the 90 and the 248kHz transducers. The use of two different frequencies could provide some indications as to which frequency is most suitable in an estuarine environment and which frequency is the best detector of bubble clouds in estuarine waters.

3.5.DISCUSSION

Additional work is needed to better understand the process of sound scattering in a cloud of bubbles, and how accurately the speed of a cloud can be estimated from a diffuse pattern.

Further work into determining the different sources of errors that should be taken into account to derive the real surface current from the pattern of bubble plumes is also important. This step should give an idea about how accurate this method is, and would allow comparisons with other more conventional methods to be made.

For this method to become practical, the data should be conveniently presented in a way that would make it easily accessible by a computer for rapid and accurate processing. There is a necessity to design the appropriate algorithm that would identify the return signal from clouds of bubbles among a background of scatterers. The algorithm should enable the correlation of successive returns from the same cloud of bubbles and derive its horizontal drifting speed from the variations of its range (from transmission) with time. The algorithm would also need to include the necessary corrections due to the vertical motion of the bubbles in the cloud.

A method for the data processing is proposed in chapter 5.

Alternatively, the useful sonographs could be processed into digital images from where the relevant information such as the slopes of the bubble plumes, the velocity of the breaking waves

and that of the groups of breaking waves could be digitally derived.

Summary

i/ A high frequency side scan transducer can be operated in very shallow waters for use as a remote sensing tool. During the experiment, targets could be detected out to a range of 120m, but the most useful information was located at range between 10 and 80m.

ii/ Among the events captured by the sonar in waters 4-5m deep are breaking waves. From the slopes of their distinctive echoes have been derived surface wave group and phase velocities.

iii/ Drifting bubble plumes can be traced to provide a measure of the near surface horizontal current along the sound beam. However, this method is dependent on the presence of bubble plumes in the water column.

iv/ In order to verify the measured parameters with measurements from other instruments, an experimental arrangement is proposed to enable the production of a 2D grid of the surface current at a particular spot of the sea surface using two transducers.

EFFECT OF FLOATING FILMS ON THE SEA SURFACE and their remote detection

INTRODUCTION

The presence of an oil layer on the sea surface is noticeable through its visible effect, leaving the surface looking glassy and calm . This property of reducing the surface roughness was commonly used even in ancient times when seamen claimed to reduce the turbulent activity of the waves during heavy storms by pouring oil onto the sea surface. In the same way, divers would spray oil onto the surface before they dived to eliminate the ripples that would otherwise form distracting patterns of sun-light beneath the surface. A full historical review, dating back to antiquity, of wave damping under the influence of an oil layer is given by Scott (1978). It relates numerous examples, recorded throughout the years, of how oil spilled on the surface of ferocious ocean waters saved lives of seamen. The three phenomena, the formation of waves, their damping once formed and the tendency of large waves to break, can all be affected by monolayers on the surface. Aitken (1883) was among the first to offer a scientific explanation to the problem of wave damping by a surface film. He showed that the phenomenon was associated with the resistance of the surface to compression.

4.1. PROPERTIES OF SURFACE FILMS

Liquid oils floating on the sea surface may have different origins. Petroleum products, which are the most harmful to the marine environment, are a direct result of the increasing use of off-shore drilling sites and of the marine transport of petroleum substances. Marine plants and organisms can also secrete oleic substances that rise to the surface and form slicks. Tank flushing and river discharge of chemical detergents of all sorts add to the already wide spectrum of slick origins.

When oil is poured onto the sea, a small part is mixed in the bulk by various mixing processes but the largest part stays at the surface where it floats.

Oil can occur in water in four different forms :

i/ A thin film a few hundreds of microns thick (sometimes less), which spreads uniformly on the water surface,

ii/ a stable emulsion (with particle sizes less than 300 microns),

iii/ a solute (the solubility of petroleum ranges from 2 to 100 mg/l)

or iv/ floating blobs and lumps.

Petroleum products contain surfactants (surface active substances) which consist of chains of hydrocarbon molecules. These surfactants will react in different ways with the underlying water according to their chemical structure. It is the presence of these synthetic surfactants in many crude oils that gives them the property to spread into thin layers. Additional surface active material can be naturally produced by bacterial decomposition and photo-oxidation processes taking place in the vicinity of an existing slick. Slicks of biological origin consist of fatty acids mainly produced by phytoplankton. The high concentrations of surfactants in these acids allows

slicks of this nature to spread into very thin films, usually referred to as monomolecular films (only a few nanometres in thickness) before they are broken up by the turbulent processes at the surface.

4.1.1. Spreading of oil on the water surface

A hydrocarbon product spilled into a calm sea will spread under the influence of gravitational forces and its viscous properties. The equilibrium thickness of the layer is dependant upon the different surface tensions involved in the film and is determined by (Garrett,1974):

$$t^2 = - 2 \frac{F}{\rho_o \, g \, (1-R)} \qquad (4.1)$$

with $R = \rho_o / \rho_w$, where ρ is density,

$F = \gamma_w - (\gamma_o + \gamma_{ow})$, where γ is the surface tension and the subscripts o,w and ow standing respectively for oil, water and oil-water interface, and g is the acceleration due to gravity.

If F is negative, the oil layer, instead of spreading out, will remain in a lens with a thickness determined by the above equation. However, most petroleum products have a positive F and will spread into extremely thin films owing to the surface chemical activity of the oil. This spreading is caused by the surface active constituents of the product. In real conditions, the oil will spread into a film with various thicknesses ranging from a few microns to a few millimetres. Microwave radiometry observations of experimental fuel and crude oil spills (Hollinger and Menella,1973) have shown that after the slick has spread for some time, there are one or more thick patches with thickness greater than 1 mm, and which accounts approximately for 90% of

the total oil volume. The extent of these regions is usually not more than 10% of the total area covered by the slick. Surrounding these lenses are large areas of significantly thinner films of 2 to 4 microns in thickness. The outermost region of a fresh spill appears only as a colourless slick in which capillary waves are damped. They carried out their experiments under wind conditions of less than 10m/s at the surface.

Under the influence of moderate wind conditions and surface currents, the film is moved with the flow of the surface water. The thickest part of the film (lens) also moves with the wind driven surface water flow. The film is usually spread along the wind axis, with the thickest part located at the downwind edge of the slick. The lens in that part of the slick acts as a reservoir which could rapidly "repair" parts of the film affected by the destructive processes of wave action, dissipation, evaporation, etc. This generally results in the slick having a clean-cut edge, with the film bearing no disruption inside the slick. At the upwind edge of a slick, the spreading of oil will,

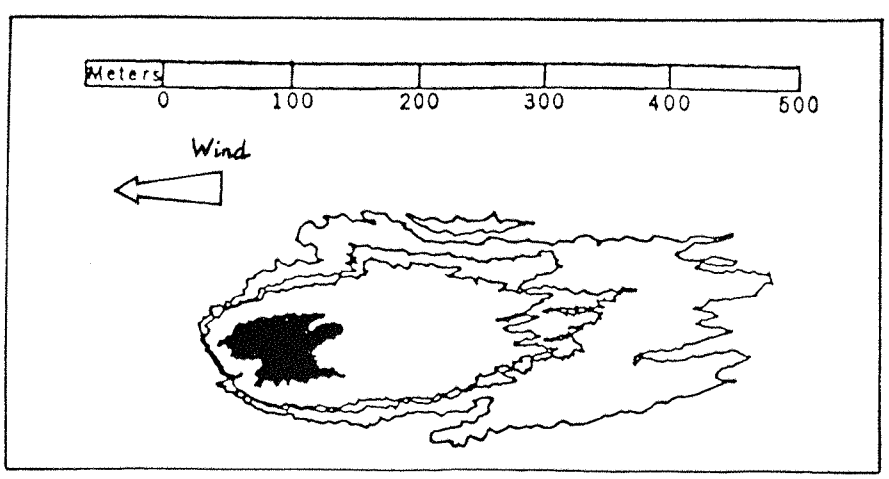

Fig 4.1 Drawing from a colour photography tracing of a No2 fuel oil slick 4 hrs after release. The dark area is the region of thickest oil (from Hollinger and Menella).

in addition, be influenced by the dynamic processes taking place near the surface (convergence zones, Langmuir cells, surface currents) making the slick form a variety of patterns. A finger-like pattern is the most usually observed in open sea experiments (Figure 4.1). It is generally found that the major axis of a slick a few hours old elongates in the direction along the wind at a faster rate than it does across the wind.

A realistic estimation of the rate at which a slick spreads must take into account such important parameters as the volume, age, density and viscosity of the oil product in addition to sea state and weather conditions. The type and concentration of surface active agents present in the oil play an equally important role, hence the wide range of models found in the literature (see for instance Elliott,1986). The practical difficulty of identifying the position of the slick edges adds to the problem of achieving accurate measurements of slick dimensions for qualitative estimates of slick sizes.

4.1.2. Wave damping by surface films

The presence in the water of liquid oils suppresses waves in the short period part of the spectrum and reduces the intensity of wave breaking (Ariel, quoted by Bortkoskii,1988; Barger et al,1970). In addition to being the most effective inhibitors of capillary waves, thin films are also the most suitable ones for quantitative experimental observations. A small quantity of oil containing highly surface active substances (e.g. oleyl alcohol) can spread into a very large slick, providing an experimental area that should be large enough to influence the surface wave system. We will be implicitly referring to this type of slicks in the subsequent sections.

The expression of the propagation velocity of small amplitude waves in deep water U, is given by (Lamb,1932):

$$U^2 = \frac{g\lambda}{2\pi} + \frac{2\pi\gamma}{\rho\lambda} \qquad (4.2)$$

where g, ρ and λ are respectively the acceleration due to gravity, density of water and wavelength of surface wave. The quantity γ represents the surface tension.

For high frequency gravity-capillary waves (small λ), the first term in eq 4.2 becomes small compared to the second term. It becomes clear from the equation that as the presence of a surface film on the water reduces the surface tension the propagation speed of the waves of small wavelength will be reduced. However, a reduction in the surface tension is not the major contributor to the wave damping process. In general, as a wave propagates the surface tends to contract at a wave crest and expand at a trough (Lamb,1932). Under the presence of a surface film, these contractions and extensions will produce differentials in the surface concentration which in turn create surface tension gradients. These local variations in surface tension will act as an elasticity which tend to oppose the wave motion (Lucassen-Reynders and Lucassen,1969). Viscous properties of soluble surface films have also been found to play an important part in the wave damping process (Davies and Vose,1965) so that the rate of viscous energy dissipation increases as a result of the alternating drag on the liquid caused by the variations in the surface tension.

Theoretically, a second type of damping can take place when surface tension gradients are present. A viscoelastic surface can accommodate two different wave modes: transverse waves, commonly known as gravity-capillary waves, and longitudinal waves (horizontal particle motion) or Marangoni waves, named after the physicist Carlo Marangoni. Marangoni waves are excited by tangential forces associated with surface tension gradients due

to the local contractions and expansions of the surface film. They are heavily damped due to the occurrence of strong velocity gradients within the surface boundary which leads to enhanced viscous dissipation - in a purely elastic film, the Marangoni wave amplitude decreases to about 7% of its original value over a distance of 1 wavelength. This has prevented early experimental detection of these waves which was only achieved in 1968 by Lucassen. The surface waves experience maximum damping when Marangoni waves are in (linear) resonance with surface waves, that is when the wave number of the surface waves at a given frequency is equal to that of the Marangoni waves. For many viscoelastic films, this maximum damping is located in the short gravity wave region (around 5Hz).

4.1.3. Effect on the surface wave spectrum

A noticeable effect of a slick on the sea surface is the relative disappearance of the visible ripples. This reduction in the surface roughness has a direct effect on the air-sea exchange processes such as momentum, gas exchange and heat. Most experimental studies (laboratory and open sea) agree that high frequency ($f \geq 2Hz$ or $L \leq 40cm$) waves are the most affected by a surface film (Yermakov et al.,1985; Cini & Lombardini,1981; Cini et al.,1983; Huhnerfuss et al,1981). However, it was also found that not only high frequency waves were affected by the film, but a significant damping of the longer waves was also observed (Barger et al,1970; Mallinger and Mickelson,1973; Huhnerfuss et al,1983).

Attempts by divers authors to assess the extent to which the low frequency components of the wave spectrum were affected by the presence of the film resulted in considerable results appearing in the literature. Although they all agree to the fact that only certain parts of the spectrum are noticeably affected

by the film, they fail to agree on the segments of the spectrum where maximum wave damping takes place. This can be partly explained by the multitude of techniques employed to achieve the measurements, the nature of the oil products used in their experiments, and the physical conditions prevailing at the time. Mallinger and Mickelson's observations in the open sea using airborne laser-wave profilometer showed a considerable reduction (54%) of the surface wave energy for frequencies between 0.3 and 0.6Hz (L= 17.3 to 4.3m). Limitations in their instruments could not provide measurements at higher frequencies. Huhnerfuss et al. made their measurements from a tower based wave measuring station. They dispersed small frozen masses of oleyl alcohol from a helicopter and measured the surface wave spectrum as the slick drifted by the measuring platform under the influence of tidal currents and the wind. Their measurements showed that wave frequencies between 0.5 and 0.7Hz (6.2 to 3.2m) were only slightly affected by the presence of the film and that significant wave attenuation was only noticed for frequencies above 0.7Hz. Barger et al. found a significant drop in the energy of wave components at frequencies of 0.4 to 1Hz (9.8 to 1.6m). Their artificial slick of oleyl alcohol was about 1 X 0.5km in size.

Viscous dissipation alone can not explain damping of large waves over length scales of a few wavelengths. Two possible processes are involved for the damping of long waves :

i/ As a consequence of the surface smoothing effect of the oil the wind velocity profile near the surface will change (Barger et al,1970) thus influencing the energy input from wind to the wave system.

ii/ Suppression of capillary waves also modifies the nonlinear wave-wave interaction of the spectral components. The significant depression of the energy spectral form in the short

wavelength gravity-capillary components of the surface waves will be expected to affect the wave system which will respond to such deviations from equilibrium with an increase in the energy transfer rate towards higher wave numbers. That is how energy would be expected to be drained away from the low frequency waves, thus leading to the damping of longer water waves (Alpers and Huhnerfuss,1989).

The other process induced by the presence of an oil film is the reduction in the frequency of wave breaking. The suppression of short waves riding on the back of on longer waves means that less energy is transferred from the wind to the wave system. It is therefore possible that the frequency of breaking might be reduced due to the fact that less energy will be injected into the waves when the surface gets smoother. Ariel's (cf Bortkoskii,1988) observations of the effect of diesel oil slicks on the sea state have shown that inside a slick the rate of breaking is reduced by a factor of two thirds. The observations were made under moderate wind conditions (6.5 to 10m/s). The size of the slick was relatively small covering an area of about 6000m^2 with the main axis about 80 to 150m along the wind direction. Barger et al.'s (1970) field work showed a total absence of capillary waves and breaking waves in an oleyl alcohol slick under winds of around 7.5m/s (at 10m). However, considering that the areas covered by the slick in the last two experiments mentioned were relatively small, no quantitative results can be drawn from the observations. The authors failed to mention by what means the breaking events were detected. If, as the papers suggest, this was carried out visually from a ship, there may be some doubt as to how well breaking waves were identified.

4.2. REMOTE SENSING OF OIL SLICKS AT SEA

Remote sensing of oil films at the sea surface is important in that it can provide useful information both for slick detection operations, and for the study of some ocean properties. Remote sensing of oil films provides an insight into how oil slicks evolve in time and about their spacial distribution. Bearing in mind the similarities between em- and acoustic-ocean waves interactions discussed in § 2.4, we will discuss hereafter experimental observations of the two types of interactions and assess the similarities and differences in their general behaviour.

4.2.1. Radar sea surface scattering : theoretical background.

A wave incident upon a rough- surface boundary is partly reflected in the specular direction and partly scattered in all directions. When transmitter and receiver are located at the same position, the backscattered component of the scattered energy is the relevant part of the return.

Ulaby et al (1982) explains how a smooth surface would reflect all the incident radiation onto the specular direction. As the surface becomes rougher, energy reflected in the specular direction gets deviated along other directions, and thus backscattering increases. Backscattering is fundamentally influenced by the roughness scale of the surface. However, the same surface may be rough for some wavelength and smooth for others; or for the same wavelength it may be either rough or smooth for different angles of incidence. A parameter representative of the surface roughness was given by Rayleigh as

$$R = 4\pi \, h \sin\theta / \lambda$$

where h is the roughness height above (or below) the mean surface level, θ is the angle of incidence, and λ is the incident wavelength.

A slightly rough surface would be defined as a surface with a Rayleigh parameter small compared to unity, whereas if $R > 1$ the surface is considered rough.

1. Near vertical incidence (90°-70°)

At near vertical incidence, sea surface backscatter is dominated by specular reflection. This is the range wherein the Gaussian distribution of wave slopes has a significant population of facets oriented perpendicularly to the incident wave. Since the surface wave facets have a large radius of curvature compared to the wavelength of the incident wave, they will act as small mirrors and reflect energy in the specular plan according to optics principles. This process is dominated by the long surface waves which modulate the inclination of the reflecting facets. Specular reflection is a dominant process at angles above 60° from the horizontal and is the process by which a maximum of the incident energy is reflected at the surface.

2. Intermediate to low grazing incidence

At intermediate angles (30°-60°), the probability of finding waves with large radii of curvature perpendicularly oriented to the incident rays decreases. At these angles, the dominant process is taken over by scattering from the surface roughness comparable in size to the radiation wavelength.

Bragg scattering

For this range of incidence angles (60°-20°), Bragg scattering is thought to be the dominant scattering mechanism. The term "Bragg scattering" is also refered to as selective grating mechanism or Crombie mechanism. The theory behind it is a result of the Small Perturbation Method. It was first developed by Rayleigh (1945) for acoustic scattering from walls, and extended to random surfaces by Rice (1951). Bragg scattering was shown

to be a first order effect for slight roughness, valid only under the assumptions that

i/ The rms waveheight of the surface roughness is small compared to the radiation wavelength, i.e. $h < \lambda / 4\pi \sin\theta$

ii/ The local surface wave slope is small.

When slightly larger wave amplitudes are allowed, second-order scattering effects become significant.

Under these conditions, and according to first order em scattering perturbation theory, the backscatter cross-section per unit area of the ocean for an incident wave propagating in the (x,z) plane is (Wright,1968)

$$\sigma_o(\theta,k) = 4\pi\, k^4 \cos^4\theta\ g(\theta)^2\ W(2k \sin\theta,0)\ , \qquad (4.3)$$

where k is the radar wavenumber, $W(k_x,k_y)$ is the two dimensional wave number spectral density of the surface roughness, $g(\theta)$ is the first order scattering coefficient and is dependant upon the polarization mode and the relative dielectric constant of the surface, and 4π is a normalization factor.

In this model it appears that only those surface waves of wave number $2k \sin\theta$ (Bragg resonance condition), travelling in the x-direction (parallel to the line of sight) contribute to the backscatter process. The nth order length of the Bragg scatterers that contribute to the process is given by

$$L_n = n\lambda / 2 \sin\theta \qquad (4.4)$$

where $\lambda = 2\pi/k$.

Although it is largely accepted that Bragg scattering is the dominant scattering process at intermediate angles, assumption i is more likely to hold for long waves since they are less steep

than capillary-short gravity waves. Thus, Bragg scattering though applicable for HF radiowave (λ = 10-100m) echo will not necessarily be valid for VHF radar where centimetre-scale wavelengths are involved. This will certainly be the case with high frequency acoustic scattering where wavelengths are of the order of a millimetre. In addition, assumption ii/ is not always valid.

Experimental evidence of Bragg scattering in the open sea, first observed by Crombie in 1955, is based on the observation of the Doppler shift of the scattered signal which corresponds to the expected phase velocity of the Bragg waves.

Composite-surface theory

In the ocean, the validity of Bragg scattering as the dominant scattering mechanism was until recently assumed at angles between 60° and 20°. Other effects such as shadowing, diffraction and wave breaking, which are excluded from the initial assumptions, were suspected to become more important at lower incidence angles.

To include the shadowing and tilting effects of short waves by the longer waves, Wright(1968) and Bass et al (1968)

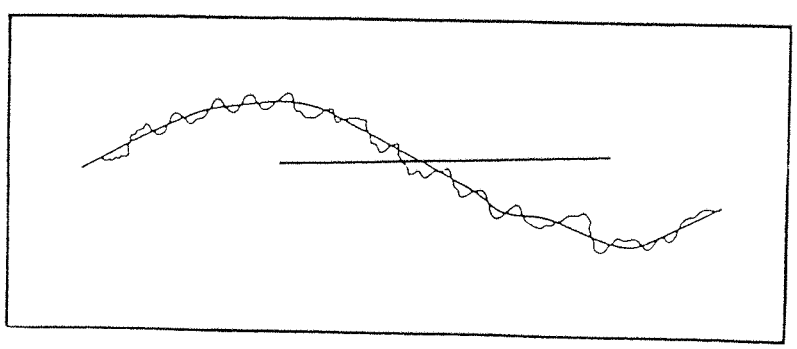

Fig 4.2 Surface can be represented as a combination of small scale roughness over-riding long waves.

introduced a composite roughness surface model (two scale model) based on the assumption that the sea surface wave spectrum can be divided into two wave number regimes: a large scale and a small scale surface waves system. The large scale waves consist of waves whose wavelength is long compared to that of the incident radiation. Superimposed on the large scale surface is a smaller wave structure composed of short wavelength gravity and capillary waves (Figure 4.2).

The model is consistent with the scattering theory and measurements because the small scale roughness is chosen to include the portion of the spectrum that may be resonant for a given radar wavelength, whereas the longer waves are chosen to provide a uniform tilting of the scattering surface. This new model has since been widely used and found some success and was particularly useful at predicting low grazing backscatter (Guinard et al,1971).

Other theories

The reader is referred to an excellent review about the evolution of the sea surface scattering theories up to 1971 by Fortuin.

We can mention the one that is based on the Kirchoff approximation, reviewed in Apel (1987). The Kirchoff approximation is the first order result of a first principle scattering theory. It is not limited to small amplitudes as is Bragg scattering. It includes the specular reflection range but, like Bragg theory, is not valid at grazing incidence.

Discussion

It would thus appear that the following may be said about Bragg theory and its application into high frequency acoustic sea surface scattering:

1.It works in the ocean for wavelengths greater than a few metres. Thus making assumption ii/ valid only for very short waves, except in conditions of exceptional calm.

2.It is not applicable for incidence angles less than 20°, or at small wavelengths for incidence angles greater than 60°.

For these reasons, it would seem that although useful as an initial aid, Bragg scattering is rarely a sufficiently accurate theory if one wishes to make quantitative deductions.

3. Sea surface scattering cross section measured by microwave and acoustics :

Both acoustic and em data collected at sea show the same behaviour of the sea surface backscatter at angles between 90° (vertical) and 25°-30°. Figure 4.3 shows an example of the variations of X-band horizontally polarized radar and sonar sea surface backscatter with incidence angle. The radar data (wind speed coded) have been collected by Guinard et al (1971) under winds of 2.5 to 24 m/s. These data points are the median values of the statistical distribution of the backscatter cross-section at fixed angles of incidence. The airborne radar (8.9GHz) was pointing upwind and had a spacial resolution of 80m. The continuous curves are best fits for acoustic data collected by Urick (1956) at three different wind speeds (2.5, 5 and 7.5m/s). Urick does not mention the acoustic frequency but it is thought to be high (a few tens of kHz). In this case the em and the acoustic wavelength would be of the same order of magnitude. Urick also fails to mention the line of sight with regard to wind direction.

It can be seen from this figure that at near vertical incidence both radar and acoustic backscatter are at a maximum. They both show a decrease of this maximum with increasing wind.

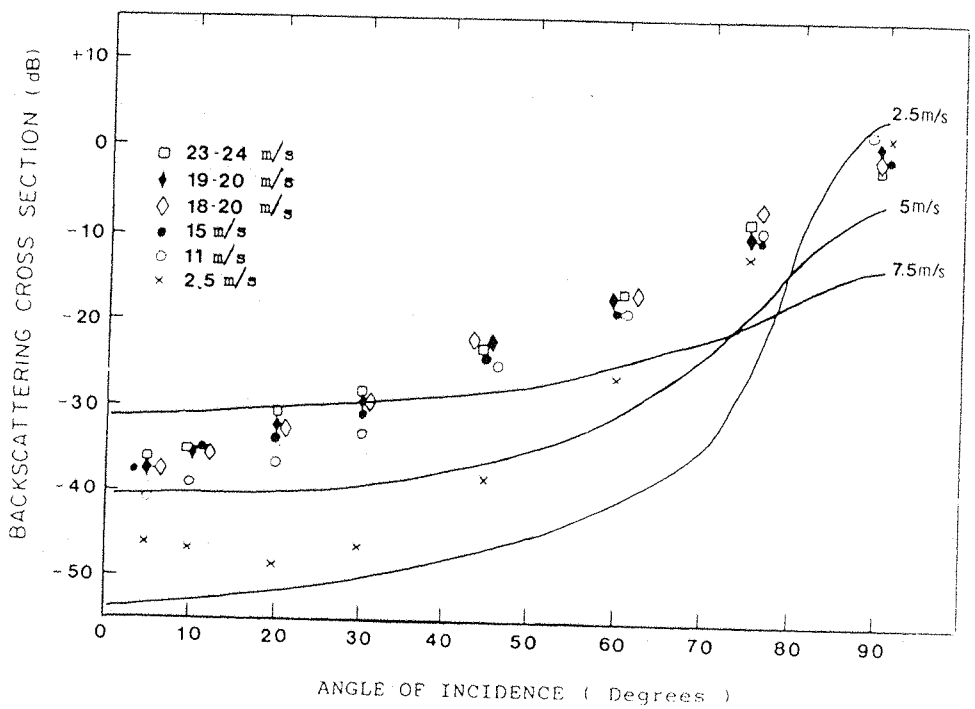

Fig 4.3 Backscatter cross section from the sea surface for radar (coded data) and sonar (curves). Radar data were collected by Guinard et al.(1971) at various wind speeds with the radar (8.9GHz) pointing upwind. Sonar curves are best fits for data collected by Urick (1956) at the wind speeds indicated.

At vertical incidence (90°), acoustic backscatter decreases by an average of 18dB for the observed range of speeds (2.5 -7m/s) whereas the radar data drops by about 6dB for a much larger range. This can partly be explained by the difference in the averaging procedures (resolution) which is not mentioned for the acoustic data.

Nevertheless, if backscatter in this region is due to specular reflection from surface waves facets, this is the general trend that would be expected from the data owing to the fact that as wind speed increases, the surface will tend to develop short ripples. As a consequence, the density of waves having a large radius of curvature (compared to the incident wavelength) is more important at lower wind speeds.

For a given wind condition and as we move away from vertical down to 60°-70° incidence, backscatter decreases steeply. This feature is characteristic both to the radar and the acoustic data.

In the intermediate range (60°-70° to 25°-30°), the slope of the fitted curves becomes less important. At fixed incidence, the acoustic return level is now seen to be increasing with increasing wind speed. This is also a direct result of the effect of wind on the surface roughness. As wind increases, the density of capillary waves, whose restoring force is wind stress, increases.

At low grazing angles (below 25°) radar and acoustic backscatter differs quite dramatically. The acoustic data reaches a steady level which increases with wind speed whereas the em data shows a drop of 5 to 8dB between 25°-30° and 0°. At these incidence angles, large areas of the sea surface, and particularly those covered by small scale roughness, are concealed by the shadowing effects of the large waves so that the rays can no longer view the whole of the surface. This is

thought to be the main cause of the observed abrupt depression of the radar data.

Shadowing effects should also affect acoustic backscatter. However, as the sea surface is not symmetrical, other processes have to be taken into account underwater. Among these is the generation, under moderate to high winds, of subsurface micro bubbles by wave breaking. The higher the wind is and the more bubbles are produced (Thorpe,1982) and the more intense backscatter becomes. Under wind speed greater than 7.5m/s, Thorpe (1983) found that bubbles were horizontally organized into an almost continuous layer, and that under lower wind conditions the bubble would appear as distinct clouds of bubbles produced in the proximity of the breakers. The effect of these bubbles (appearing in any of these two forms) would be expected to be significant at any incidence angle. As a consequence, backscatter should be expected to increase with wind speed. The only region where this has not been observed is at near vertical incidence where scattering is dominated by specular reflection.

4.2.2. Microwave remote sensing of oil slicks at sea: experimental observations.

Scattering of electromagnetic waves in the visible (Cox and Munk,1954) and microwave (Table 4.1) spectral bands is influenced by the presence of oil layers. Many large scale experiments have contributed to a better understanding of radar backscatter from contaminated surfaces (JONSWAP75, MARSEN79). Microwave radar frequencies are usually used because their range of wavelengths is similar to the length scales of the surface roughness affected by the oil.

Table 4.1 is a summary of observations made between 1973 and 1986 of artificially produced oil slicks, using radars operating in the Ku-band and C-band (see Table 4.2 for frequencies and

Author (year)	Frequency of sensor and Polarization	Viewing angle range from vertical	Type of oil	Relative Reduction in backscatter cross-section	Maximum damping (angle)	Wind conditions
Krishen (1973)	13.3GHz (2.25cm) VV - polarized	20° - 50°	crude	5 - 10dB	undefined	2.5-9.0 m/s
Huhnerfuss et al (1978)	13.9GHz (2.16cm) VV - polarized	47°	oleyl alcohol	7.3dB	single incident angle	3.5-4.4 m/s
Johnson & Croswell (1982)	13.9GHz Doppler scatterometer	20° - 60°	Larosa (crude)	8 - 11dB	30° - 35°	5 - 7 m/s
			Murban (crude)	9 - 14dB		
Singh et al (1986)	13.3GHz HH - polarized	20° - 60°	Alberta Sweet Mixed	8 - 12dB	30° - 35°	3 - 6 m/s
				7 - 8dB		10 - 14 m/s
	5.7GHz (5.26cm) HH - polarized		Blend (crude)	10 - 13dB	40° - 45°	3 - 6 m/s
				8 - 9dB		10 - 14 m/s

Table 4.1 Summary of oil slick observations using microwave sensors.

wavelengths). Since the magnitude of the physical effects of the slick on the surface roughness is dependant upon the chemical nature of the slick, its thickness, and the concentration of the surface active agents, the results are only consistent relative to the experimental conditions at which they were observed. However, the ability of the microwave sensor to detect the oil slick, in all four examples, proves that slick detection is possible by microwave radars. It is the smoothing of the surface that translates to the radar sensor as a reduction in the surface backscatter strength of the signal. All of the sensors were operating at oblique incidence angle (20°-70°). This is the angular range where Bragg scattering is thought to be the dominant scattering process at the sea surface (eq 4.3). Damping of capillary waves which are the major contributors of

Designation	Frequency	Central Wavelength cm.
L band	1 - 2 GHz	20
S	2 - 4 GHz	10
C	4 - 8 GHz	5
X	8 - 12.5 GHz	3
Ku	12.5 - 18 GHz	1

Table 4.2.

Bragg scattering will therefore have a direct effect on the scattering cross section of the sea surface at these angles. The angle at which Singh et al. observed a maximum reduction in the radar signal is in good agreement with the previous measurements of Johnson and Croswell (30°-35°) for the Ku-band case. For

first order Bragg scattering, eq 4.4 yields to surface waves of wavelengths between 1.8cm and 2.25cm as the waves that are the most affected by the oil film.

4.2.3. Spatial modulation of the surface roughness in a slick

One question relating the effects of the contaminated sea surface to the interpretation of remotely sensed microwave signatures is the thickness gradient of the film across the slick, and whether or not these thickness variations induce spacial variations of the capillary waves density distribution, and its subsequent effect on radar backscatter strength.

Capillary waves can be damped and restored over relatively short fetches (a few wavelengths) compared to longer waves. Yermakov et al. (1986) for instance observed a strong damping of capillary waves in an olein (technical grade oleic) and vegetable oil slick of small dimension not exceeding 10m along the wind direction. There is a critical thickness (Linde et al.,1984) and concentration of surface active material (Tailby et al,1970) at which the damping rate is greatest. Further increase in thickness decreases damping and ripples may again begin to appear. Davies (1962) suggests that this phenomenon is connected to the presence of two interfacial surfaces along which propagate two surface waves of different wavelengths. The closeness of the two surfaces facilitates the process of energy exchange carried by the waves and leads to a change in the character of the flow. An increase of the interfacial distance diminishes these effects and can possibly reduce the damping process.

The existence of this damping peak suggests that spacial variations of the surface wave energy spectrum (especially high frequency waves) might be present in a slick. These gradients will be more pronounced in slicks made of oil substances of

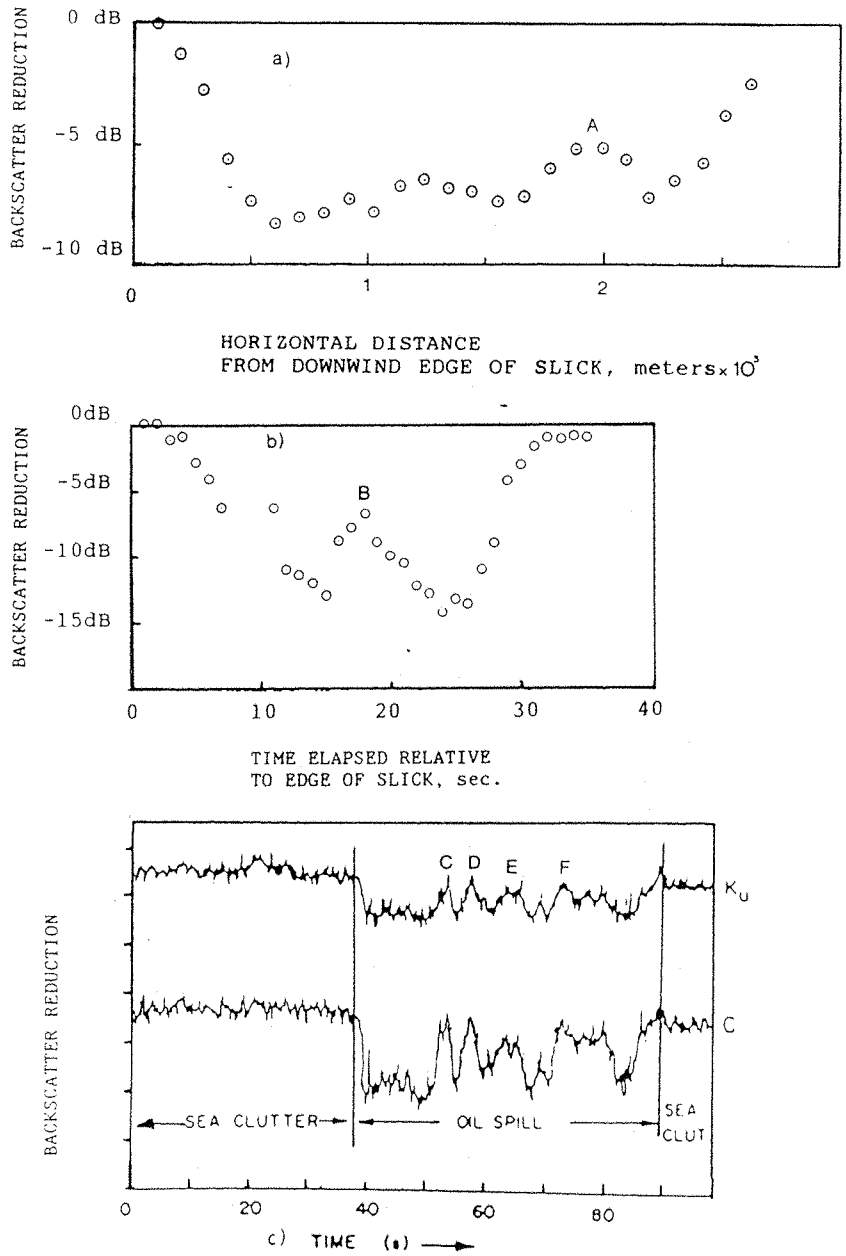

Fig 4.4 Depression of radar backscatter signal across an oil-covered surface:
a) & b) at 13.9GHz (Johnson & Croswell,1982) averaged over a 30°-35° incidence angle bin. Altitude is 1500m (a) and 450m (b).
c) at 13.3GHz (Ku) and 5.7GHz (C) (Singh et al,1986). The sensor were inclined by 45° and the plane was flying across the long dimension of the spill (3.5km). The vertical tick marks are 10dB apart.
For details on weather conditions, oil types etc refer to Table 4.1.

low concentration of surface active agents - as in some heavy crude oils. This effect is well illustrated in Figure 4.4 which shows Johnson and Croswell and Singh et al's backscatter reduction across an oil slick using C- and Ku-band airborne microwave sensors. The circles in Figures 4.4a & b (Johnson and Croswell) are data points of constant value each averaged over a specific distance (≈100m along the airplane's track) across a crude oil slick. Figure 4.4c also shows the backscatter reduction across a crude oil slick but here the data sampling rate is much higher than on the two previous figures.

All three figures show a reduction in the backscatter signal of the order of 10dB near the edges of the slick. This reduction is quite sharp and follows a uniform return signal from the areas outside the slick (4.4c). Inside the slick, backscatter is on average uniform and fluctuates around a level which is in general smaller than outside the slick edges. There are however some regions within the slick (see for instance regions marked A,B,C,D,E and F on the figure) which are different from the overall backscatter in the slick. These areas show unexpected increases of the backscatter of as much as 10dB in some cases (4.4c). These regions are thought to be areas in the slick where the film has been disrupted, or as suggested earlier these could be areas of very thick oil where ripples begin to appear.

4.2.4. Effect of oil on the sound speed profile

The presence of an oil film on the sea surface can affect the propagation of electromagnetic waves incident on the sea surface by altering the dielectric properties of the reflecting air/water interface (Wright,1968; Valenzuela,1978). The magnitude of the dielectric effect is primarily a function of film thickness. Significant variations can be expected only when

the surface film thickness exceeds 1mm, but since most experimental films are monomolecular or very thin (an average thickness of a few tens to a few hundred microns), there are no significant changes in the dielectric properties of the surface.

By analogy, sound propagation can also be affected by the presence of dissolved oil in the upper layer. This water/oil mixture, sustained by continuous vertical mixing processes, can change the sound speed profile close to the surface and hence affect sound propagation. Very few data of quantitative measurements of dissolved oil below the surface following an oil spill are available. During their numerous experiments in the North Sea, the Warren Spring Laboratory have taken samples of water at various depths in order to estimate the concentration and depth penetration of the oil in the water (this is particularly important with regard to the environmental effects of oil spillage, and whether the use of chemical dispersants increases or decreases the harmful effects, WSL Technical Report). The average concentrations were found to be very small in the first 5m from the surface and even lower below. In most of their experiments (private communication), including the one we took part in (see next chapter), the concentrations varied between 10 and a few hundred ppb. The WSL's observations also showed that most of the oil appeared in a dissolved condition.

Using the simple mixture theory (Urick,1975), the speed of sound c in a mixture of two liquids (oil and water) is given by:

$$c = c_o \left(\frac{1}{1 + \beta \, K_w/K_o} \right)^{1/2} \qquad (4.5)$$

where β is the concentration of oil in the water, K the compressibility coefficient for water (w) and oil (o) and c_o the speed of sound in clean water.

Since $\beta << 1$ and that K_o and K_w are of comparable magnitude, we can assume that the dissolved oil has no significant effect on the speed of sound.

Summary

The main conclusions to be drawn from this chapter and which will be of importance when we come to analyze our observations are

i/ We expect specular reflection to dominate the acoustic scattering process at near vertical incidence. Between 90° and 65°-70° and for a given wind speed, backscatter should fall sharply. The amount by which backscatter falls depends on the wind conditions. At near vertical incidence, backscatter is expected to increase with decreasing wind speed. Between 60° and 25°, backscatter should be influenced by the small scale roughness and should have a strong wind dependence. At the lower grazing angles, other processes come into account. Among these processes is scattering from bubble clouds. Their contribution to the mean scattering cross section is thought to extend from 60°-65° to very low grazing. However, this contribution will be most significant at low grazing angles.

ii/ Ku-band microwave observations of oil slicks show a depression in the scattering cross section of 8-15dB inside a slick (Figure 4.4). We believe this is associated with the damping of capillary - high frequency gravity waves by the surface film.

THE OIL SLICK EXPERIMENT

5.1.MAIN OBJECTIVES

The main objective of this experiment was to measure the relative acoustic backscatter from the sea surface as a function of incidence angle for both contaminated and clean surface, and to compare a number of signatures under both surface conditions.

The main questions that were to be answered following these observations were:

i/ Does an oil-slick affect the level of high frequency acoustic backscatter ?

ii/ If such system were to be used for oil slick detection, what would be the optimum scanning angle ?

iii/ Are similarities to be found between sonar and radar scattering from an oil covered surface?

In order to provide the answers (given later in § 6.4), an experiment involving the observation of an oil slick in the open sea, using a high frequency (248kHz) side scan sonar was conducted.

The comparison between the two types of surfaces (clean and slick) under the same conditions will provide a measure of the reduction in backscatter due to the surface-smoothing effect of the oil in the short gravity and capillary wave region. The range of wind speed (4.0m/s - 11.5m/s) enabled comparisons to be made at different winds typical of commonly encountered conditions.

5.2.EXPERIMENTAL DESCRIPTION

5.2.1.Experimental arrangements

On two different occasions in 1987 (May and July), experimental cruises were carried out in the southern North Sea, in collaboration with the *Institute of Oceanographic Sciences* and the *Warren Spring Laboratory* (WSL) aboard the research vessel *SEASPRING*.

The WSL is a pollution control laboratory whose aim is to monitor and control the excess of oil input to the sea from illegal sources (oil tank flushing,power stations, oil rigs etc) and to trace and predict the drift of slicks following oil spill incidents.

A small boat operating from Seaspring was collecting samples of sea water at different depths in and around the slick, and an airplane equiped with different sensors (see section 5.3.3) took part in the experiment aimed at monitoring the horizontal spreading and the vertical diffusion of the oil. The observations were made at a location centred around 52°10'N and 02°22'E (Figure 5.1), where WSL have permission to discharge oil for research purposes. Water depth in the area was around 45m.

Four types of oil substances were used to obtain the artificial slicks required for the experiments (see Table 5.1 for details).

For the crude oil slicks, the oil was discharged from the side of the ship a rate of about 500 l/min while the ship was

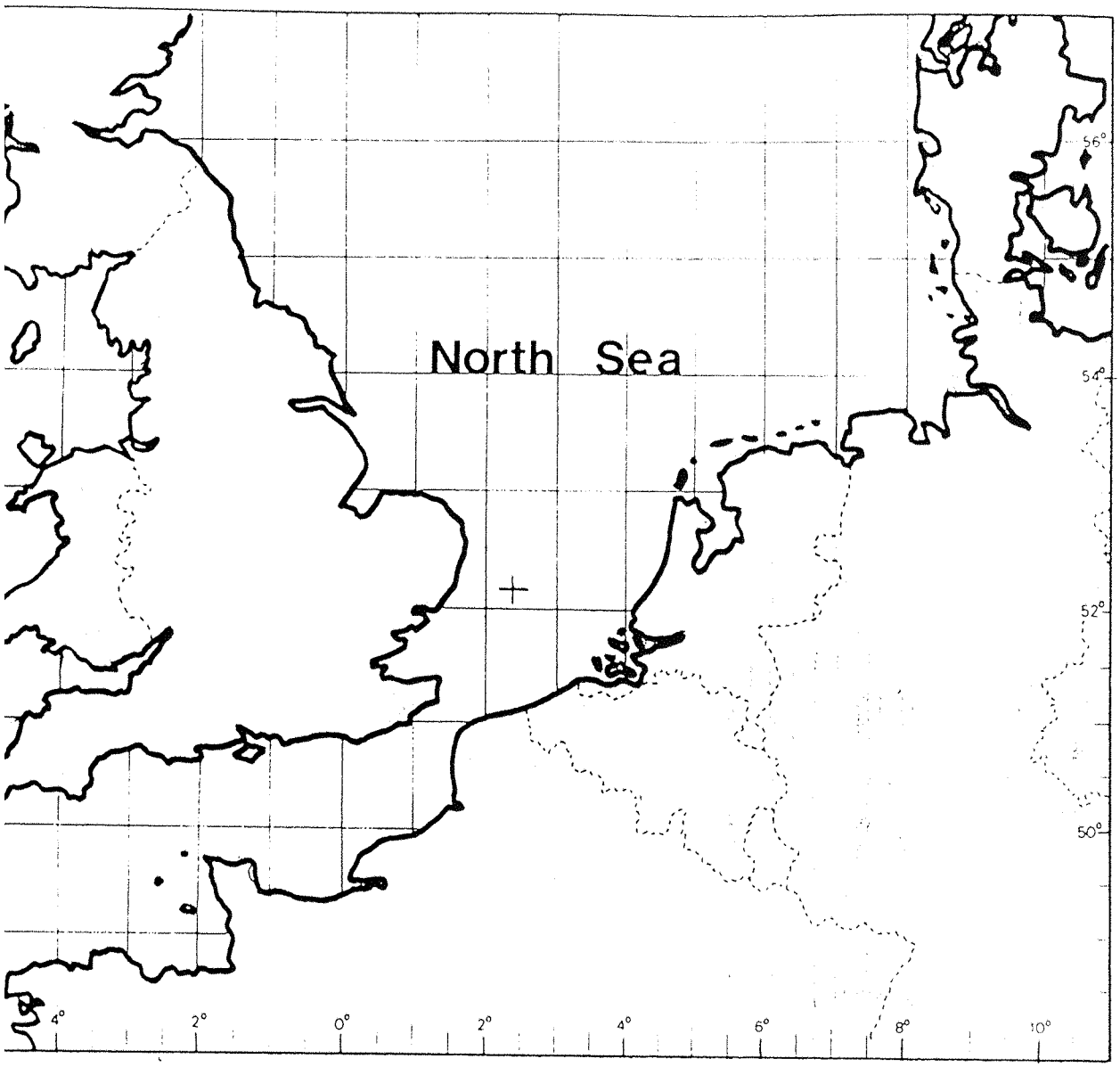

Fig 5.1 Experimental area.

Day	Oil	Oil vol. / Slick area	Oil properties	Wind speed	Corresp. sonogr. (Fig No)
06.05.87	1:1 mixture of medium fuel and diesel oil	2.5 m	$\eta \approx 50$ Cp $\rho \approx 900$ kg/m	7 - 9.5 m/s	6.6, 6.7
07.05.87	Oil + 2% disp.	0.4 m	no data	7 - 9.5 m/s	no sonogr.
07.07.87	Medium fuel oil	7.5 m	n. d.	7 - 11.5 m/s	6.4, 6.5
08.07.87	Oleyl alcohol	5km X 1.5km	n. d.	4 - 6 m/s	6.3

Table 5.1 Slicks characteristics

sailing in an increasing spiral pattern (Figure 5.2). The oleyl alcohol,used on the 08.08.87, was discharged after several parallel runs (8 in total) to make a carpet of about 5km X 1.5km. The discharge pattern of the oleyl slick can clearly be seen on the SARL image (Figure 5.3b) taken some 1 hour after the release operation ended. The figure shows the slick as a series of long stripes of about 5km.

The slicks generally followed the spreading pattern discussed in section 1.1 of chapter 3, stretching gradually along the wind direction. Figure 5.3 is a sequence of infrared (left) and ultraviolet (right) images of the slick taken on 07.07.87 from the airplane. It shows the evolution of the slick in the period 20min to 1 hour after the release of oil. The highlights on the IR images are the regions of the slick where oil is the thickest (Huhnerfuss et al.,1986). These regions lie in a spiral pattern similar to that followed by the ship during the release operation. Figures 5.3b and 5.3c show SLAR images of the same slick (Fig5.3c) on the same day and 25 hours later (Fig5.3b) combined with the oleyl alcohol slick. The general features (eg the shape) of the medium fuel oil slick are similar on both the IR/UV and the SLAR images, but on the radar images, the extent of the slick tended to be generally larger than on the IR/UV images. This suggests that radar waves are more sensible to very

small film thicknesses (as it is expected to be found on the edges of a slick).

Once the oil was discharged, several runs across the artificial slick, heading across the wind and up/downwind were

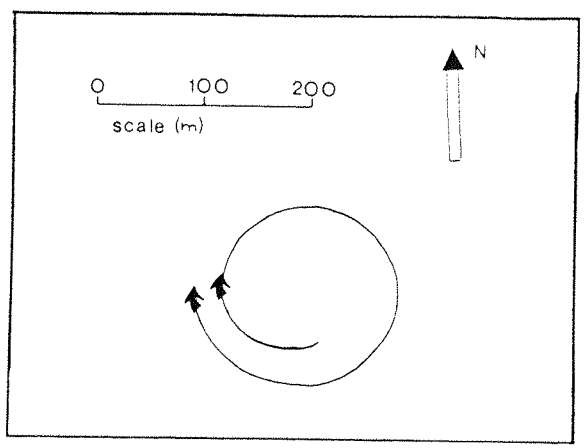

Fig 5.2 Spiral pattern followed by ship during oil release. Final diameter on July 7th was around 250m.

performed. Figure 5.4 is a sketch of the medium fuel oil slick derived from a combination of the features observed on the IR/UV images (Figure 5.3). The dark areas are the regions where oil is the thickest. The dotted areas are those detected by the IR sensor, while the total surface of the slick is derived from the UV image (see IR/UV image at 12:14 in Figure 5.3). The figure also shows the approximate courses of the towing vessel for the different runs performed across the slick on that particular day. Ideally the runs should have been performed with the vessel on the outside edges of the slick in order not to disrupt the film. However, this proved to be extremely difficult to achieve owing to the difficulty in identifying the slick edge with accuracy.

The towing speed, estimated relative to the water, was kept as steady as possible during each run so that backscatter from the surface would be uniformly distributed along the survey

a.

b.

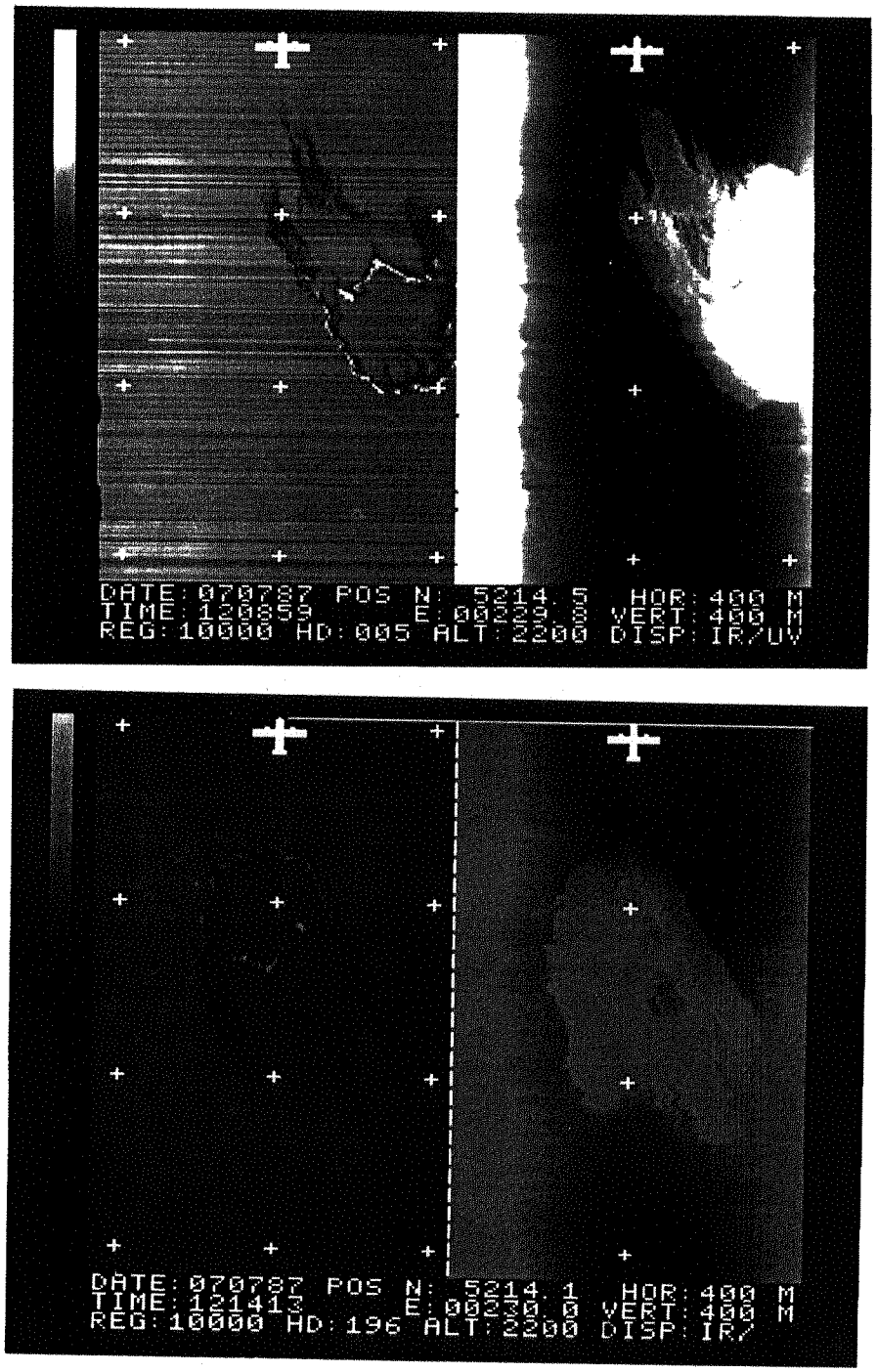

Fig 5.3 Series of IR (left) and UV (right) Line Scan images of the slick shown in chronological order, 20mn to 1hour after release.
Airplane position, heading, altitude together with time (add 1 Hour), and distance between crosses (Vert & Hor) are indicated.

c.

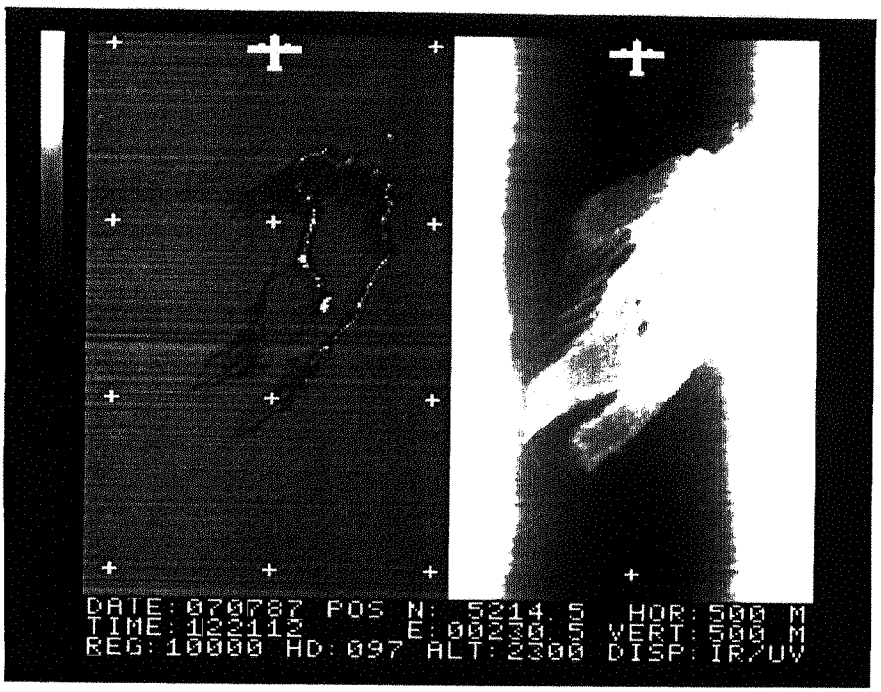
DATE:070787 POS N: 5214.5 HOR:500 M
TIME:122112 E:00230.5 VERT:500 M
REG:10000 HD:097 ALT:2300 DISP:IR/UV

d.

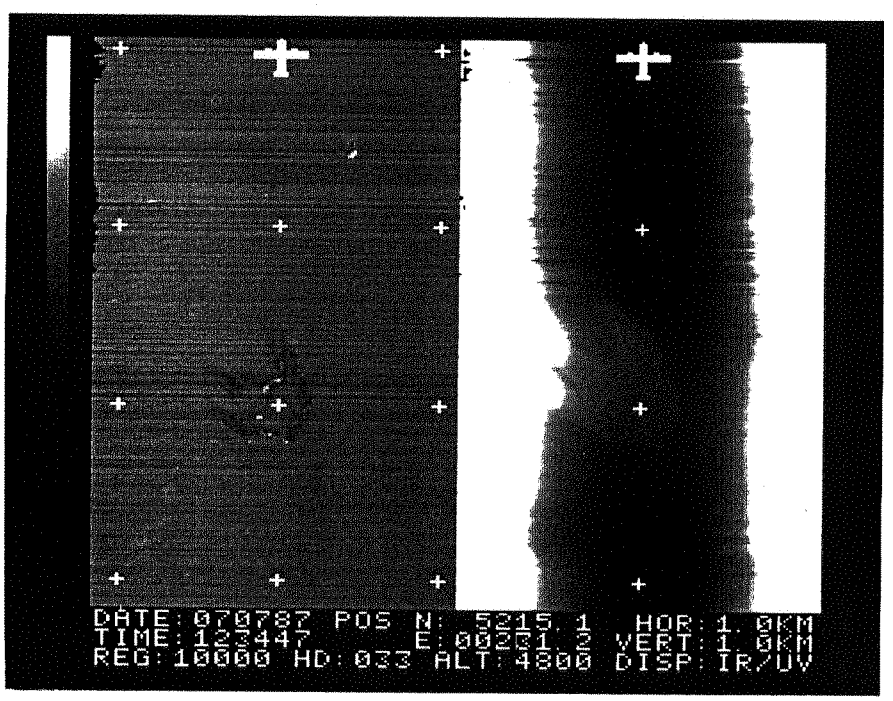
DATE:070787 POS N: 5215.1 HOR:1.0KM
TIME:123447 E:00231.2 VERT:1.0KM
REG:10000 HD:033 ALT:4800 DISP:IR/UV

e.

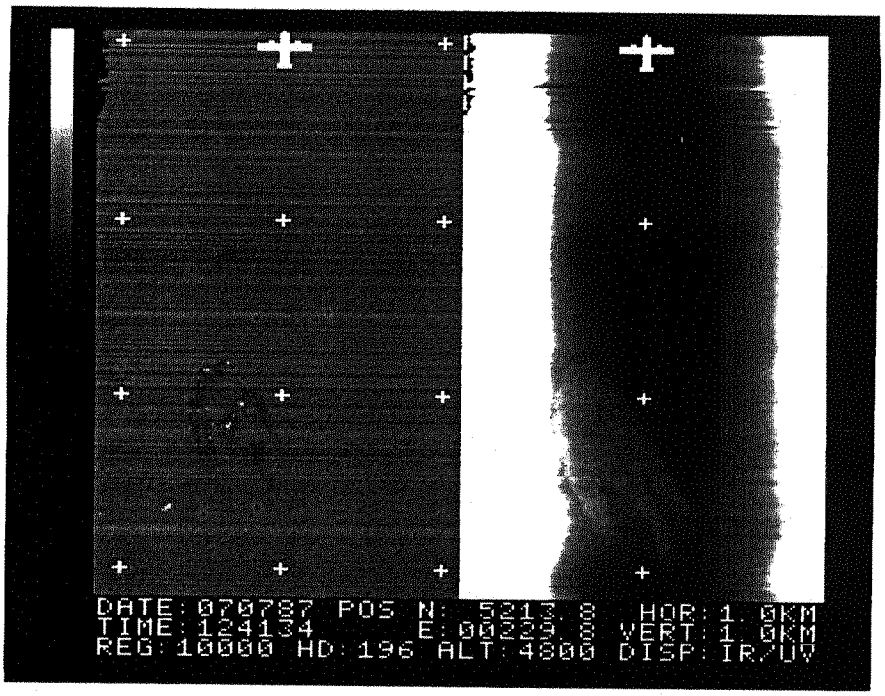
DATE:070787 POS N: 5213.8 HOR:1.0KM
TIME:124134 E:00229.8 VERT:1.0KM
REG:10000 HD:196 ALT:4800 DISP:IR/UV

f.

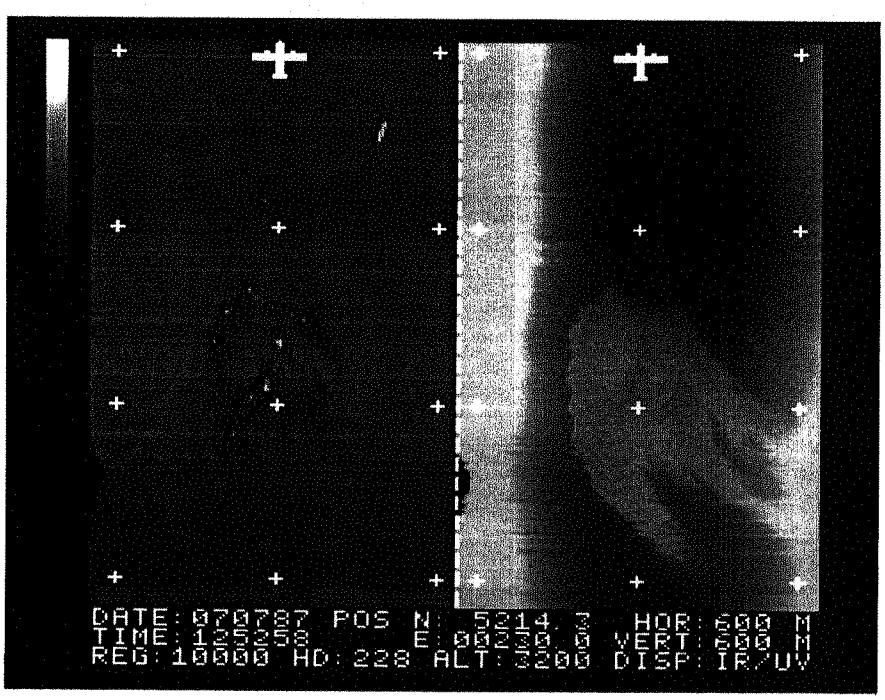
DATE:070787 POS N: 5214.3 HOR:600 M
TIME:125258 E:00230.0 VERT:600 M
REG:10000 HD:228 ALT:3200 DISP:IR/UV

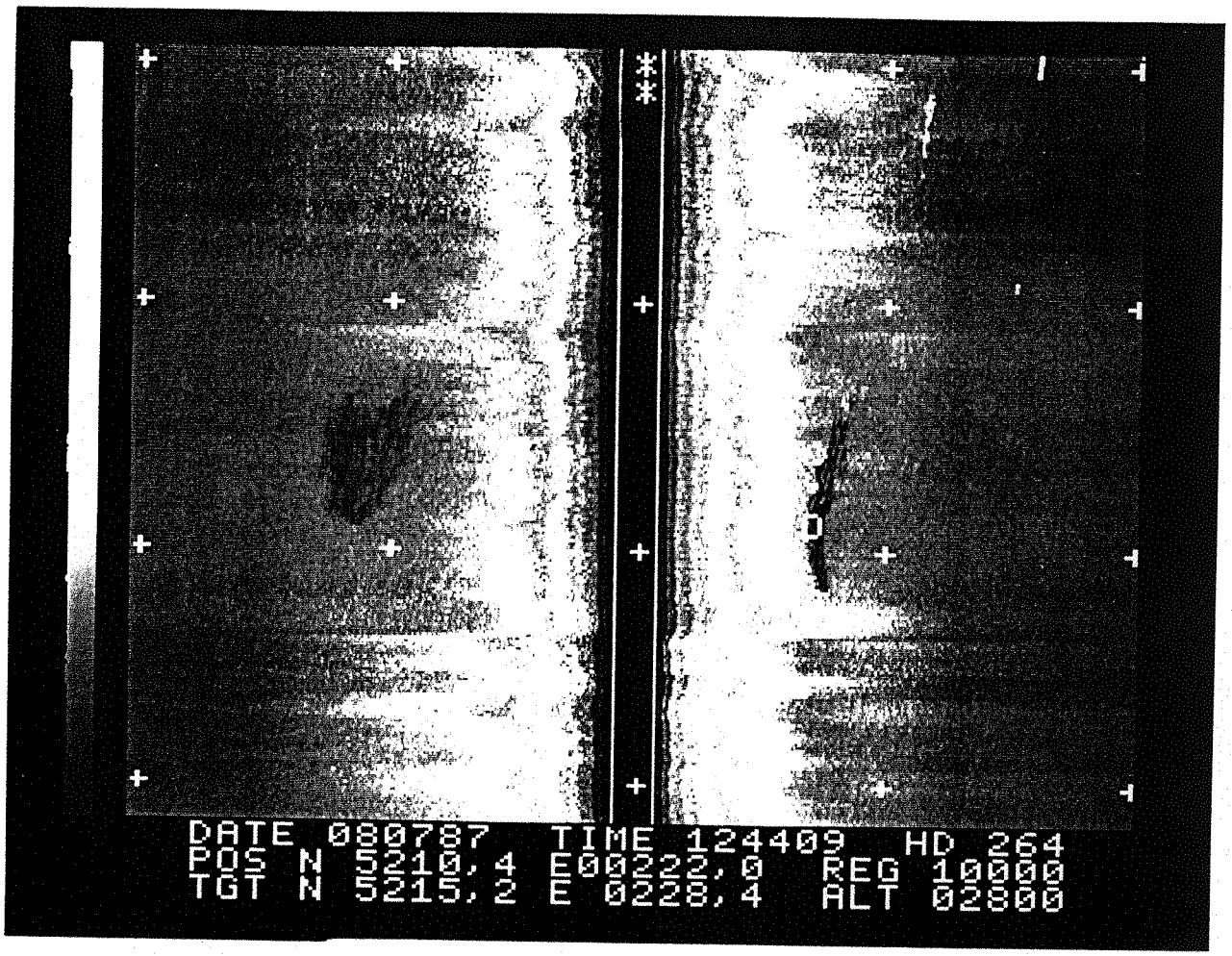

Fig 5.3b SLAR image of the fuel oil slick (left) 25 hours after release, and the oleyl alcohol slick (right) about 1 hour after release. The aircraft (heading 264°) is flying down the centre of the image. looking at both sides. The crosses are 10km apart.
Highlights show areas of intense backscatter, whereas dark areas indicate low backscatter.

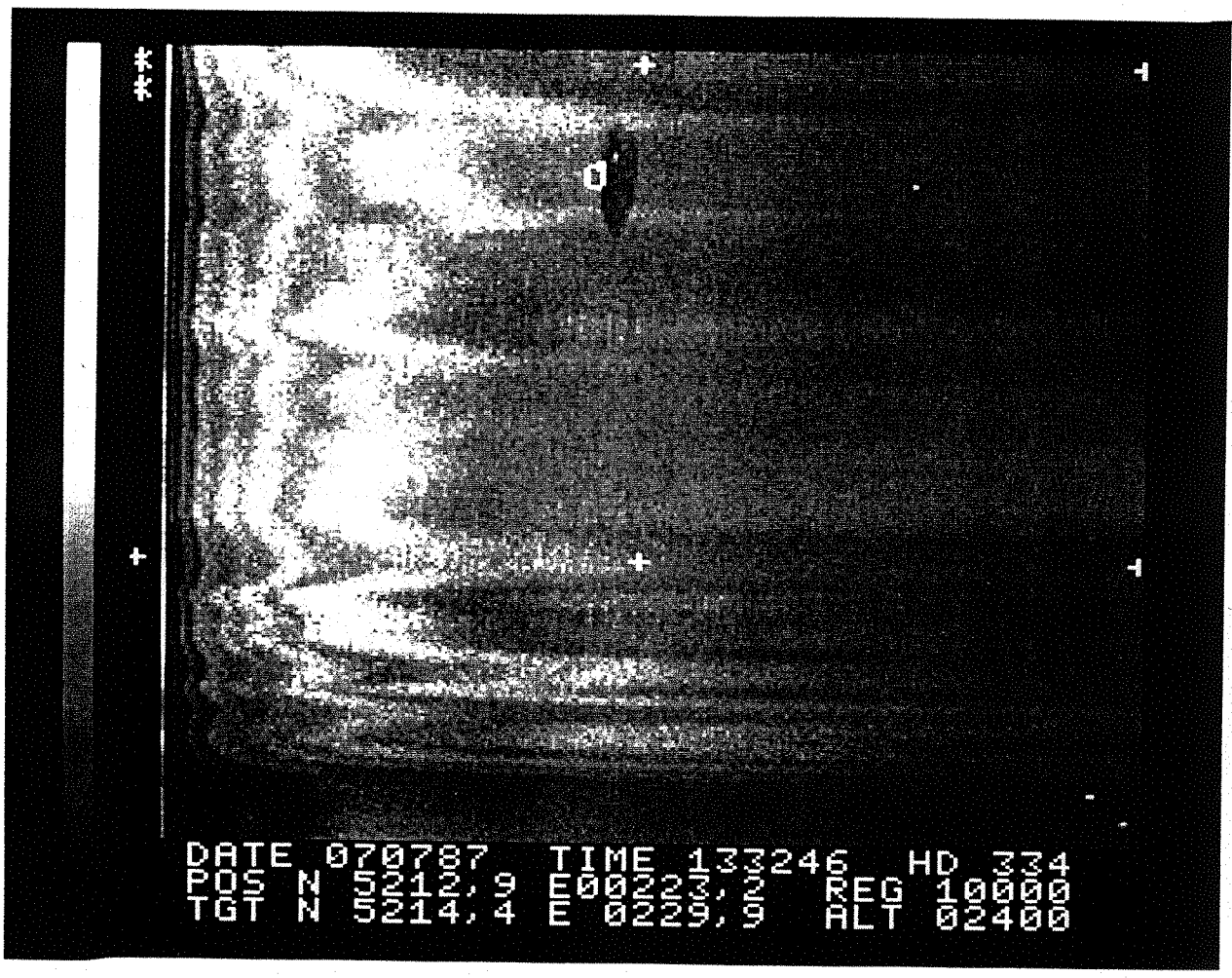

Fig 5.3c SLAR image of the fuel oil slick (07.07.87) about 1 hour 40min after release. The aircraft is flying along the left hand edge of the image, heading 334°. The crosses are 10km apart. At 0 is the reflection from the research vessel stationed on the edge of the slick.

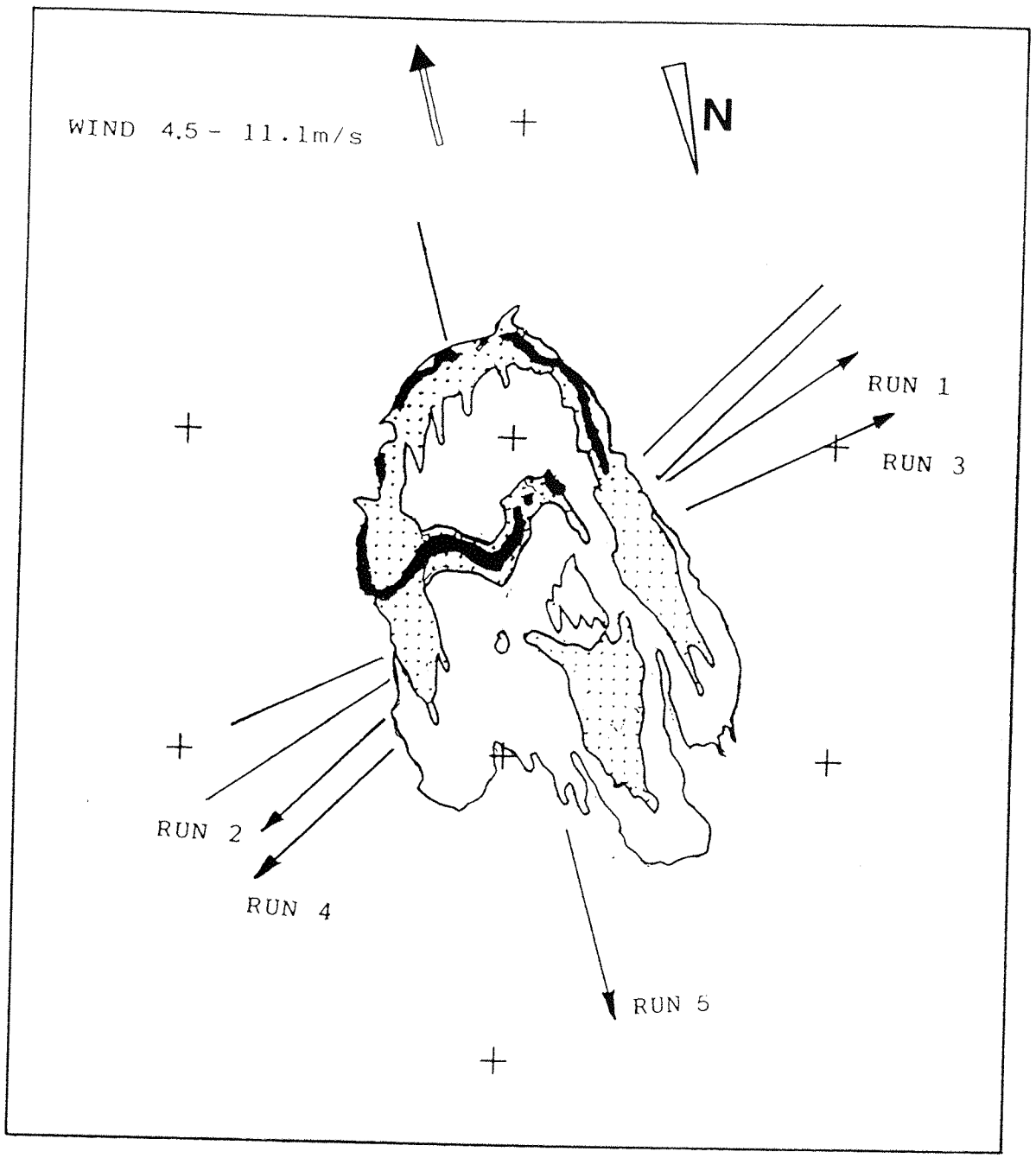

Fig 5.4 Sketch of the slick 1 1/2 hour after release derived from the IR/UV images shown on Fig 5.3.
The figure also shows the approximate courses of the survey ship as they were performed across the slick on July 7th.The crosses are 400m apart in both directions.

track.

Long runs in water free of oil were made before and after entering the slick to allow comparison of the backscatter signal from slick and clean surface to be made over large distances (typically a few hundreds of meters).

5.2.2. Weather Conditions

Wind speed and direction were monitored by a masthead anemometer located at a height of 10m above sea surface. There were no continuous recordings available at the time, so instantaneous readings were made four times for each experimental run, at intervals of about 10min.

Wind was constantly blowing from the North. On 06.05 and 07.05, wind was from 340°-010°, varying between 7.0 and 9.5m/s during the trials.

On 07.07.87, wind was from 330°-360° starting at 2.5m/s at 08:00 and continually increasing throughout the morning before reaching a maximum of 10.5-11.0m/s at 14:00. It then stabilised at this speed for almost two hours before falling steadily to 7.5m/s by the end of the day. And on 08.07.87, wind was low, varying between 4 and 6m/s during the experiment.

During the periods when wind was higher than 6-7 m/s, the significant waveheight was not more than 1.5m (as observed from the deck), with a period of about 5s (corresponding to a wavelength of around 40m), characteristic of swell waves in the area.

On 07.07, measurements of air and sea surface temperature were taken. The temperatures remained more or less constant throughout the experimental period with T_{air} varying between 14.5 and 16.8°C and $T_{surface} \approx 14.0$°C.

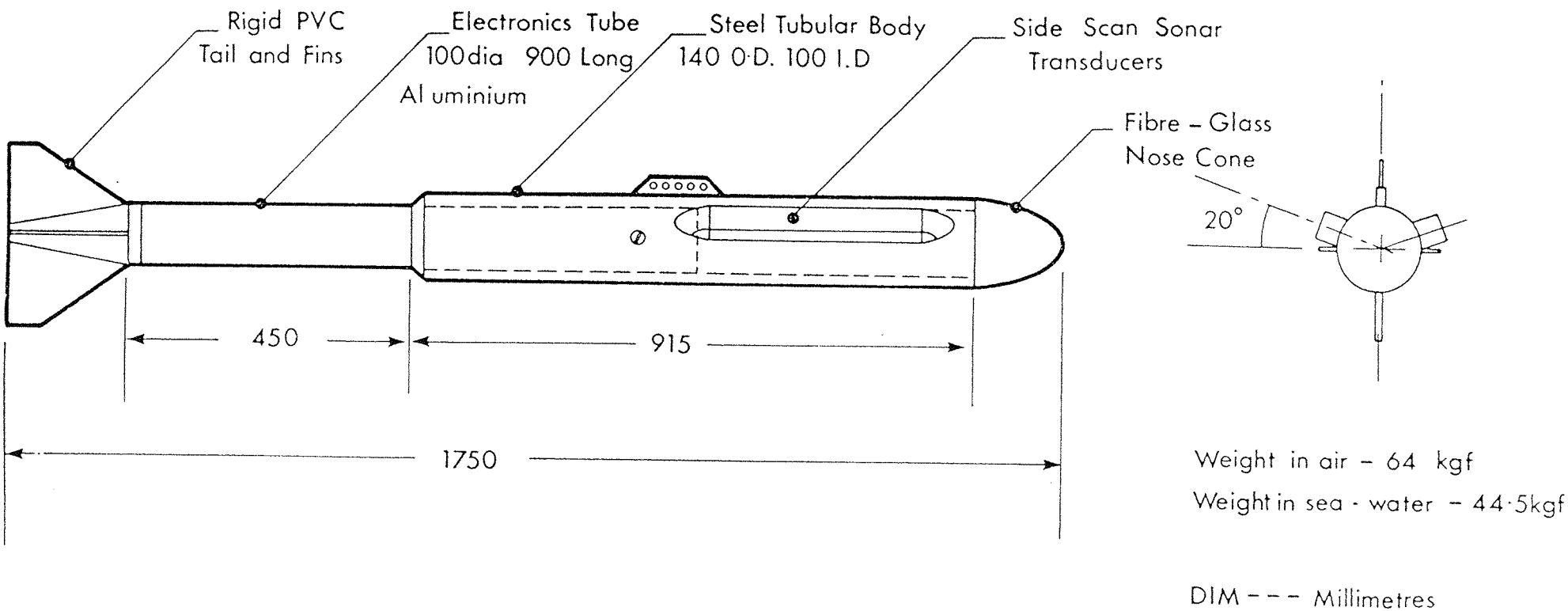

Fig 5.5 Drawing of the sonar in its metal steel housing.

5.3.EQUIPMENT

5.3.1. Sonar System

The acoustic system used during the experiment was originally designed as a side-scan sonar (see characteristics in Table 5.2). It was mounted on a steel fish (Figure 5.5). The beam pattern (Figure 5.6), shows the angular distribution of the transmitted acoustic power. The diagramme was experimentally determined at IOS and refers to relative values.

Parameter	Value
Signal Frequency	248 KHz
Transmitted pulse	
Peak power	100 W
Pulse Length	0.08ms/0.2ms
Repetition rate	4Hz , 8Hz
Sound Beam	
Dimension (3dB cutoff)	35°X 1°

Table 5.2 Sonar system characteristics.

Only one transducer, looking starboard, was used during the experiment. A dummy transducer was mounted symetrically to keep the structure in balance in the water. The transducer was positioned in such a way that the axis of the main sound beam was pointing upwards to the surface at an angle of 20 ± 1 degrees from horizontal (Figure 5.7). An electric switch would allow the use of the transducer both as a source and as a receiver. This switch transforms the transducer into a receiver as soon as the trigger pulse is transmitted to allow reception of the echo, and

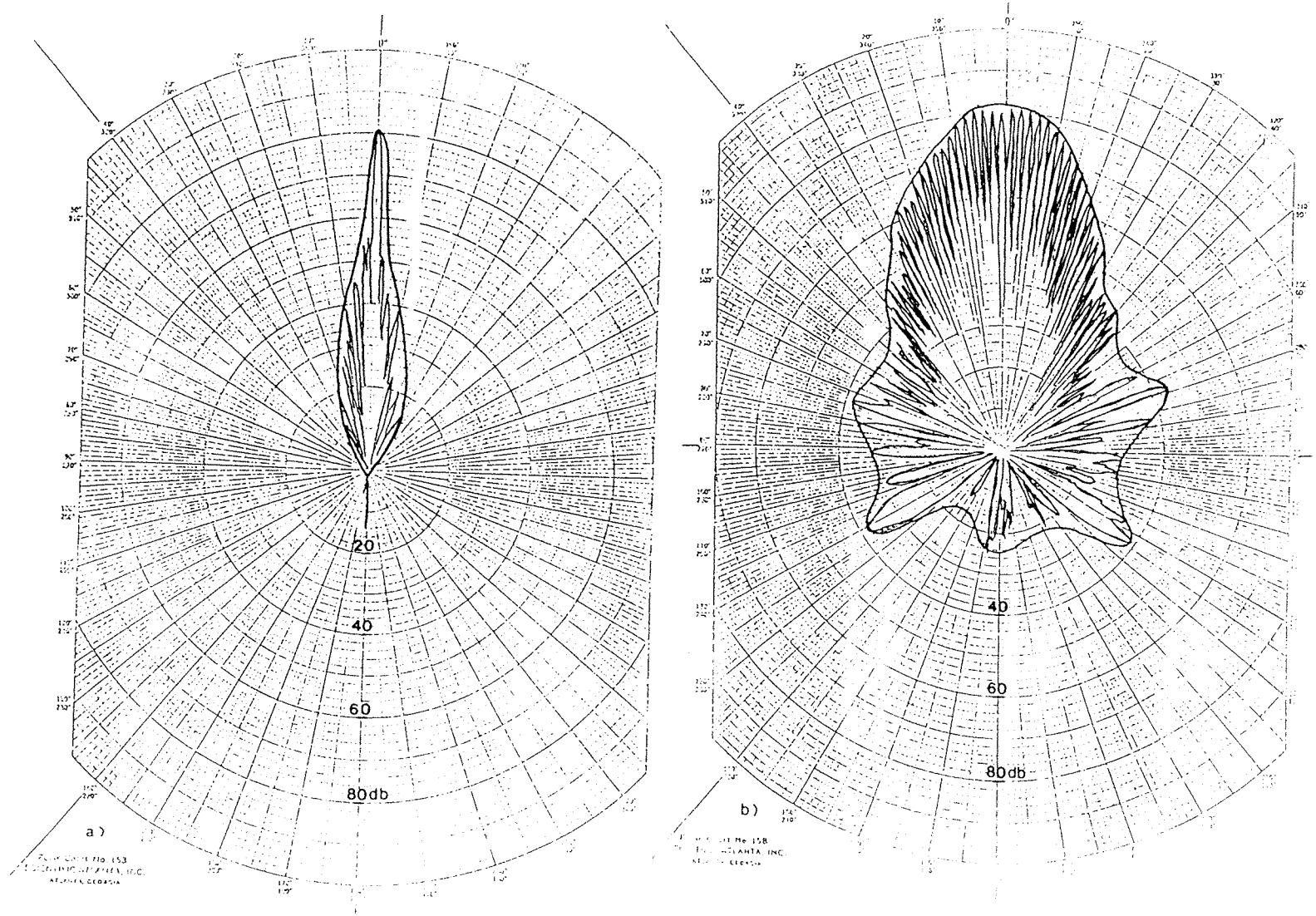

Fig 5.6 Experimentally determined beam pattern of 248kHz transducer used in our experiments showing the beam a) in the horizontal and b) in the vertical plane.

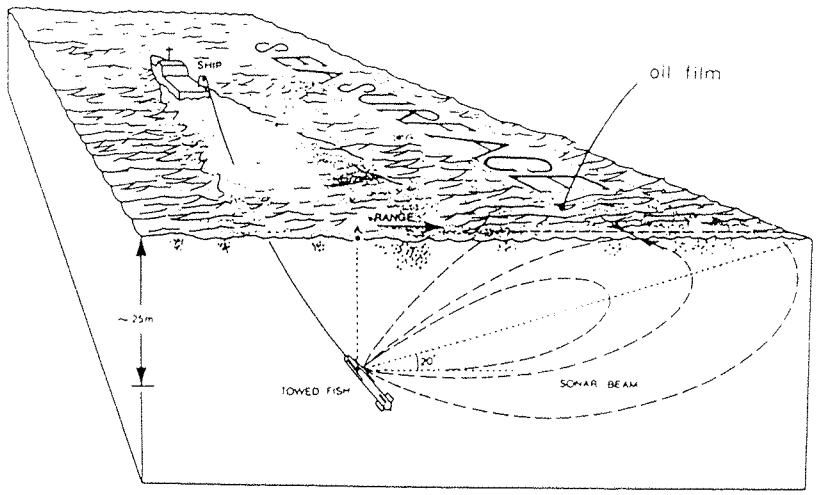

Fig 5.7 Sketch showing survey ship towing the sonar across the slick. The axis of the main beam is pointing to the sea surface at a 20° angle from the horizontal. Maximum range along the surface was about 150m.

then switches the transducer back into a transmitting device just before sending the next pulse.

The fish was towed using an 8-core metal cable, laid through a large pulley mounted at the stern of the ship. The amount of cable that was put out would determine the depth at which the sonar operated (usually 20 - 25m below the surface). The towing cable was attached to a specially designed fairing in order to reduce the drag effect on the fish (IOS internal Report n°270, March 1987). As a consequence, vibrations of the cable were considerably reduced, thus significantly reducing pitch and yaw of the fish.

5.3.2.Recording equipment

1.Graphic recorder

A graphic recorder was used to translate the strength of the acoustic backscatter into an image (sonographs). In the recorder, a set of three stylii moves across a chart in a direction perpendicular to the chart's length, starting at one edge at the time of transmission and marking the chart as the echoes are received. The chart then moves slightly forward, so that each sweep is adjacent to the previous one and visual

correlation of the echo pattern is possible. Axis on the sonographs are time (horizontal) and time-delay (vertical) of echo. Whenever possible, they are generally converted into spatial scales for convenience. Time-delay converts into horizontal range on the surface (Figure 5.8) extending from a point vertically above the transducer using the relation

$$x = (r^2-d^2)^{1/2}$$
$$= (c^2.t^2/4 - d^2)^{1/2} \qquad (5.1)$$

where d is depth at which the sonar is operating.

Horizontal scale is either converted into distance along the ship's track (if the sonar is being towed), or kept as it is.

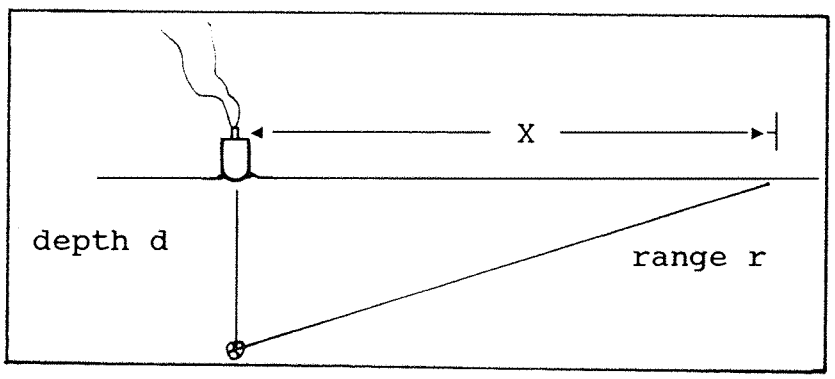

Figure 5.8 Geometrical configuration

The recorder used was an EPC model 3200. It had a dynamic range of 23db with a resolution of 16 tone shades (4bits) from black to white, the darkest shades expressing the strongest echo. The availability of a digital output on the EPC was not exploited due to the lack of an adequate memory storage unit.

The trigger pulse, provided by the EPC's internal clock, was generally set at a rate of 1/4s (4Hz), and sometimes at 1/8s (8Hz).

2.Magnetic tape recorder

A UHER magnetic tape recorder (see Table 5.3) was used at the same time to record the analog signal. This would enable subsequent replays of the different runs. These recordings formed the basis of the digitizing work. The dynamic range and frequency band the tape recorder offered were reasonably adequate for the kind of signal we were expecting as well as matching the performances of the equipment that was used. Replays from the tape recorder to the graphic recorder showed very few discrepancies with the original images.

Parameter	Value
Frequency response	35 - 20,000 Hz
Dynamic range	> 56dB
Tape speed	19 cm/s
Tape dimensions	6.3-0.06 mm
Tracks	Left: Trigger pulse Right: return signal

Table 5.3 Tape recorder specifications

5.3.3.Photography and airborne sensors

Sets of photographs were taken every 30s or so for each run with the camera pointing at the area of the surface that wasinsonified by the main beam. The aim was to see how well the recorded acoustic signal could be correlated with features observed on the surface. The camera used was a Minolta XG1, with a focal length of 45mm. The films used were high resolution 50 to 100 ASA.

The airplane was equipped with three types of sensors: Infrared and Ultraviolet Line Scanners, and a Side Looking Airborne Radar (SLAR). The UV images showed the extent of the

area covered by the oil which can be regarded as the outline of the total slick, while the IR images revealed the location of the relatively thick oil regions within the slick. The images combining returns from both sensors contain information about the height, heading and location of the airplane. They were very useful in localizing the slick and estimating its orientation, as well as correlating slick sizes with those derived from sonar records. Examples of these images are given in Figure 5.3. The SLAR images (see Figures 5.3b and 5.3c) also proved to be helpful in detecting the slicks and estimating their extent.

5.4.DATA PROCESSING

5.4.1.Introduction

The sonographs obtained throughout the experiments provided the first stages of the acoustic analysis. However, the inability to perform fast and efficient processing directly on the sonographs meant that an alternative way of processing the

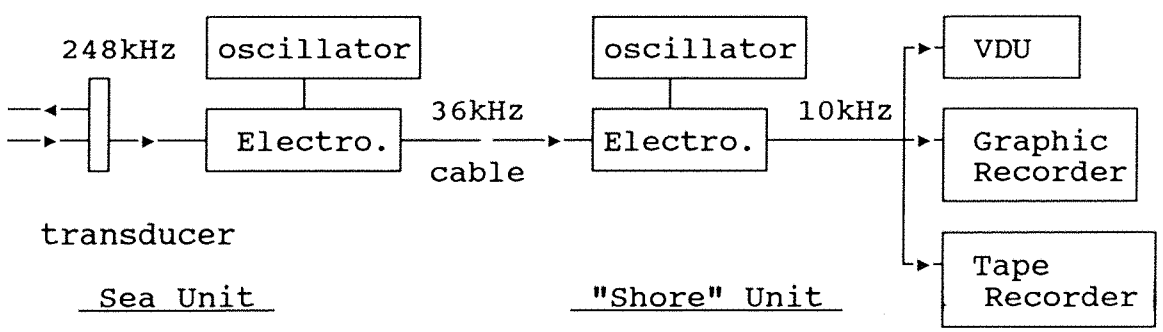

Fig 5.9 Block diagram of experimental set-up.

data was needed. The return signal, available on tapes (Figure 5.9) in analog form, was later digitized.

5.4.2.Heterodyning method

The carrier frequency was of no particular value at the analysis stage. We used a heterodyning method (Figure 5.10) to reduce the carrier frequency to a frequency that could allow better handling of the signal by the electronic circuits and also cut losses through long cable propagation. The method consists of mixing the received signal with the signal from an oscillator emitting at a constant frequency. The mixed signal is then sent through a low band pass filter in order to remove the high frequency signal. The resulting signal has an envelope similar to the original one, but the frequency of the new carrier is equal to the difference of the frequencies.

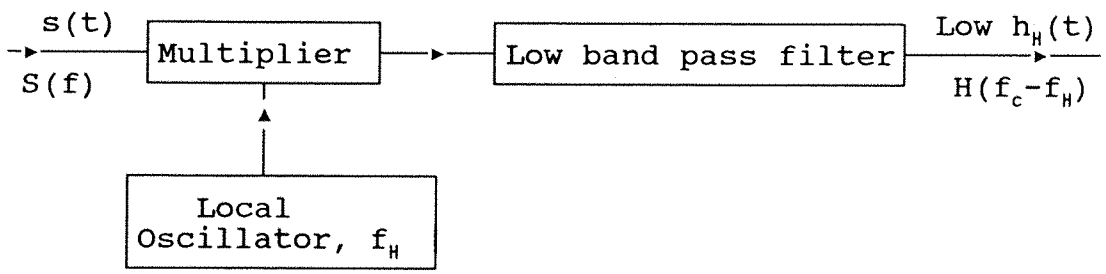

Fig 5.10 Heterodyning of high frequency signal

5.4.3.Digitization

Using a full wave precision rectifier (Figure 5.11), the signal is then rectified, filtered (to remove the frequency of the carrier to eliminate any interference with the sampling rate) and passed through an Analog/Digital Converter (A/DC) (Figure 5.12). The filter used was a Buetterworth analog active filter. The cutoff frequency f_o is determined following successive tests. The procedure followed was to play back the tapes onto the

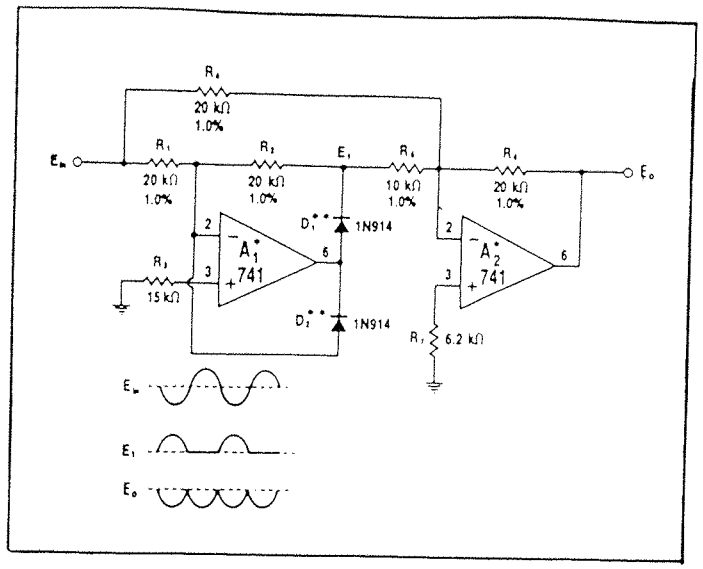

Fig 5.11 Diagramme of the full wave precision rectifier used in the data processing.

graphic recorder via a low-pass filter. The cutoff frequency is then progressively reduced down to the limit where features on the new sonographs start differing or disappearing when compared to the original sonographs.

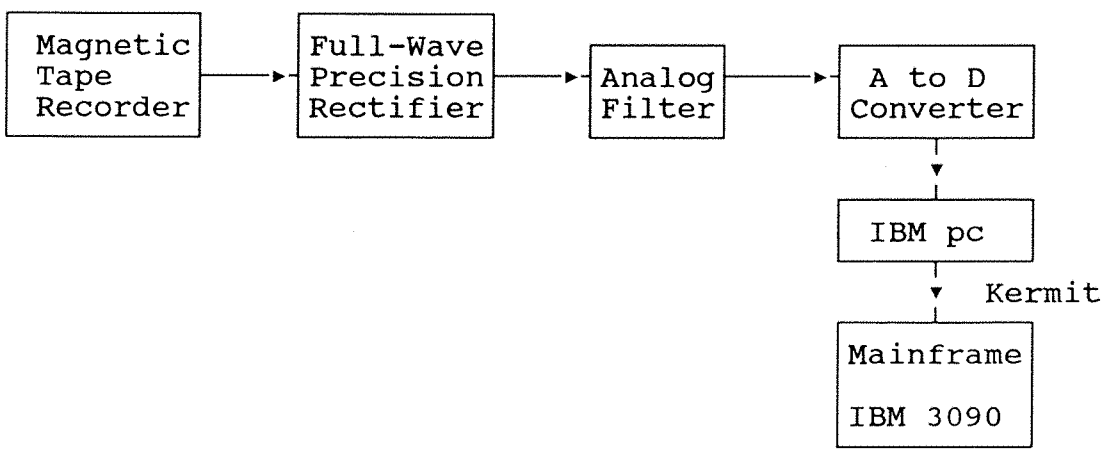

Fig 5.12 Block diagramme of data processing arrangement

Ideally, the sampling frequency (f_s) on the A/DC should be at least four times that of the filter so that a full wavelength can be sampled at four different points. After carrying out tests with sampling frequencies $f_s = 4f_o$ and $f_s = 2f_o$ and comparing the results, the latter sampling rate has been adopted as it did not show any difference with the former. The main reason why

such procedures were carried out was to cut down on memory storage capacities needed to a level which still produced qualitative results. This enabled to reduce the cost as well as the processing time.

The A/DC used for the processing was a DATALAB 2000, kindly lent by the Institute of Sound and Vibration Research at Southampton University. The sampling rate ranged from 0.5μs to 200ms and the recording capacity was 4kBytes at a time. The sampling frequency selected to process the data was 2kHz, which allowed a total sampling period of 2.048s at a time. With the repetition rate of the transmitted pulse equal to 4Hz, only 8 full consecutive echoes could be recorded at any one time. These echoes were then stored in different files on floppy discs which were later transferred to an IBM 3090 mainframe computer for processing (Figure 5.12) using the Kermit file transfer package.

5.4.4.Suggestions for future data processing

The analysis procedure described above was very time consuming owing to the absence of adequate equipment. In effect, the A/DC used during the digitization operation was designed for transcient signals such as shocks or impacts, which last for a fraction of a second and have low repetition frequencies. Sonar signals on the other hand carry a mass of information and usually come in succession, at a higher rate. The A/DC system was therefore inadequate in that the sonar signal needed to be partitioned into packets of 2s interval each, allowing not more than eight full successive echoes per operation to be digitized.

We recommend that if future digital analysis is to be carried out, then an adequate system would need to be used. The system should consist of a digital signal processing unit (DSP), which incorporates a digital filter, the A/DC and a parallel microprocessor. Parallel processing has become nowadays the state-of-the-art in the data processing fields, as it enables

many simultaneous operations to be carried out on the data. This allows real time processing of the data, fed from the tape recorder to the system. The data is managed from a PC which acts as a link between the DSP, the display unit, the mainframe and the storage unit; although for the two latter, a direct connection is possible (Figure 5.13). The digital storage unit should enable enough data to be stored momentarily while processing is under way, before the data is stored on tapes.

It appears that recording of the sonar signal by Video Cassette Recorders (VCR) onto high quality commercial video tapes has found some success (Alan Hall, private communication). This is mainly due to the high dynamical range offered by today's standards on most VCRs, to their wide availability on the market, and to the relatively low costs.

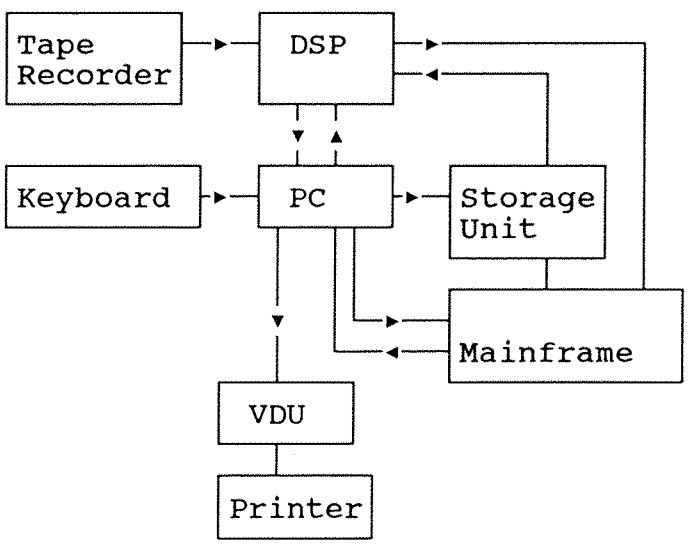

Fig 5.13 Block diagramme of suggested processing arrangement.

INTERPRETATION OF DATA

6.1.THE SONOGRAPHS

6.1.1.Description

The sonar was generally towed at a greater speed than the mean surface currents so that scatterers passing across the sound beam, and in particular the clouds of bubbles entrained by subsurface water flows and eddy motions (see Chapter 3), will only appear as single stationary targets on the sonographs.

Figure 6.1 for example is a sonograph obtained during the May trials. The ship, heading in a straight course into the wind at a speed of about 1.6m/s, was sailing in water free of oil. Winds were high (about 10m/s) from the north. On this sonograph, time is running from right to left and transmission is from the bottom of the record (for more details about sonographs, refer to Chapter 3).

Assuming the ship's speed V_s is constant, the horizontal scale converts into a linear distance along the ship's track. This is particularly useful to estimate the dimension of the observed phenomenon.

The vertical scale (on the right hand side) represents horizontal distance along the surface in the direction of the beam, starting from a point vertically above the sonar (see Figure 5.8).

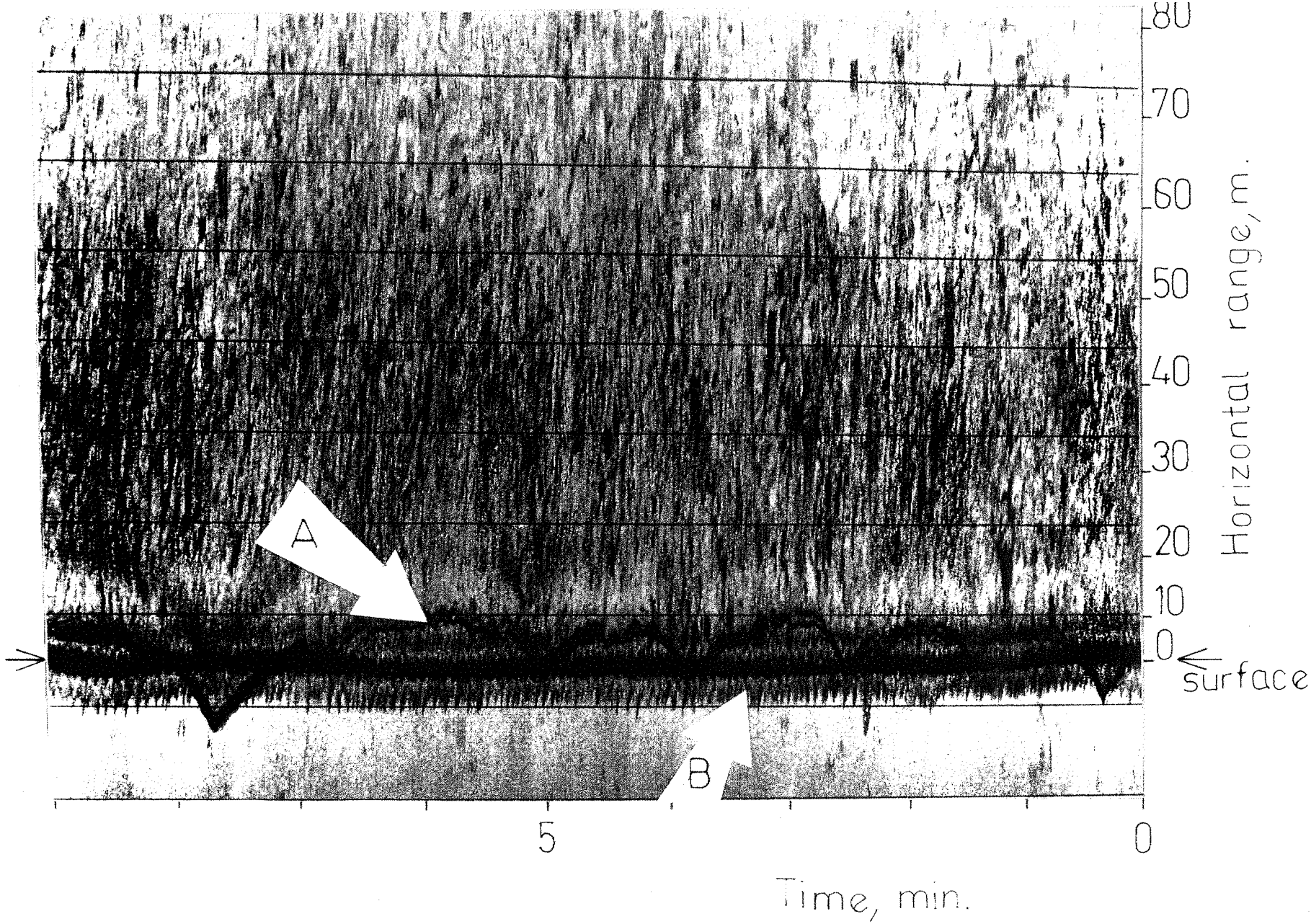

Fig 6.1 Example of sonograph record obtained with the ship heading into the wind. The sonar was operated in clean water at 25m depth. Ship speed was about 1.6m/s.
Bottom (A) and surface (0 range) reflections are indicated. Arrow B shows the presence of a scattering layer located immediately below the surface.

6.1.2.Surface and bottom reflections

In this sonograph, reflection from the sea bed vertically below the sonar from one of the beam's side lobes is marked A. The reflection is characterized by an irregular variation of its range from the sonar, according to the sea bed topography. The sea bed around the experimental area consisted of asymmetrical sand waves whose crests extended along the East-West. This explains the fluctuations in the bottom-reflection patterns on most sonographs obtained when the ship was heading on a North-South course.

A second echo of similar intensity (at 0 horizontal range) can be seen. It is the reflection from the surface vertically above the sonar. It is quite distinct from the bottom reflection in that it looks relatively smooth overall due to the sonar being kept at a constant depth by the relatively constant speed of the ship. Another difference lies in the presence of a scattering layer situated immediately below the surface reflection. This scattering layer (marked B on the sonograph) consists of air bubbles generated by the ship's propellers and entrained below the surface by turbulence. Their presence was visible throughout the experiment and tended to get more intense as the ship's speed was increased, or disappear when the ship was stationary. The backscatter recorded between 0 to about 80m is that from the surface along the beam and from scatterers in the water column.

Occasionally, scatterers can be seen at mid-depth between the sonar and the bottom (or the surface). They mainly consist of fish whose swim bladders can also act as good acoustic scatterers (Urick,1975).

6.1.3.The oil slick

1.Photographs

As can be seen on Figure 6.2, the presence of the oil has affected the short wave-high frequency wave spectrum in the

a)

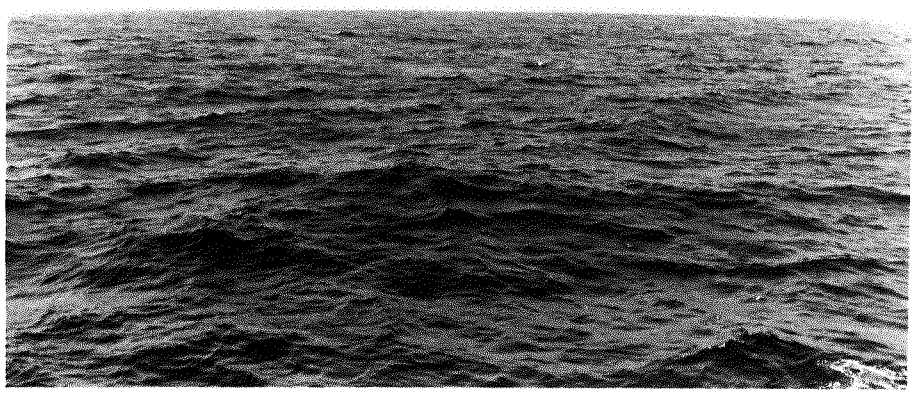

b)

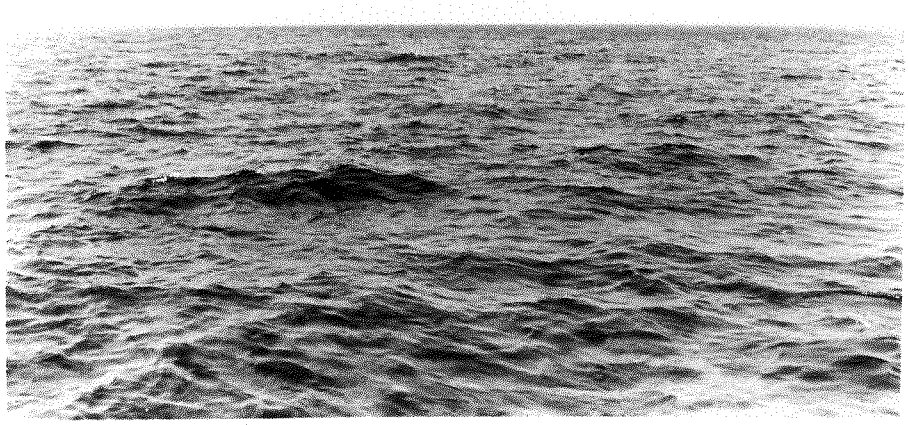

Fig 6.2 Photograph of the sea surface a) in clean and b) in slick water.
In the near field, ripples can be seen to have disappeared from the oil-covered surface, but notice that the larger waves still cause breaking at their crests.

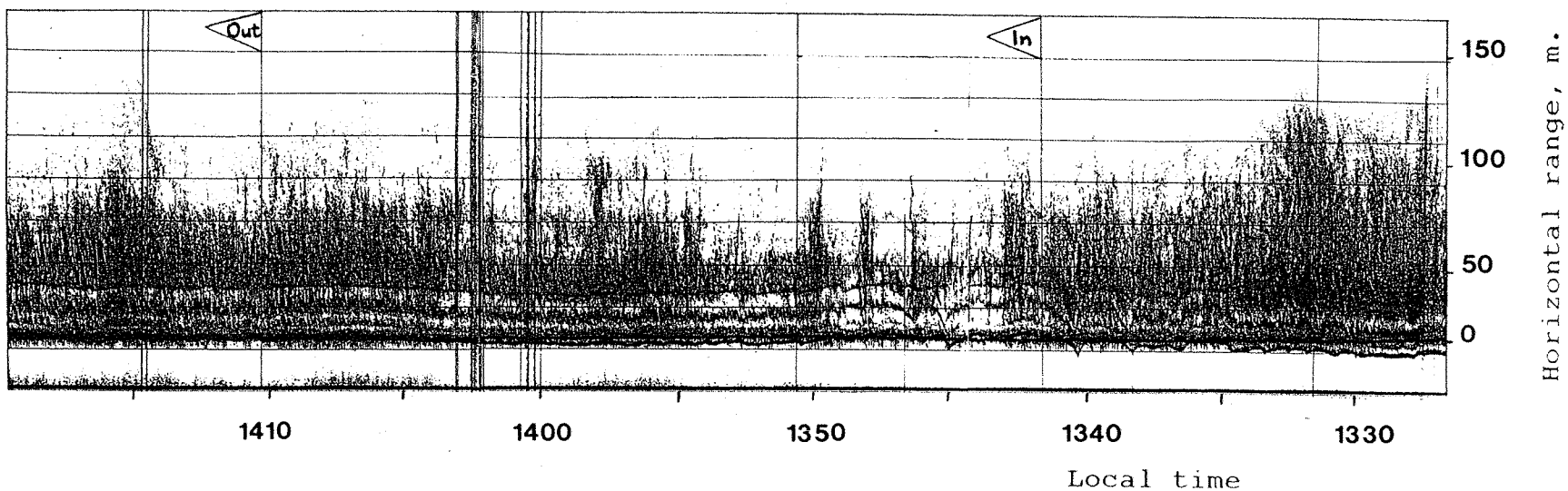

Fig 6.3 Sonograph of the sea surface across an oleyl alcohol slick (08.08.87, V_s=2m/s, W_{10}= 4-6m/s,sonar pointing downwind). The arrows (In and Out) indicate the approximate edges of the slick as estimated from the ship. The occasional wide vertical lines seen between 14:00 and 14:15 are due to some interference with the radio signals transmitted between the aircraft and the ship.

slick. On these photographs, taken at 6min intervals with the ship heading across the wind (from right to left on the photographs), the camera was pointing (a) outside and (b) inside the slick. Wind speed was about 11.0m/s. The entering and exiting edge of the slick are slightly visible on the right hand side of the pictures. While no significant damping of the long waves was visible, the small ripples on the other hand have been seriously affected and have almost completely disappeared in the near field in Figure 6.2b.

2.Sonographs

Sonographs from three of the four experimental days are shown in Figures 6.3 to 6.7. The runs were performed crosswind with the sound beam pointing either upwind or downwind. The small arrows (In and Out) indicate the approximate edges of the slick estimated from the deck at the moment the ship was either entering or exiting the slick (for details on the wind conditions, please refer to §5.2.2).

Figure 6.3 is a sonograph of the oleyl alcohol slick (08.07.87) taken under relatively low wind. The signal intensity is seen to be reducing as soon as the sonar enters the slick surface, but the exiting edge of the slick is not so obvious. The backscatter intensity within the slick is however seen to be periodically decresing and increasing. This is probably due to the way the oleyl was spread (see §5.2.1 and Figure 5.3b), where variations in the film thickness would be expected to be present, and would therfore lead to variations in the surface backscatter across the slick (§4.2.3).

The sonographs in Figures 6.4 and 6.5 were taken during the same day (July 7th) in succeeding runs (see Figure 5.4 for the ship courses). On this day, the sonar was generally towed at mid-water. As a result, the surface and bottom echoes overlapped on some occasions (Figure 6.4). In Figure 6.5, the two echoes

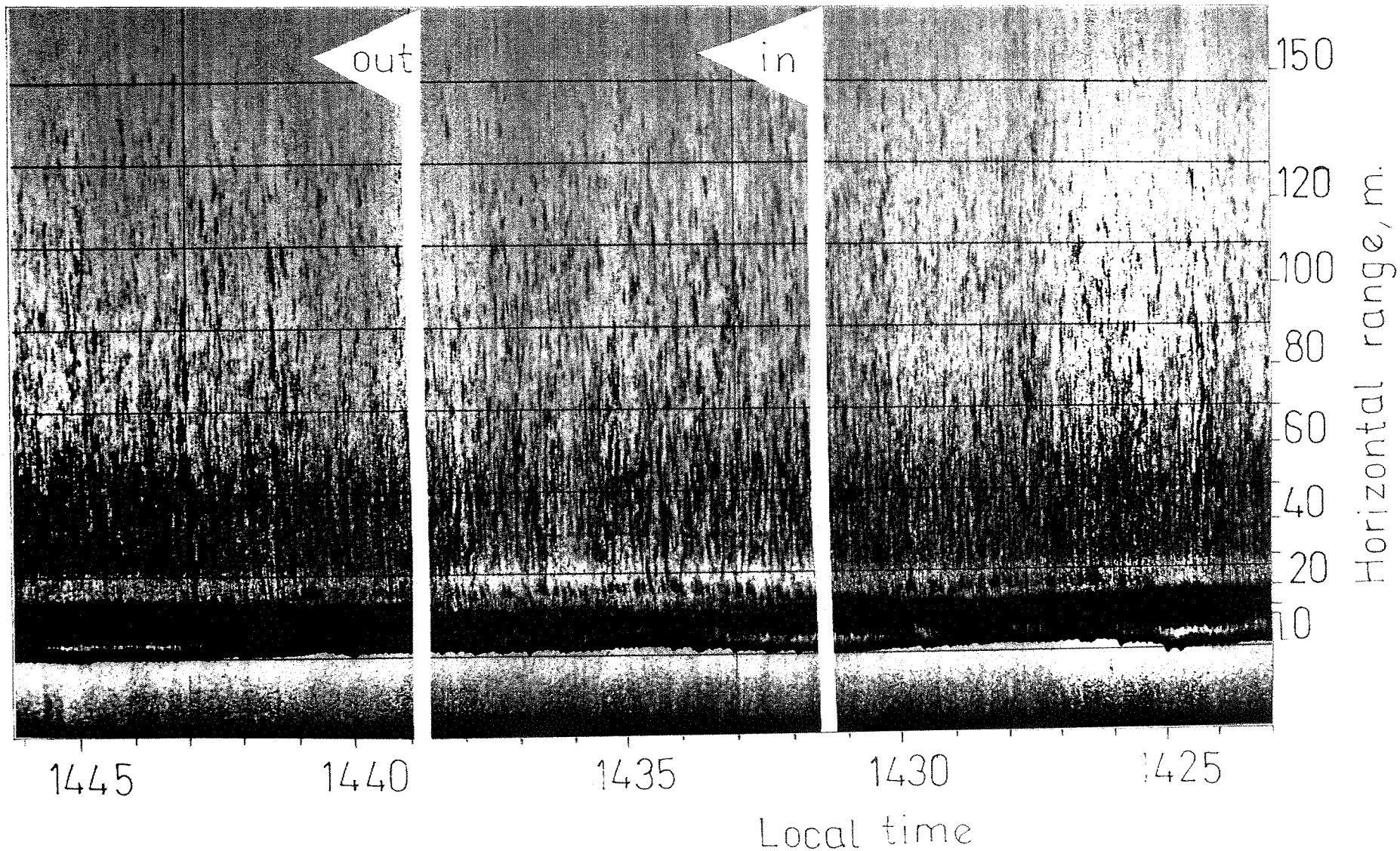

Fig 6.4 Sonograph of the sea surface on 07.07.87 (RUN2: upwind, W(10)= 11.1m/s, V_s= 1.58m/s).

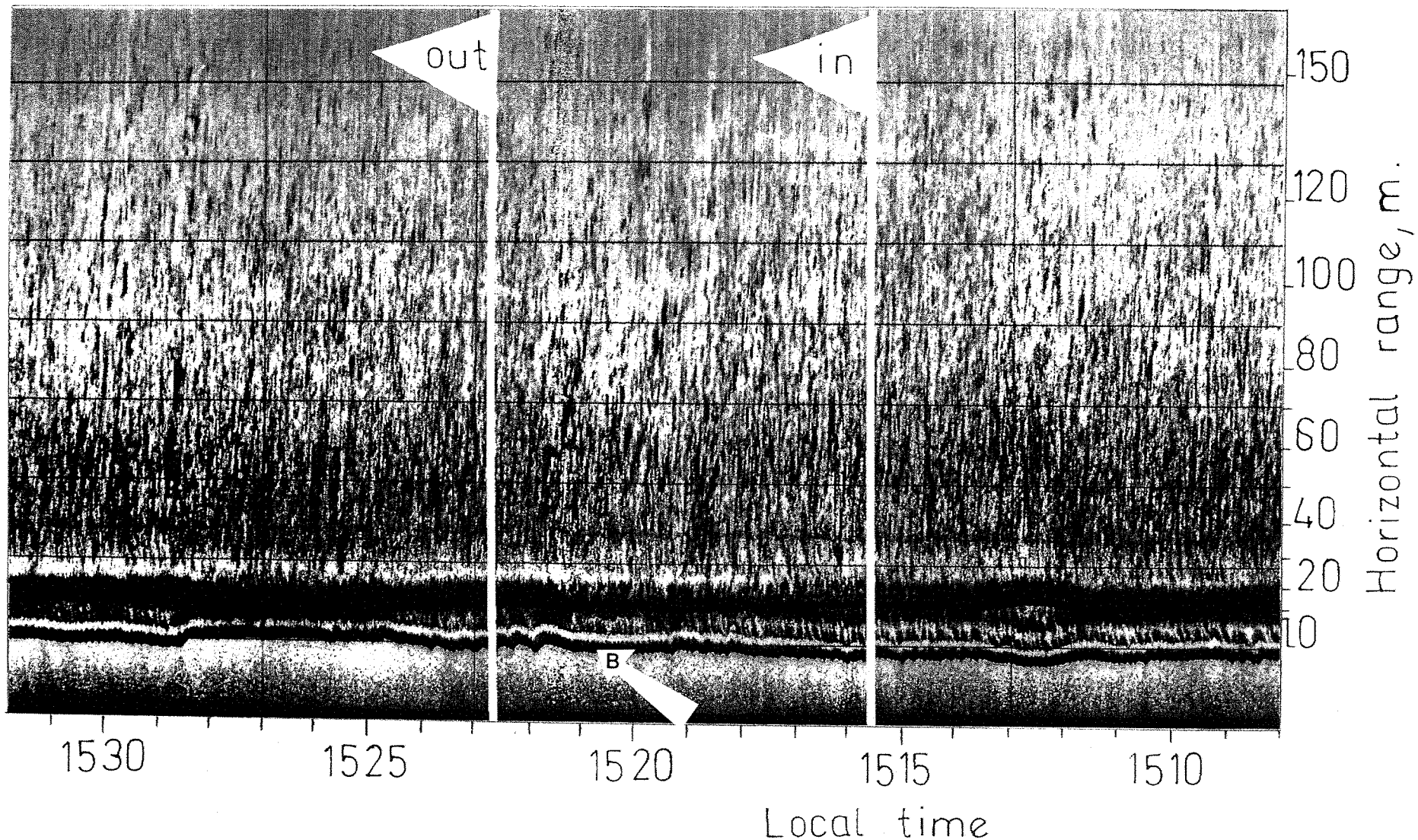

Fig 6.5 Sonograph of the sea surface on 07.07.87 (RUN3: downwind, W(10)= 9.5m/s, V_s= 1.6m/s).Arrow B shows echo from the sea bed.

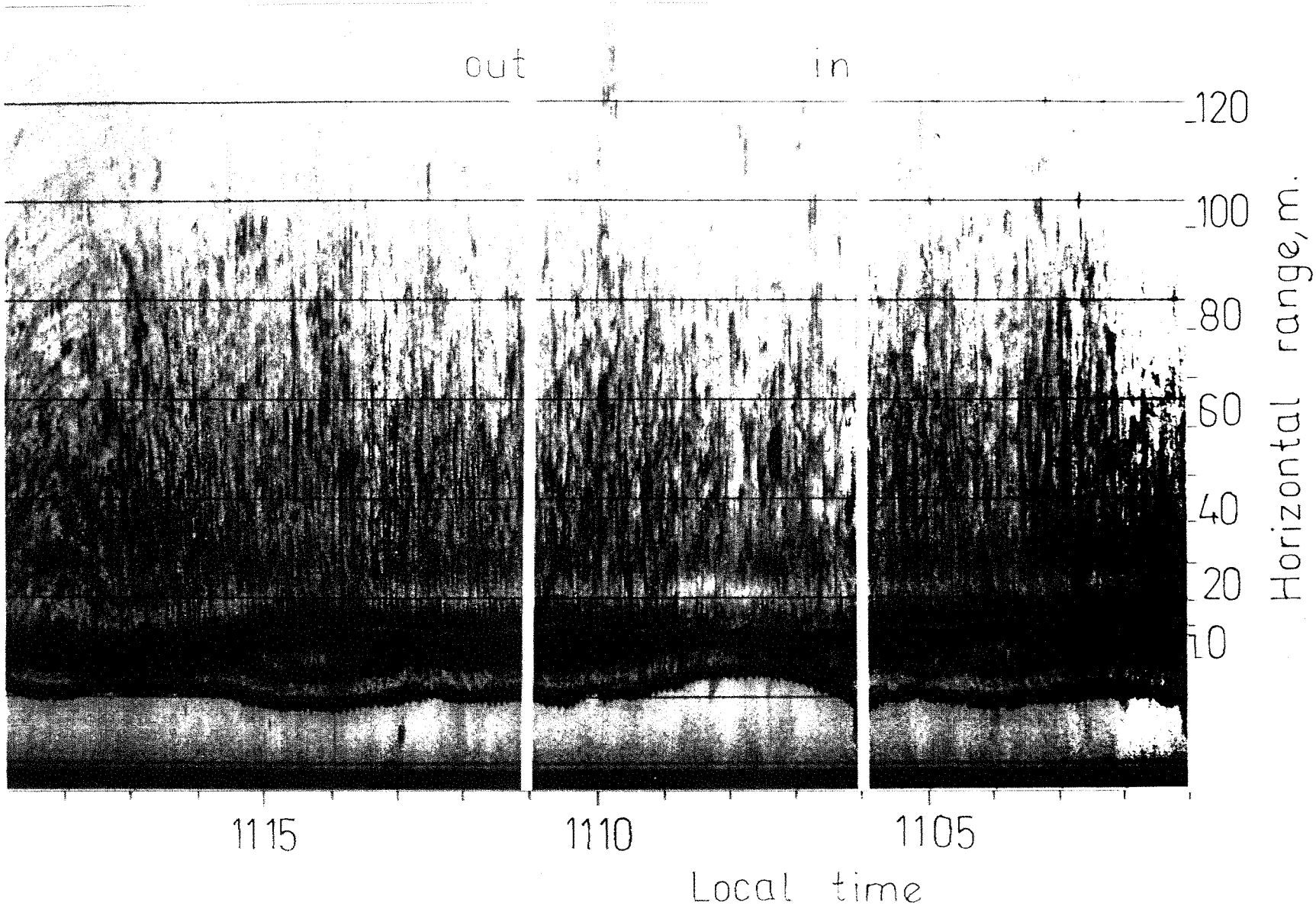

Fig 6.6 Sonograph of the sea surface on 06.05.87 (upwind, W(10)= 9.5m/s, V_s= 1.42m/s).

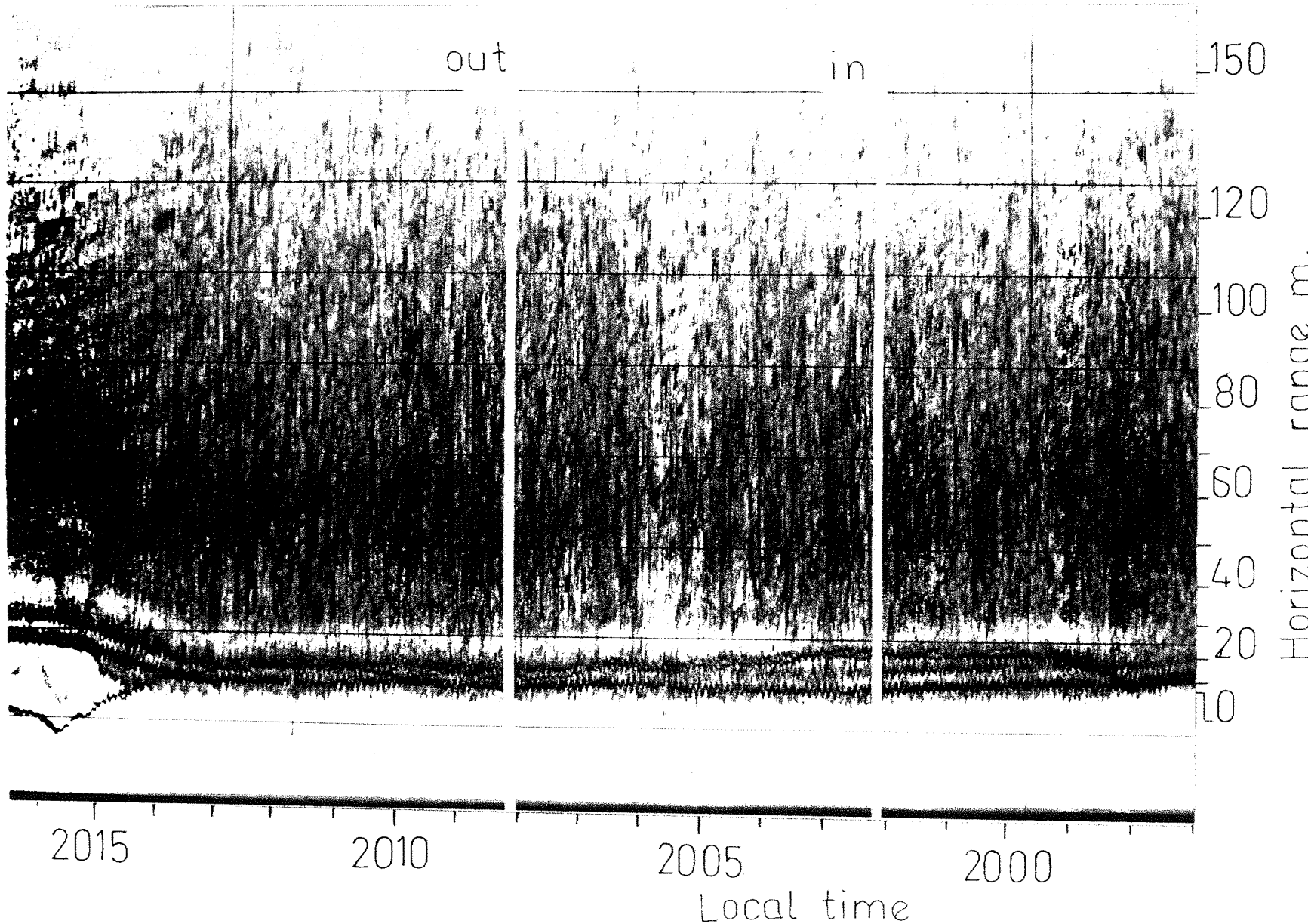

Fig 6.7 Sonograph of the sea surface on 06.05.87 (downwind, W(10)= 9.5m/s, V_s= 1.66m/s). The separation of the surface from the bottom echoes at the end of the sonograph was associated with a turn started at the end of the run.

are slightly distinct from each other, with the sea bed received first (B). A second echo of the sea bed gathered by a side lobe can be seen moving almost parallel to B. In Figure 6.7, a turn (of the survey vessel) was started at the end of the run (at about 20h14min). As the vesel slowed down, the sonar is seen to be lowering down and appears on the sonographs to be getting closer to the sea bed. Another consequence of the slowing of the vessel is a considerable reduction of the intensity of the sub-surface backscatter.

By visually comparing the section within the In and Out arrows and that outside the arrows, there is a clear evidence (particularly in Figures 6.3,6.4,6.6 and 6.7) that the presence of the oil has affected the level of acoustic backscatter. This difference in backscatter is particularly visible at intermediate range (20-60m).

6.2.INTERPRETATION OF DIGITIZED DATA

6.2.1. Remarks

i/ The surface vertically above the transducer being contaminated by the ship's wake, geometric calculations showed that the first 20° from vertical incidence were irrelevant in the analysis. We will therefore ignore this part of the records in our subsequent analysis.

ii/ Recording facilities were only available on 07.07.87. Consequently, the following discussion will only relate to this day. RUN1 to RUN4 were all performed on that day.

6.2.2. Experimental results

1.Oil film thickness

To estimate the oil film thickness across the slick, we estimated the extent of the slick from the UV images in Figure

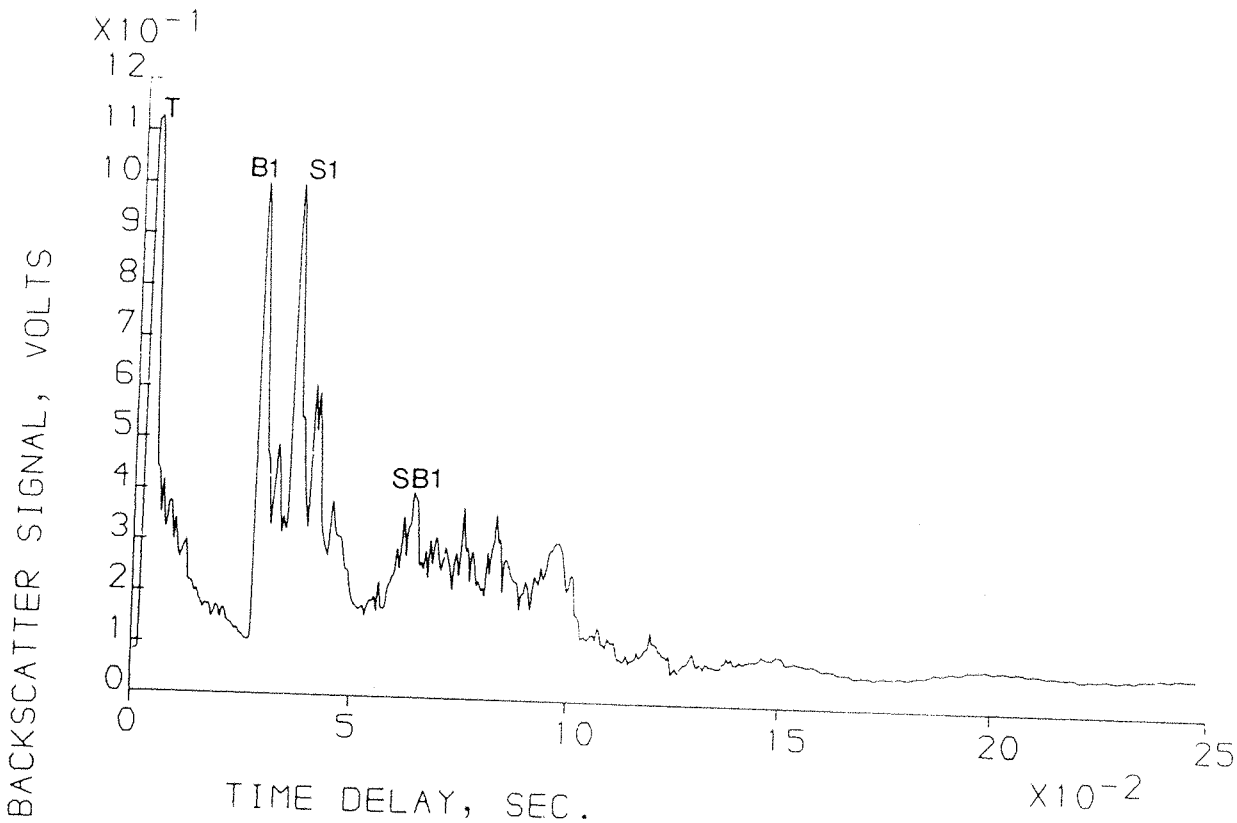

Fig 6.8 Acoustic backscatter from 248kHz sonar. Transmission (T), bottom reflection (B1), surface reflection (S1), and bottom-surface reflections (SB1) are indicated.

5.3, 24min after the release operation ended. If we assume that all of the oil released was floating on the surface, the average thickness of the film would be circa 25.5 microns. The concentrations of subsurface oil in the top 5 metres from the surface, measured on that day were below the instrument's detection threshold (100 ppb). According to Neil Hurford (private communication), the level of oil concentration would be expected to be around 50 ppb. If we take into account the amount of oil that has dissolved in the water, the oil that has evaporated and the fact that only a small amount of the total oil volume (about 10%) occupies most of the slick area (see §4.1.1.), the 25.5 microns thickness of the film should be reduced to a much smaller figure.

2.Variation of the return level with wind speed and surface type

To quantify the angular reduction in backscatter, we averaged the return signal from successive echoes under both surface conditions. Averages for three consecutive runs (2,3 and 4) are shown in Figures 6.9 to 6.11. Before discussing these, let us first examine in more details one full single echo to explain some of the features appearing on the return signal.

Figure 6.8 for example is the resulting average of eight successive echoes (i.e. each data point is the arithmetic mean of the data points at the same range for 8 successive echoes) from an oil-free surface. In this figure the first sharp peak at time t=0 (T) is the transmission. The peak following T (B1) is the first reflection from the sea bed vertically below the sonar. S1 is the first reflection from the surface. It is usually higher than B1 as sea surface is a better sound reflector than the bottom. The chronological occurrence of B1 in relation to S1 depends solely on the position of the transducer relative to the surface/bottom. A third peak (SB1) of smaller importance may be apparent from time to time. Its

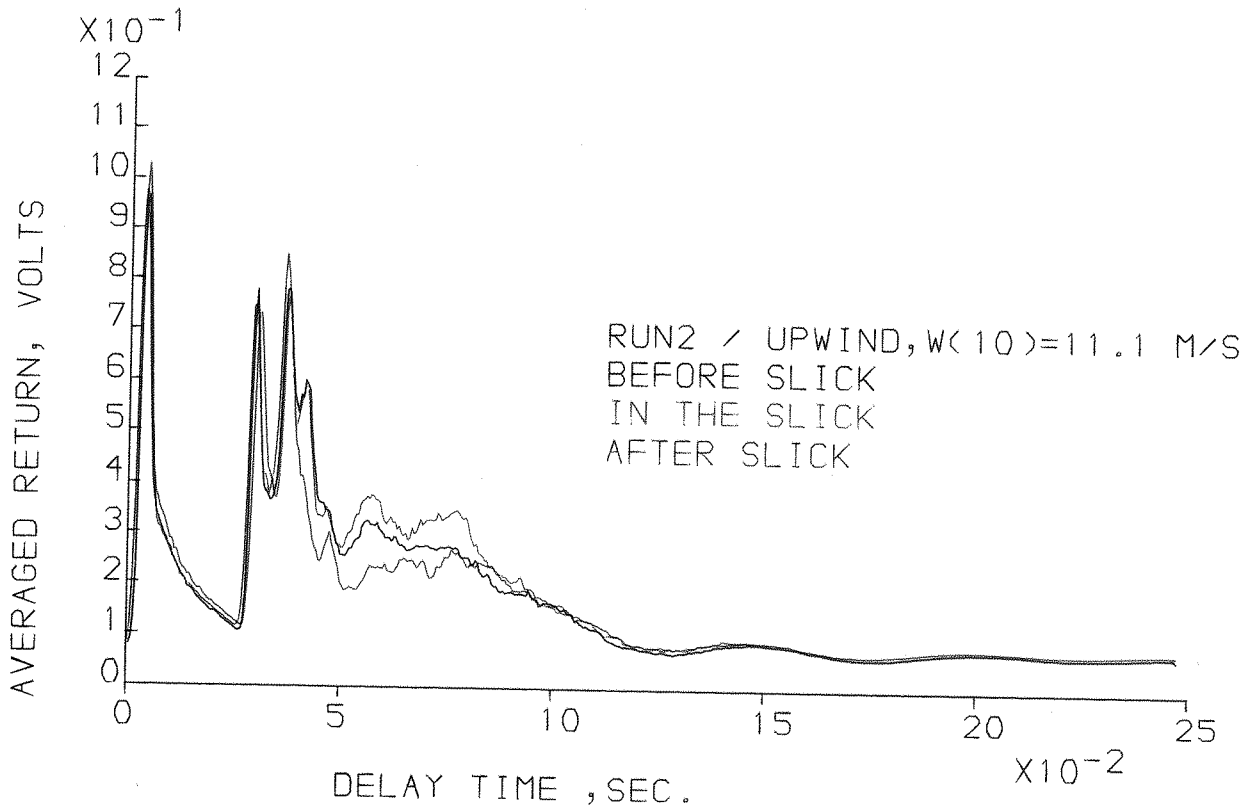

Fig 6.9 Acoustic sea surface backscatter from RUN2 over clean water before and after entering the slick and underneath the slick,averaged over a distance of 70m along the survey track.

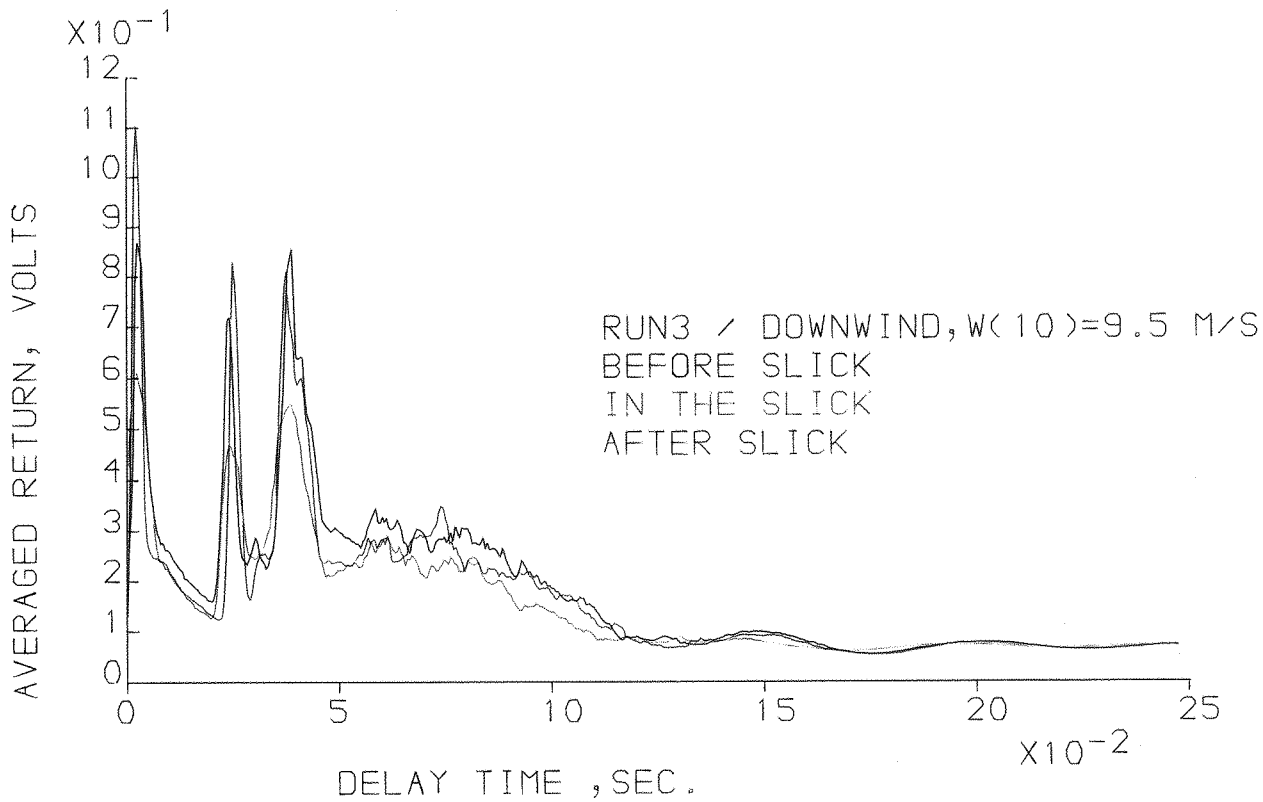

Fig 6.10 Acoustic sea surface backscatter from RUN3 averaged over 70m.

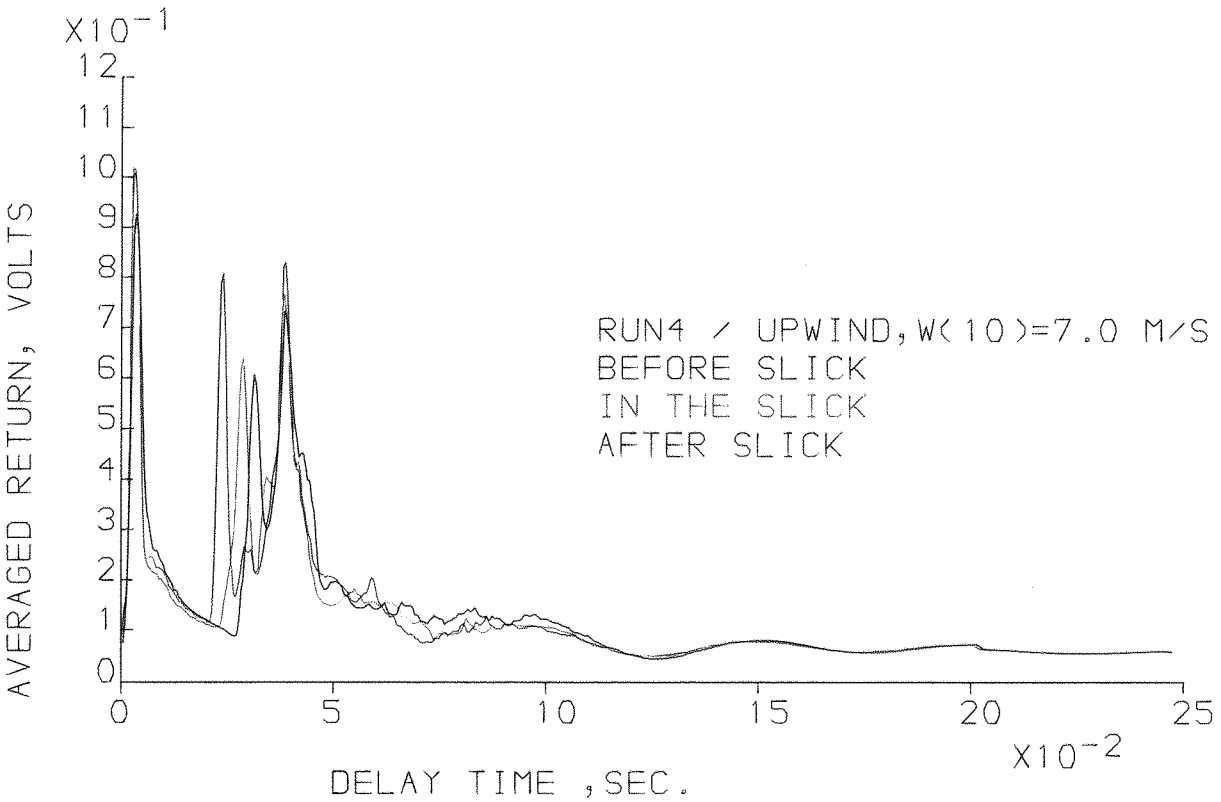

Fig 6.11 Acoustic sea surface backscatter from RUN4 averaged over 70m.

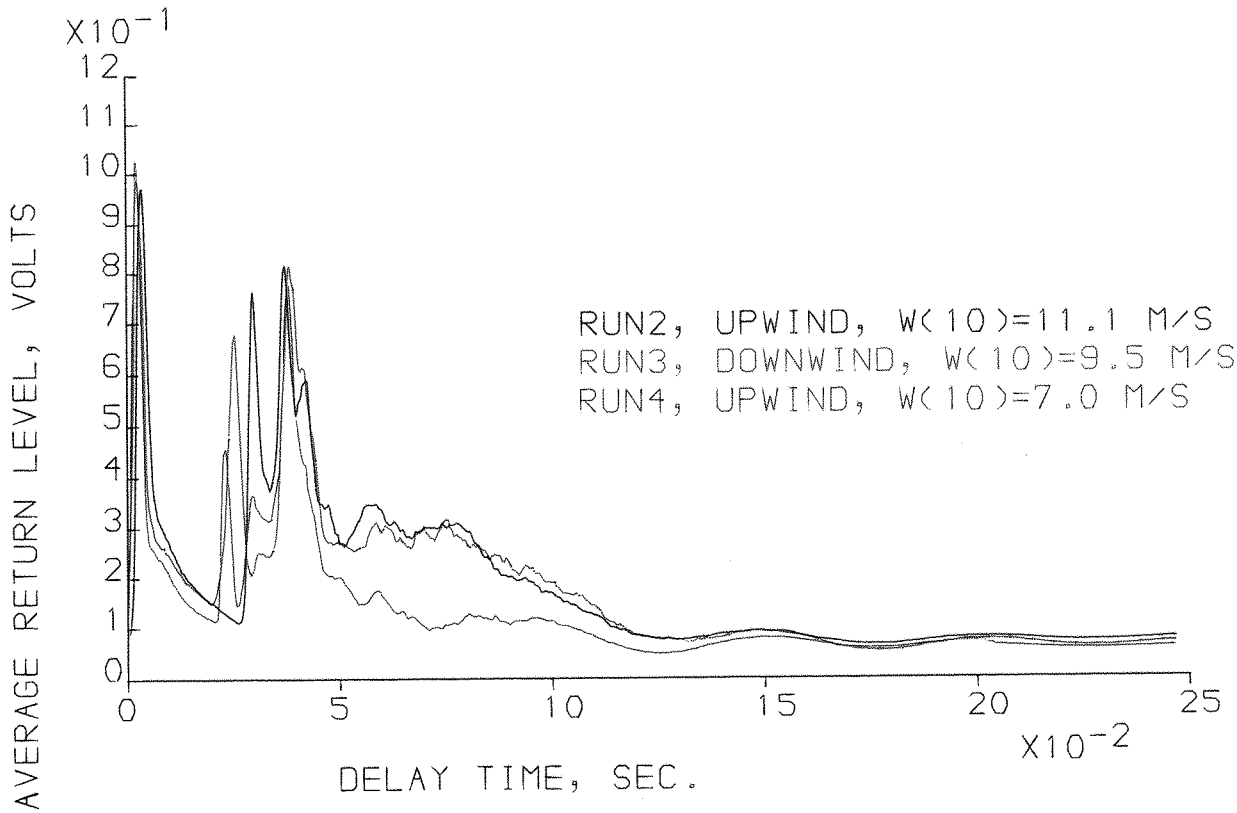

Fig 6.12 Plots of averages of the acoustic backscatter from RUNS 2,3 & 4 in clean water.

presence depends mainly on the reflection properties of the sea bed and consists of the sum of the reflections from the sound rays travelling vertically between the transducer-bottom-surface-transducer and the transducer-surface-bottom-transducer. The "dip" located between S1 and SB1 is a result of the anisotropic distribution of the acoustic energy of the sound beam (see Figure 5.6).

I can offer no physical explanation for the occurrence of the low frequency fluctuations seen about 12.10^{-2}s after transmission. The most probable origin of these fluctuations is a parasitic noise introduced by the electronic components of the equipment during the digitizing procedures described in the preceding chapter. A lack of adequate hardware prevented us from reproducing the digital data for comparison with the original records.

The echo starting from S1 represents the sum of contributions from various scatterers and reflectors located on the surface as well as within the water column. Their arrival time after transmission increases with range. The high frequency fluctuations in the backscatter are almost certainly associated with individual scattering events located on the surface or within the water column. Figure 6.12 shows the backscatter level at three different wind speeds. For the three runs considered, the figure shows that the backscatter level decreases as wind speed decreases, emphasizing the fact that the scattering process is generated at the surface or in the adjacent layer rather than being some artefact of the electronics. Averages over substantial spatial scales (typically of the order of 70m, or 240 pulses) should allow the filtering of the odd scatterers visible int the 8 pulse average of Figure 6.8, and only leave us with the mean backscatter level from the surface.

Figures 6.9 to 6.11 show plots of the backscatter from RUNS2,3 and 4 averaged using a similar procedure to that of

Figure 6.8. The averages were performed over a horizontal distance of 70m along the survey's track in water clear of oil before and after entering the slick and within the slick. These runs were made with the sound beam pointing either upwind or downwind. Between the first and the last of these runs, wind speed decreased from 11.1 to 7.0 m/s. Surface reflections on the three curves are located at the same range from transmission as the fish was kept more or less at the same depth during the runs by the constant survey speed. On these three figures, the surface backscatter is not as "spiky" as in Figure 6.8, suggesting that the averaging procedure acted as a filter to the high frequency scatterers. In Figure 6.9 the slick was $2^{3}/_{4}$ hours old and wind was about 11.1m/s. Backscatter level can be seen to be substantially greater under the clear surface than under the slick. On the next run (Figure 6.10), the return from the clean surface has come closer to that from the slick but still remains greater overall. On the following run, the slick was $4^{1}/_{2}$ hours old and the effect of the oil film on the backscatter have diminished as all three curves are almost at the same level. By that time, wind speed had dropped to 7.0m/s.

3.Differential backscatter between slick and clean water

In Figure 6.13, we have plotted the angular differential backscatter $\Delta S(\theta)$ for upwind and downwind observations to show the difference in the backscatter levels between the slick and clean surface using

$$\Delta S(\theta) = \bar{S}_c(\theta) - \bar{S}_s(\theta), \qquad (6.1)$$

where $\bar{S}_c(\theta)$ and $\bar{S}_s(\theta)$ are the averaged backscatter from clean surface and from the slick respectively derived from Figures 6.9 to 6.11. From the figure we can notice that for upwind

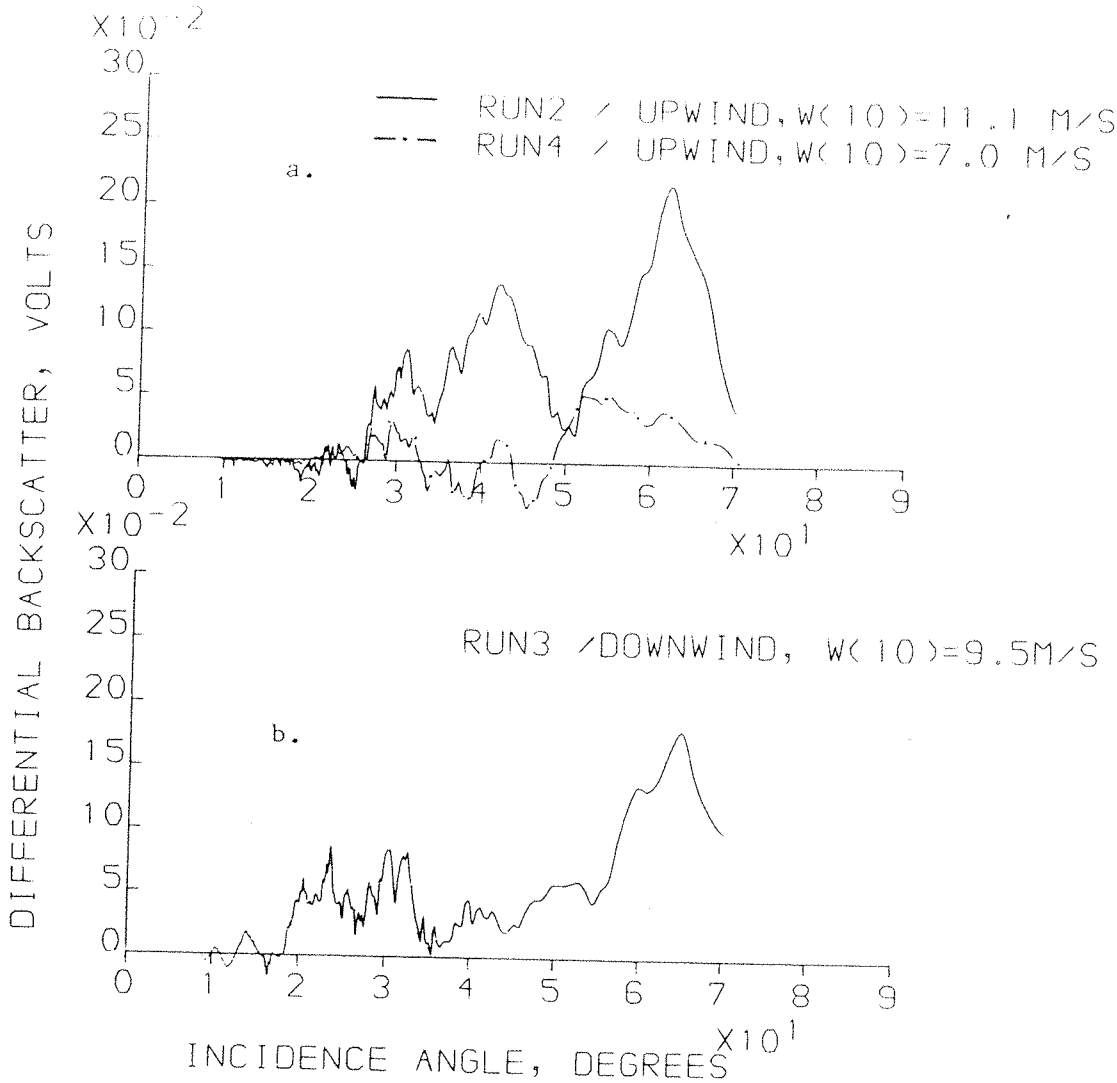

Fig 6.13 a) Upwind backscatter reduction for RUN2 and RUN4, and b) downwind backscatter reduction for RUN3.

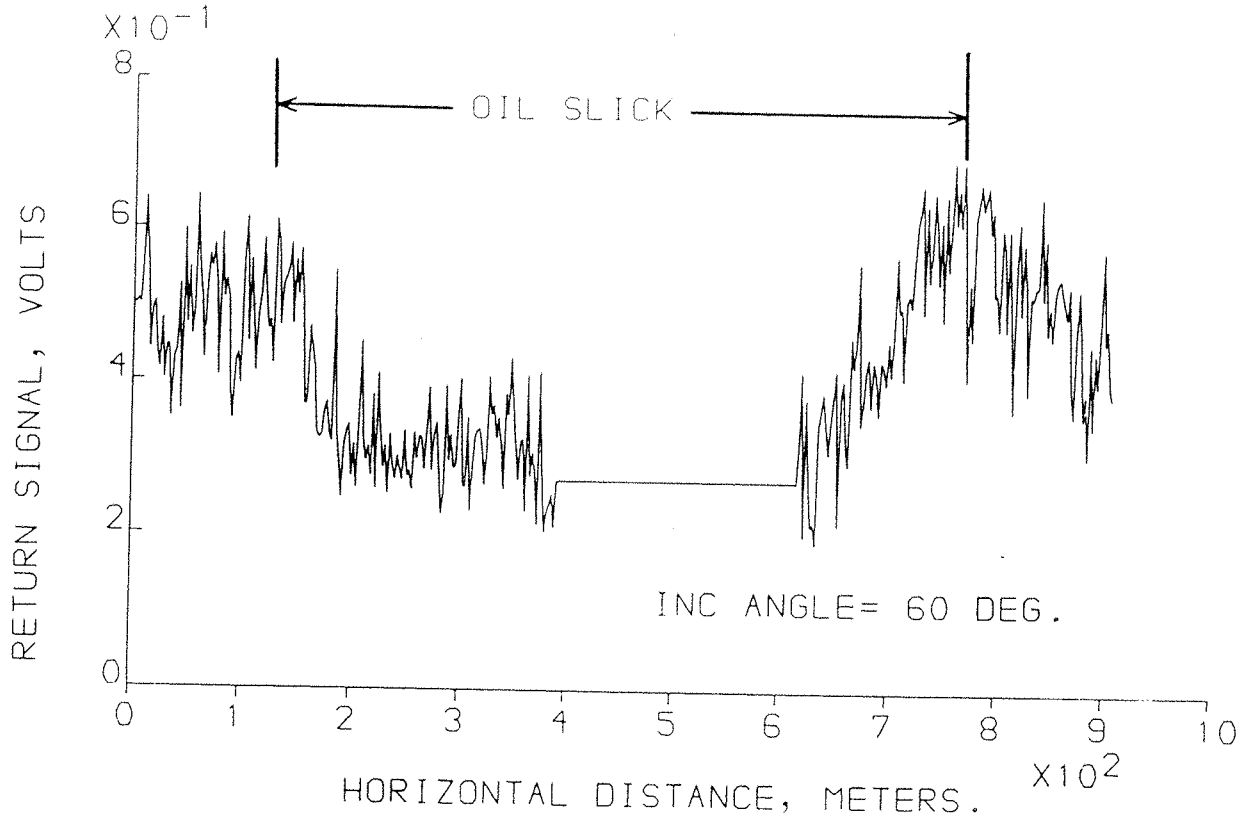

Fig 6.14 Cross section of slick (RUN2) at 60° incidence. Each data point is averaged over a distance of 5m across the ship track (angular bin 60°-52°) and 3.1m along track.

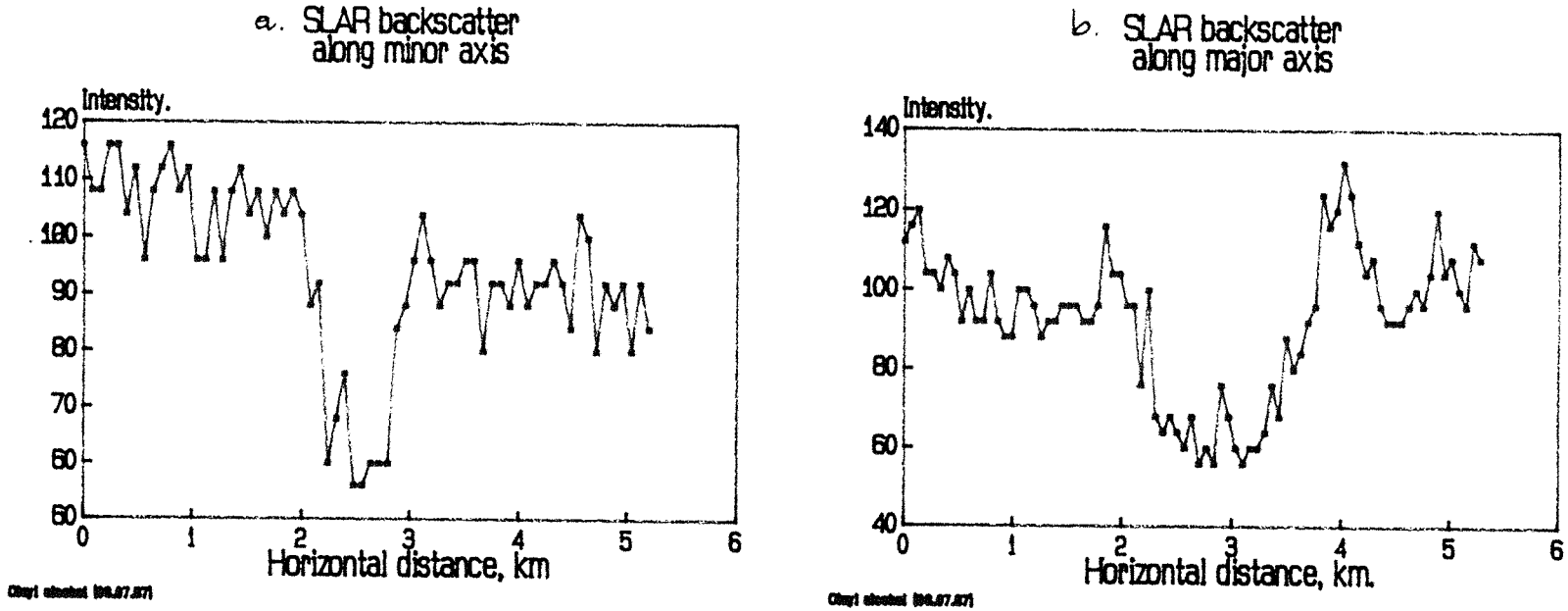

Fig 6.14b Radar sea surface backscatter of the fuel oil slick (07.07.87) a) along its minor axis, and b) along its major axis. The data is derived from the pixel intensity (resolution 80m X 66m) of the SLAR images (Fig 5.3c) of the slick. The sudden depression of the signal intensity is due to the presence of the oil.

observations, $\Delta S(\theta)$ goes through a maximum located around 55°-60° before it slowly reduces to 0 at 40° for 7.0 m/s winds and at 25° for 11.1 m/s winds. For downwind observations a similar behaviour of $\Delta S(\theta)$ is observed with the maximum reduction at 60°-65°.

4.Frequency of wave breaking in the slick

Figure 6.14 shows the acoustic backscatter across the narrow dimension of the slick taken at a constant bin angle of incidence (θ =60° -52°) derived from RUN2 (Figure 6.4). Each data point is averaged over 8 successive returns. This is equivalent to a horizontal distance along the survey track of about 3.1m. Prior to this, the data from each echo was averaged over a distance of 5m (60° -52°) across track. So every data point represents the backscatter averaged over an area of the surface equivalent to 15.1m^2. Fig 6.14b, on the other hand, is the radar sea surface backscatter taken at about the same time as RUN2 was being performed. The data points are derived from the intensity of the pixels of the corresponding SLAR image (Fig 5.3c). The spatial resolution of the pixels is about 80m X 66m. The radar cross-section is taken about 350m downwind of the sonar cross section.

A regrettable error of judgment led to the acoustic signal recording to be interrupted while a new tape was being loaded onto the magnetic tape recorder. This resulted in a portion of the return signal to be missing. This period has been represented by a straight line on Figures 6.14 and 6.15.

In Figure 6.14, the edges of the slick (as observed from the ship) coincide with a reduction in the backscatter level of about 0.15V (≈ 5dB). The size of the slick derived from Figure 6.14 is also in good agreement with that observed on the UVLS images reported in the preceding chapter (Figure 5.3). The same can be said about Figure 6.14b where the slick edges correspond to a sudden decrease in the radar backscatter intensity, although the

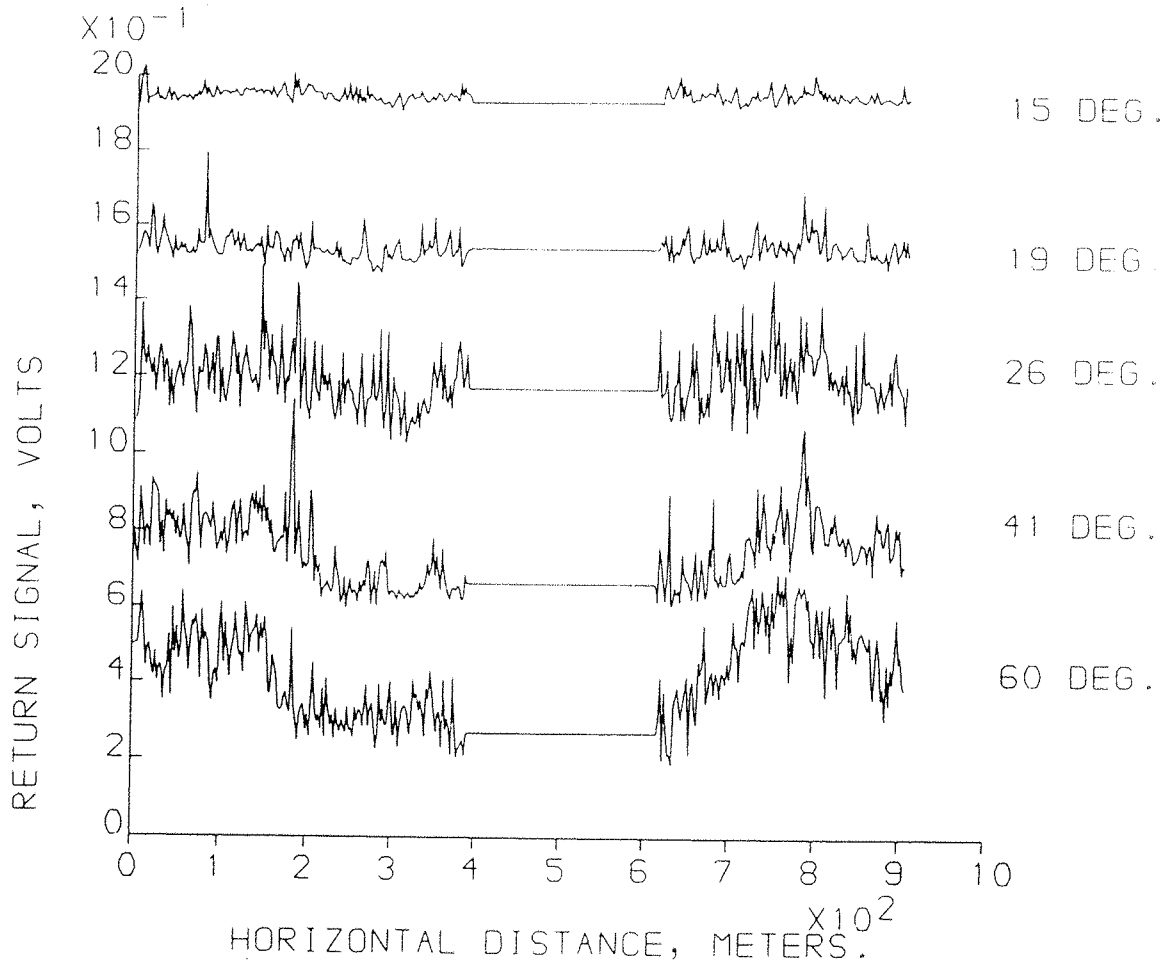

Fig 6.15 Cross section of slick (RUN 2) at various incidences for the same area of the surface as in Figure 6.14 (15.1m^2).

size of the slick derived from this figure is slightly larger (20%) than that derived from Figure 6.14. The fact that the radar and the acoustic backscatter cross-sections correspond to different sections of the slick might be one of the reasons for this discrepancy. The other reason is that radar might be more sensitive to the presence of small quantities of oil than sonar. On both figures, the mean backscatter level from the surface free of oil is in general greater than that from the slick.

Figure 6.15 shows the acoustic backscatter across the same dimension ($15.1m^2$) of the slick at smaller angles (41°,26°,19°,15°) together with that at 60°. Backscatter from the smaller angles have each been offset by +0.46V with respect to the angle immediately preceding it.

The reduction in the backscatter level caused by the presence of the oil film can still be noticed at 41° and 26° with the slick edges being in good agreement at the three highest incident angles. The backscatter from lower incidence (19° and 15°) looks scarcely affected by the presence of the slick. It also look more uniform than at higher incidence, except for some occasional spikes (at distance ≈ 10,100,250 and 650m for 19° incidence). The spatial frequency of these spikes is more important at higher incidence angles.

Phillips (1988) suggested in a recent study of microwave-ocean wave interactions that a significant component of the scattering from the ocean surface may be due to short episodes of high scattering cross-section associated with individually breaking waves. Farmer and Vagle(1988), in the open sea, and Melville et al (1988), in a wave tank, also observed the occurrence of spikes in the (passive) acoustic backscatter from the sea surface which were associated with surface waves breaking or close to breaking. It would appear reasonable to assume that the spikes observed in Figure 6.15 might be associated with individual, strong scattering events where breaking waves would

be the most probable candidates. As the grazing angle decreases, shadowing effects become more important and only the large breaking waves can leave a detectable signature. This would explain the higher frequency of the peaks at greater incidence.

The other candidate would be random noise generated by the ship and other natural mechanisms. Considering that the signal was filtered during the processing stages (see § 5.4.3) and was time and space averaged later, we suspect that most of the randomly generated noise should have been filtered out and that this source is less likely to be at the origin of the observed spikes.

A simple statistical analysis (presented in Appendix A) has been carried out on Figure 6.15's data. The results are reported in Table A1. We can see that the mean backscatter at all five incidence angles is greater outside the slick than inside the slick, and that the difference decreases as the angle decreases. There is not a large difference in the standard deviation data, which indicates that backscatter is similarly spread around the mean level for both types of surfaces. The distributions of scatterers shown in Figures A1 to A5 are positively skewed in general, which is a sign that high scattering events are present in both surface types. If these scatterers are associated with individually breaking waves, there is no evidence from the skewness coefficients shown in the table that the surface film has affected the rate of breaking during these observations. This result confirms the visual observations made from the ship where no significant reduction in the whitecaps inside the slick was noticed (see Figure 6.2).

5.Angular dependence of the backscatter cross-section:

In order to derive the acoustic sea surface scattering cross-section from the signal received at the sonar as a function of incidence angle, the various attenuation processes discussed in

§ 2.2.2 have to be taken into account. Here, we consider each one of these processes, and evaluate how much each of them affects the signal on its way out and back.

The arrival time of the echo has been translated into an angle. A simple calculation transforms the time delay T into grazing angle θ (see Figure 3.2), knowing the sonar depth d and c using

$$\theta = \sin^{-1}[\, d/r \,] = \sin^{-1}[\, 2d/cT \,] \qquad (6.2)$$

a. Loss across the air/sea interface

Transmission at the air/sea interface was found to be insignificant. We can therefore assume that all of the energy transmitted will remain in the water column.

b. Attenuation due to absorption

For a 248kHz sonar, the absorption coefficient derived from Figure 2.1 is

$\alpha_a \approx 0.1$ dB/m

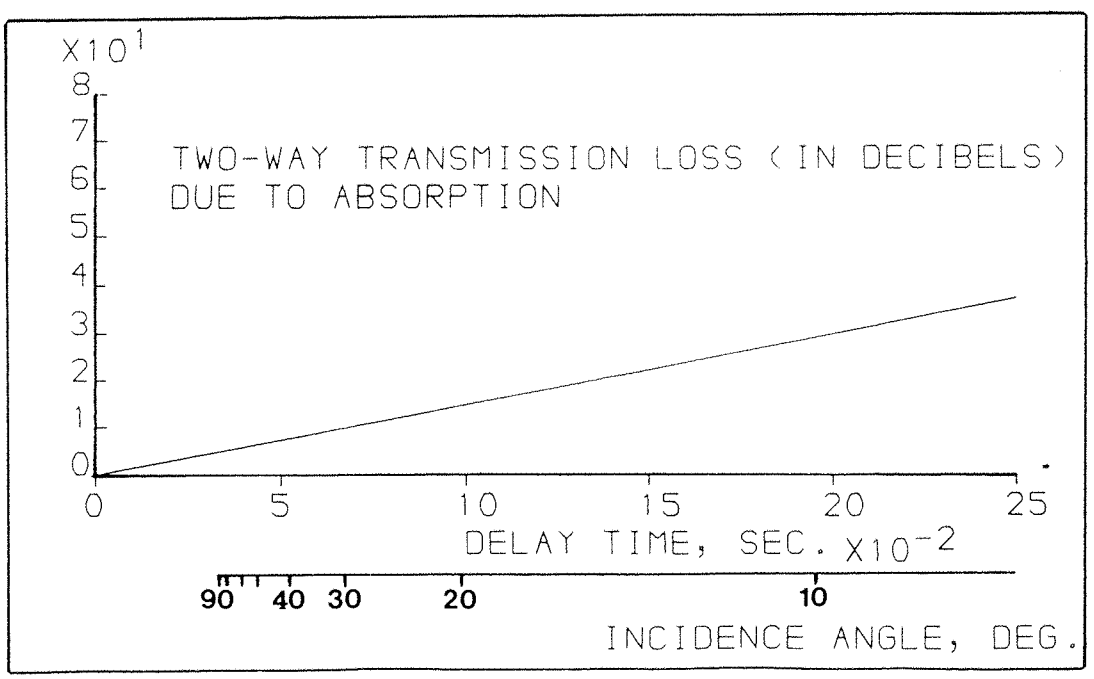

Fig 6.16 Loss of acoustic energy by absorption in sea water versus time delay, and incidence angle (the sonar is assumed at depth 25m) for 248kHz sonar.

Assuming sound rays are straight lines over the rather small distances considered in this work, we have plotted the two-way attenuation due to absorption in Figure 6.16.

c.Loss by refraction

For the range of distances covered by the sound rays (not more than 200m each way), loss through refraction is negligible and can therefore be ignored.

d.Outward spreading of energy

Considering that our source is directional, there is no significant spreading outside the main sound beam. In fact, the distribution of the acoustic pressure within the main lobe accounts for about 90% of the total power (Somers M.L., private communication).

The angular energy distribution is given by the shape of the beam, shown in Figure 5.6. In Figure 6.17, we have reproduced this data in a cartesian diagram. The reader should bear in mind

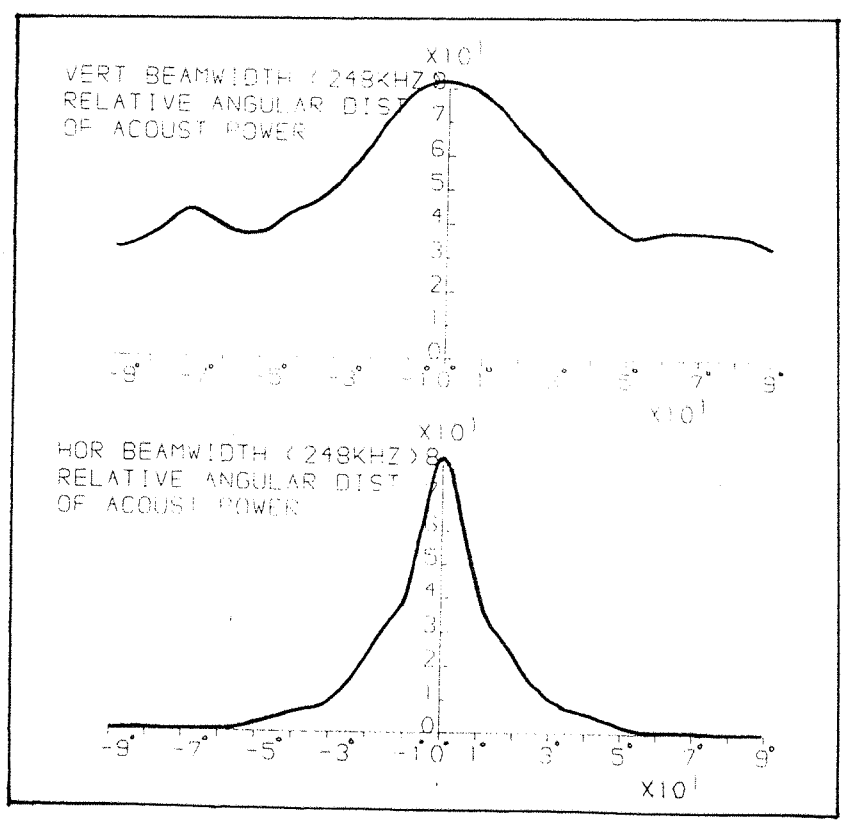

Fig 6.17 Angular distribution of transmitted acoustic power.

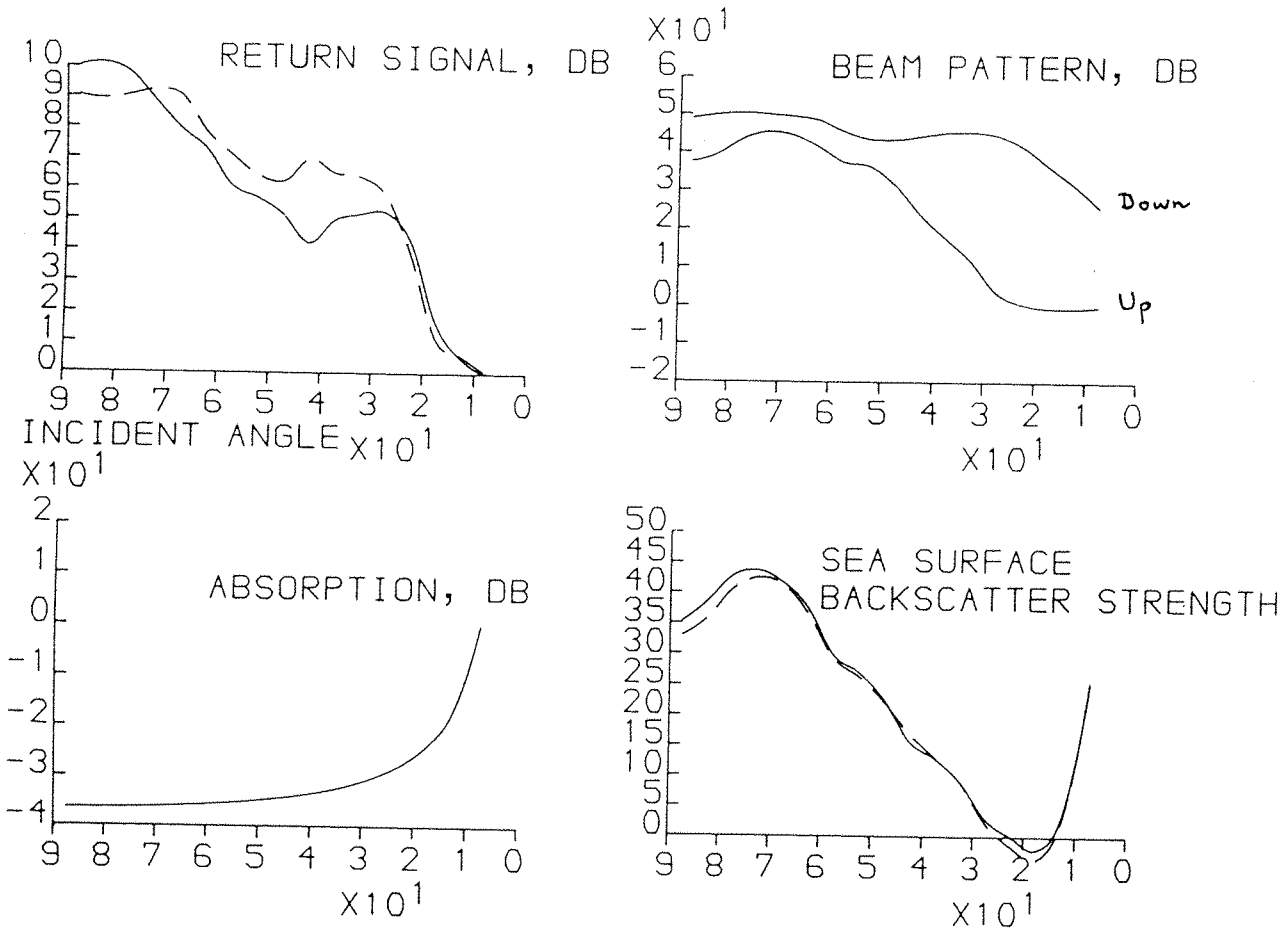

Fig 6.18
a)Return signal vs angle of incidence for slick (— —) and clean (——) surface from run 2.
b)Transmitted acoustic power around the sonar beam. Up is the sea surface bound lobe, and down is the sea bed bound.
c)Loss of energy through chemical absorption.
d)Scattering cross section from the sea surface under slick(— —) and clean (——) water, corrected for absorption and power distribution.

that the main axis of the beam was tilted upwards by 20° during the experiments.

One source of high return that must be taken into account and removed from the return signal is the reflection from the sea bed. Considering that the sonar was operated at mid-water, the bottom-bound sound lobe of the side scan sonar reflected at the bottom and the sea bed return therefore contributed to the total return signal. We have assumed a smooth bottom with no energy loss at the interface. This assumes that the sea bed can be considered as a perfect reflector. The validity of this assumption lies in the nature of the sea bed which in our case consists of large sand waves of wavelengths much longer than the incident wavelength. The type of sand (coarse, fine, etc) is also important in defining the degree of smoothness, but this parameter remains unknown as no measurements have been taken in this direction. To simplify the analysis at this stage, the return signal has been corrected from the sea bed contribution by having the bottom-bound lobe shape removed from the signal, after carrying out a correction for absorption. We also ignored multiple echoes in this analysis.

The two curves in Fig 6.18d show the variation of the backscatter strength from the sea surface (clean,— —; and slick, ——; run2) with incident angle, for a wind speed of 11.1m/s. The figure summarises the correction stages described above. The shape of the distribution of the upwards and downwards transmitted power (Fig 6.18b) is removed from the signal received at the recorder (Fig 6.18a). Energy lost by absorption (Fig 6.18c shows absorption for a typical depth of 25m) is then added to the signal. For the reasons given in §6.2.1, the data between 90° and 70° in Figures 6.18a and d should be discarded. Note that the vertical scales between figures 6.18a and 6.18d are different.

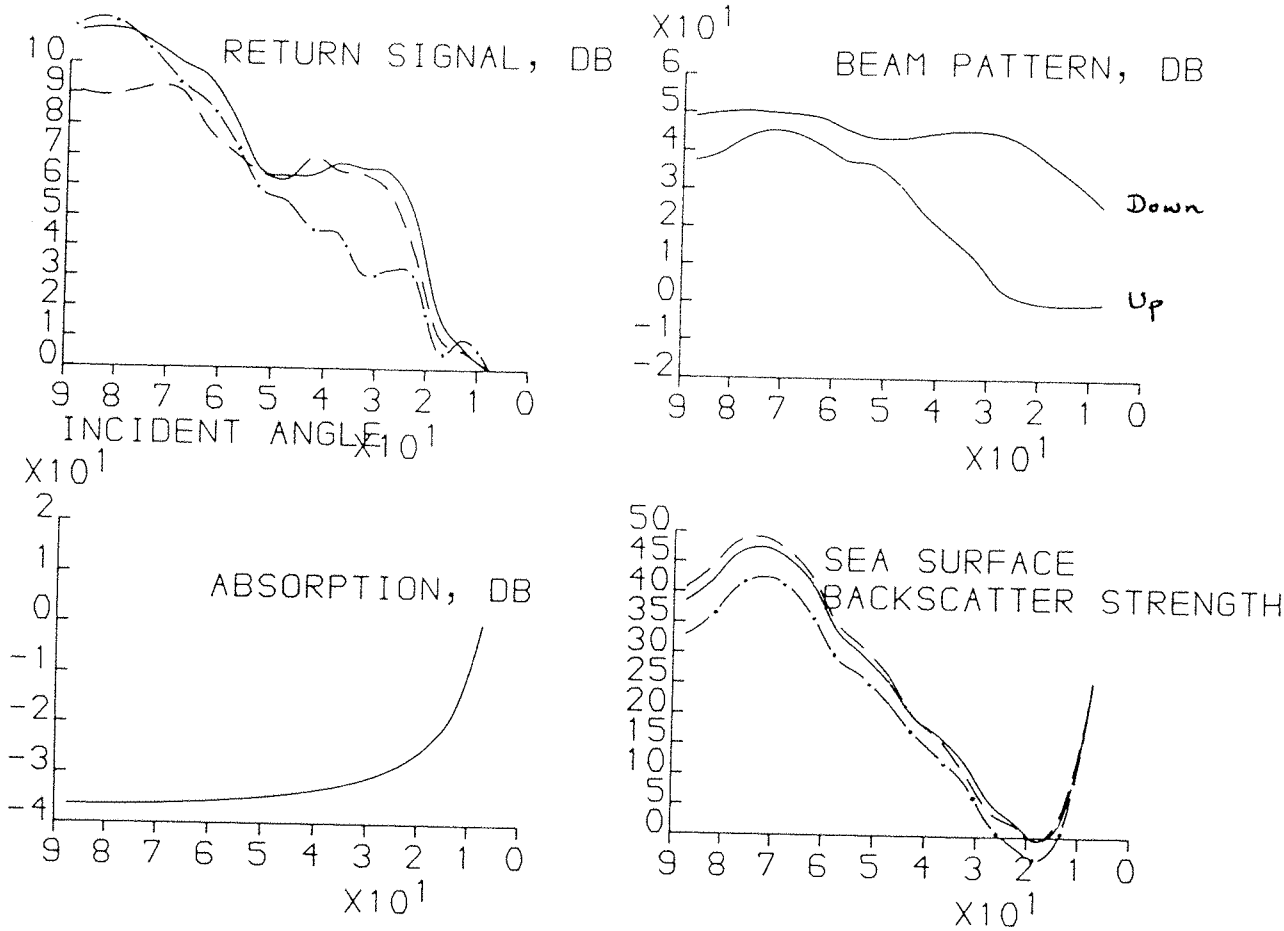

Fig 6.19
a)Return signal vs angle of incidence from clean water at W_{10}= 11.1m/s (— —), 9.5m/s (——) and 7.0m/s (—·—).
b)Transmitted acoustic power around the sonar beam. Up is the sea surface bound lobe, and down is the sea bed bound.
c)Loss of energy through chemical absorption.
d)Scattering cross section from the sea surface for the three wind speeds mentioned, corrected for absorption and power distribution.

The scattering cross-section at three different wind speeds is shown in Figure 6.19d, using the same procedure as the previous figure (the same remarks as Figure 6.18 apply to figures 6.19a and d).

The data reported in Figures 6.18 and 6.19 is relative to the signal strength at 10° incidence, which was taken as the reference level.

From the last two figures in 6.18 and 6.19, it appears that for intermediate angles (70°-25°), backscatter decreases as the angle of incidence decreases. The slope of the depression is about 1 dB/deg and is double that of radar observations made by Guinard et al (1971) under the same wind conditions (Figure 4.3). For lower incidence, the backscatter reaches a minimum level (around 15°-20°) and is seen to start increasing quite rapidly. The fact that we omitted to include the angular dependence of the bottom backscattering strength (BBS) (it was taken as constant in the analysis) could be at the origin of the observed increase at 15°-20°. A compilation by Urick (1975, p245) of high frequency (24-100kHz) measurements for a variety of sea bed types shows that, for sandy (and sand mixed) bottoms, the BBS decreases gently between vertical and about 20° (slope varying between zero and 0.5 dB/deg), and that between 20° and the horizontal the BBS suddenly reduces by 15 to 20dB. Our assumption of a perfectly reflecting loss-less sea bed might also have played a part. According to Urick (1975), the loss between the vertical and a low grazing ray incident upon a sandy sea bottom could be as high as 20db.

Our intention at the onset of the experiment was primarily to look at the surface backscatter and not the bottom, and very few efforts have been channelled in that direction. Ideally we should have been working in an area with a depth allowing the fish (usually towed at about 25m depth) to be at least in the top fifth of the water column. However, should any further work be

carried out in similar conditions, the analysis of the sea bed type to determine its acoustic characteristics should be taken into consideration.

So to summarise the two Figures presented (6.18d and 6.19d), these should not be taken as representative of the sea surface backscatter but should only be regarded as curves enabling comparisons to be made between the different sea surface types and conditions that where prevailing during the experiments.

6.3.COMPARISON BETWEEN ACOUSTIC AND EM BACKSCATTER FROM AN OIL SLICK

The acoustic results show some similarities with the Ku-band radar observations of Singh et al (1986) and Johnson & Croswell (1982) shown in Figure 4.4.

First they all succeeded in detecting the presence of the slick in the background of the sea surface backscatter signal, with a reduction between clean water and the slick signal of the same order of magnitude (5db with the sonar for 7-11.1m/s winds, and 8-12db with radar for 3-7m/s winds).

Radar and sonar showed the existence of a critical angle of incidence (from horizontal: 50°-60° for sonar, and 55°-60° for radar) where the depression in the backscatter signal is maximum.

If we assume that the dominant backscatter mechanism at this frequency and angular range is Bragg scattering from short wavelength gravity-capillary waves, then, as suggested before, the shape of the backscatter depression curve may be indicative of a selective damping process by which particular waves of small wavelength are damped more than others under the influence of the oil. By referring to eq 4.4 and considering our experimental arrangements, this would lead, for first order Bragg scattering, to a selective damping of surface waves of wavelength of 6mm.

However, in the em experiments (Table 4.1), the results show that the depression of backscatter is more important at lower wind speed, whereas in our case the depression showed to be decreasing as wind speed decreased. It might be that the ageing slick in our experiment has lost some of its damping characteristics and ripples were beginning to appear again, but it is impossible to explain the reasons of these differences at this stage as the amount of data collected during our experiment was not sufficient. The weather conditions and sea state are also important as they influence the shape of the surface wave spectrum and must therefore be closely monitored before any qualitative comparisons can be made.

6.4. Summary

Following the results obtained during the North Sea experiment, we can draw the following conclusions:

i/ The damping effect of the oil on the surface waves has played a major role in the sudden depression of the acoustic backscatter in the slick (Figure 6.14). A depression of 5dB was noticed under winds of 11.1m/s, and decreased as wind speed decreased.

ii/ For upwind and downwind observations, the backscatter depression was maximum at incidence angle 50°-60° (figure 6.13).

iii/ The depression of radar and sonar backscatter in a slick is of the same order of magnitude (§ 6.3), but radar is the most effective detector. They both show the existence of a critical angle of incidence where the depression is maximum.

iv/ Acoustic backscatter from the clean sea surface varies with the angle of incidence and also has a wind speed dependence (Figures 6.18d and 6.19d).

The other results concerning the behaviour of the slick and its effects on the sea surface can be summarized as follow

v/ No significant reduction in the rate of surface wave breaking inside the slick was noticed.

vi/ As the slick ages and wind speed drops, the differential backscatter between slick and clean surface becomes less important.

vii/ The spreading of the slick was in good agreement with that predicted in § 4.1. A $t^{1/2}$ growth along the minor axis (Appendix B), and a faster growth along the major axis with the slick forming a finger pattern at the downwind edge were observed.

We suggest that, if further evidence of the effect of an oil slick on the sea surface backscatter is needed, the use of a second transducer operating at a different frequency (preferably a few tens of kilohertzs difference) will reveal more information about the nature of the backscatter. For instance, the dummy transducer on the other side of the steel tube (see § 5.3.1) could be replaced by a genuine transducer, and would enable, when operated simultaneously, comparisons of the backscatter to be made under the same wind and sea conditions.

CONCLUSION & SUGGESTIONS

In this chapter, presented in two main sections, a summary of what has been achieved throughout the present work is combined with a discussion of ideas for future work. The first of these sections is about the results achieved during the experiment and the second about the value of side scan sonar as an alternative remote sensing tool and its possible applications.

7.1. CONCLUSIONS

The usefulness of a simple side scan sonar for detecting and observing oceanographic processes taking place close to the sea surface has been demonstrated by the large amount of valuable data collected during the experiments.

The same sonar (248kHz) was used in a stationary mode and in a towed mode (see Chapter 2). In the first mode, the equipment was operated in an unusual way, in the very shallow waters of a river in the Southampton estuary. The (high frequency) sonar allowed targets at a range up to 120m to be detected. The sonographs have revealed some useful information about a variety of physical processes taking place at or close to the surface of the water. Among the events captured by the sonar in waters 4-

5m deep were surface waves breaking individually and in groups. In particular, the sonographs provided information about the direction of propagation and the spacial distribution of clouds of bubbles formed by these breaking waves. It also revealed some information about the redistribution of bubble plumes in the wake of a ship and by other dynamical processes. This information could not have been obtained from one mooring, and could be obtained only to a limited extent by an array of moorings.

The results from the North Sea experiment showed that an oil slick can be detected by using high frequency (248kHz) sonar and that this result was directly related to the changes in the small scale surface roughness induced by the oil. A depression of 5dB between clean water and a slick with an average oil thickness of 25.5 μm (in reality, this figure should be reduced by up to one order of magnitude in most parts of the slick) was observed under winds of 11.1m/s. This depression tended to decrease as wind speed decreased and as the oil slick became older. The observation of a critical angle of incidence (55°-65°) at which the depression reaches a maximum suggests that there might exist a mechanism of selective damping of the surface waves, although Bragg scattering have been ruled out owing to the improbable validity of the theory's assumptions. The experimental results also showed that the frequency of wave breaking at high wind speeds (11.1m/s) was not affected by the presence of the oil film.

7.2. SUGGESTIONS

Side scan sonar: a remote sensor for the future?

The advantages of extensive time coverage, high resolution at short range, low cost and flexibility in deployment make a simple side scan sonar a very valuable research tool, especially

in situations where conventional instruments are difficult to deploy.

These advantages need to be weighed against other remote sensing instruments such as radars which have a wider coverage area, a good spacial resolution and a more quantitative interpretation of the backscatter signal owing to the strong theoretical background underpinning radar sea surface backscatter. However, radars (such as Synthetic Aperture Radars) are far more expensive and hence cannot usually be used in over extended periods for any one experiment nor can they resolve ocean features near the sea surface with the same resolution as HF sonars.

A simple and cheap acoustic imaging system such as an oceanographic sonar will be particularly useful when

1.The observed features have a strong acoustic scattering strength, and are therefore easily identified on the sonographs
2.The spacial dimensions of the feature lie within range of the operational sonar swath, typically a few hundred metres
3.A time-series is required over an extended period or at frequent intervals.

There are however some disadvantages of using a sonar, and particularly when it is used in a towed mode. Among these disadvantages, we can mention the fact that the area vertically above the sonar and which is indicative of the behaviour of the backscatter signal in the specular direction is contaminated by the survey ship's wake. Navigation difficulties under rough weather conditions can also be a disadvantage when rapid surveys are necessary.

The potential power of an oceanographic sonar lies in the improvement of the processing velocity of the large amount of data that is gathered. A close to real-time display of the data

in a useful form will certainly put the sonar in the forefront of oceanographic remote sensing tools. This was shown by its ability to detect clouds of bubbles and to infer measurements of the near surface currents. Applications in harbours and areas of dense shipping where strong current velocity changes are expected will certainly be of interest.

Some suggestions were made in chapters 3 and 5 as to how the data processing could be improved.

The alternative technique proposed in chapter 3 involves image processing of the sonographs. This technique requires the sonographs to be in digital form. The features appearing on the digital image would, with the help of a digital table, be used to derive measurements such as the scattering strength of the observed feature and its velocity in the sonar direction.

This technique will require a higher resolution graphic recorder (costly), and might take longer processing time, but by being selective on the quantity of sonographs to be digitally-imaged, this technique might prove to be more suitable, and could prove to be a better alternative when sonars are used in a stationary mode.

One possible application of the oceanographic sonar would be the monitoring and protection of areas (fishing farms, coastal areas,etc) which are vulnerable to oil pollution. This would bring the running costs down and ensure a round the clock monitoring regardless of day or night.

However, we believe that an oceanographic sonar can only be used for research purposes at this stage, and that more experimental evidence of its usefulness, and a better understanding of the theory behind the acoustic scattering properties of the sea surface are needed before it could become a commercially viable product.

Appendix A

COMPARISON BETWEEN THE DISTRIBUTION OF SCATTERERS IN A SLICK AND OUTSIDE A SLICK

A simple statistical analysis has been carried out on Figure 6.15's data. First we have divided the data from each angle of incidence into three distinct data sets containing the backscatter from the surface before and after the slick and from the slick surface. For each data set (of N data points) we then calculated the mean level, the standard deviation and the skewness coefficient using expressions

$$\text{Mean backscatter} = \bar{X} = \frac{\sum_{i}^{N} X_i}{N}$$

$$\text{Standard deviation} = Sd = \frac{\left(\sum_{i}^{N} (X_i - \bar{X})^2\right)^{1/2}}{N-1}$$

$$\text{Skewness} = Sk = \frac{\sum_{i}^{N} (X_i - \bar{X})^3}{(N-1).Sd^2}$$

The data (reported in Table A1, next page) is plotted in Figures A1 to A5, and shows the distribution of scatterers in 0.02V increments at 5 different angles of incidence: 60°,41°,26°,19° and 15°.

Angle of incidence	Mean Backscatter (V)	Standard Deviation(V)	Skewness (V)	Position /slick
60°	0.513	0.091	-0.011	Before
	0.354	0.095	0.070	In
	0.482	0.099	-0.016	After
41°	0.333	0.074	0.101	B
	0.209	0.056	0.075	I
	0.362	0.083	-0.021	A
26°	0.262	0.067	0.043	B
	0.238	0.081	0.044	I
	0.299	0.085	0.070	A
19°	0.144	0.038	0.063	B
	0.132	0.034	0.026	I
	0.149	0.043	0.075	A
15°	0.078	0.016	0.022	B
	0.075	0.017	0.009	I
	0.080	0.022	0.004	A

Table A1.

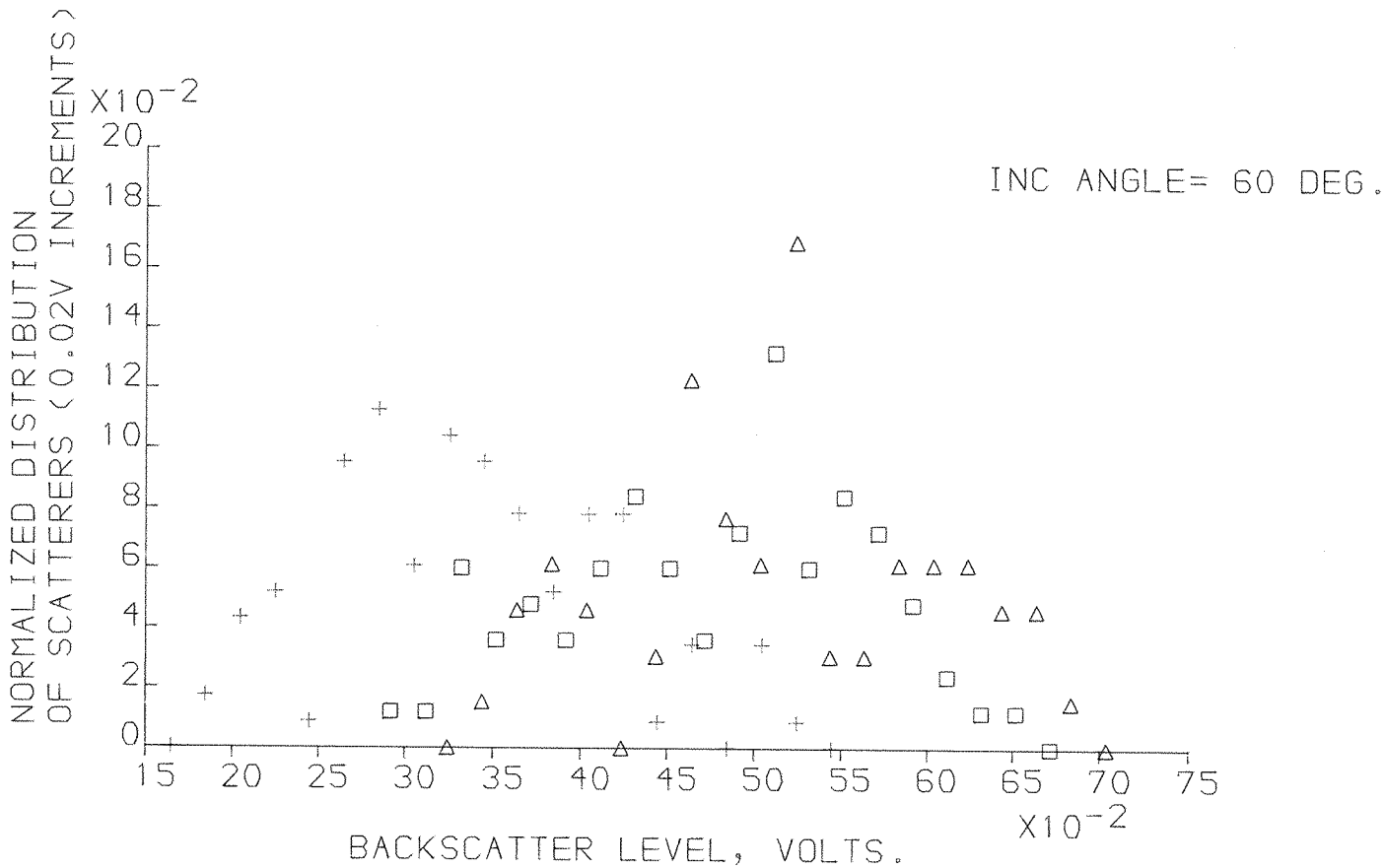

Fig A1 Distribution of sea surface scatterers derived from the sonar signal before entering the slick (△), in the slick (+) and after exiting the slick (□) at 60° incidence. Each data point is averaged over an area of 15.1m^2 of the surface.

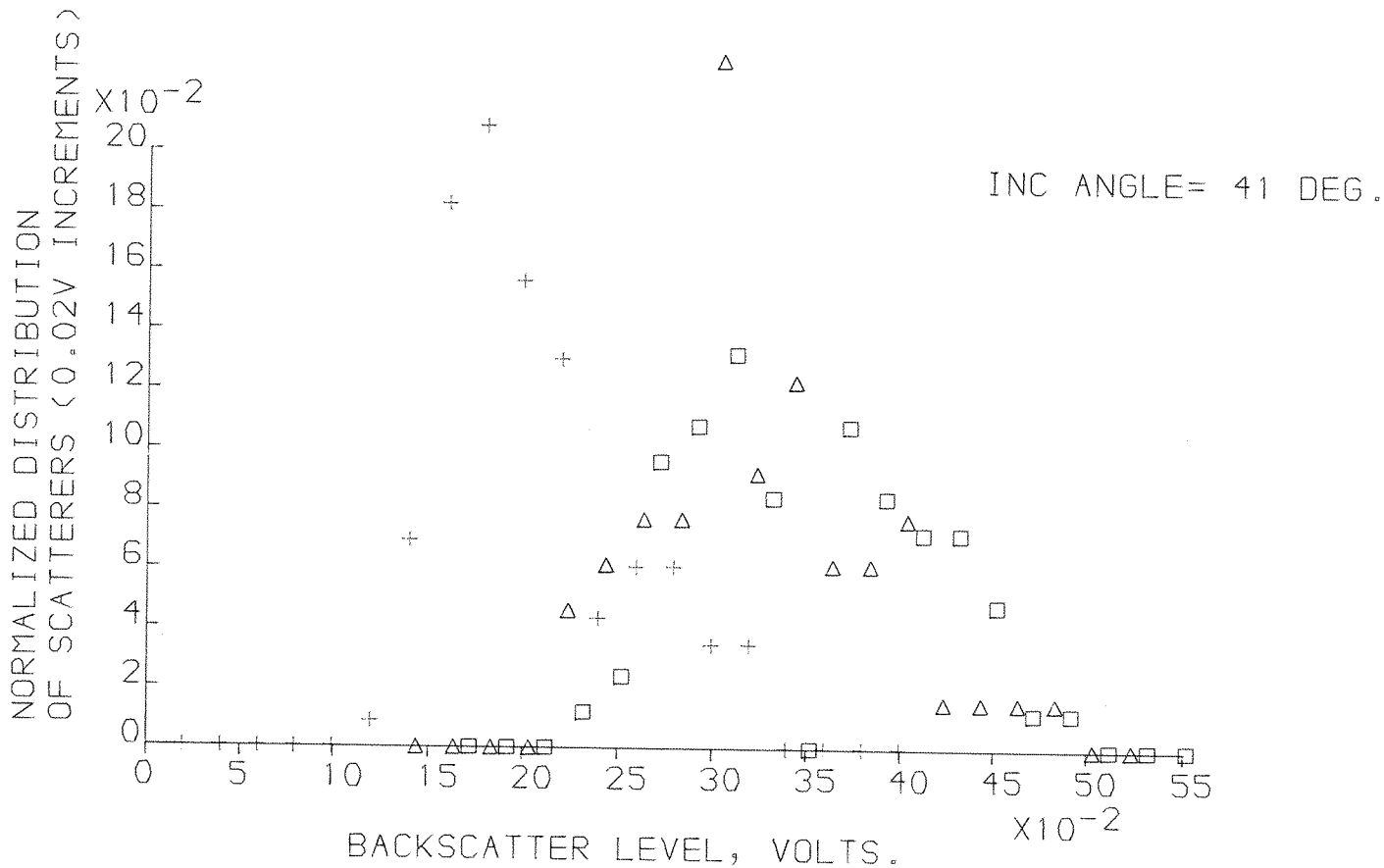

Fig A2 Distribution of sea surface scatterers derived from the sonar signal before entering the slick (△), in the slick (+) and after exiting the slick (□) at 41° incidence. Each data point is averaged over an area of 15.1m^2 of the surface.

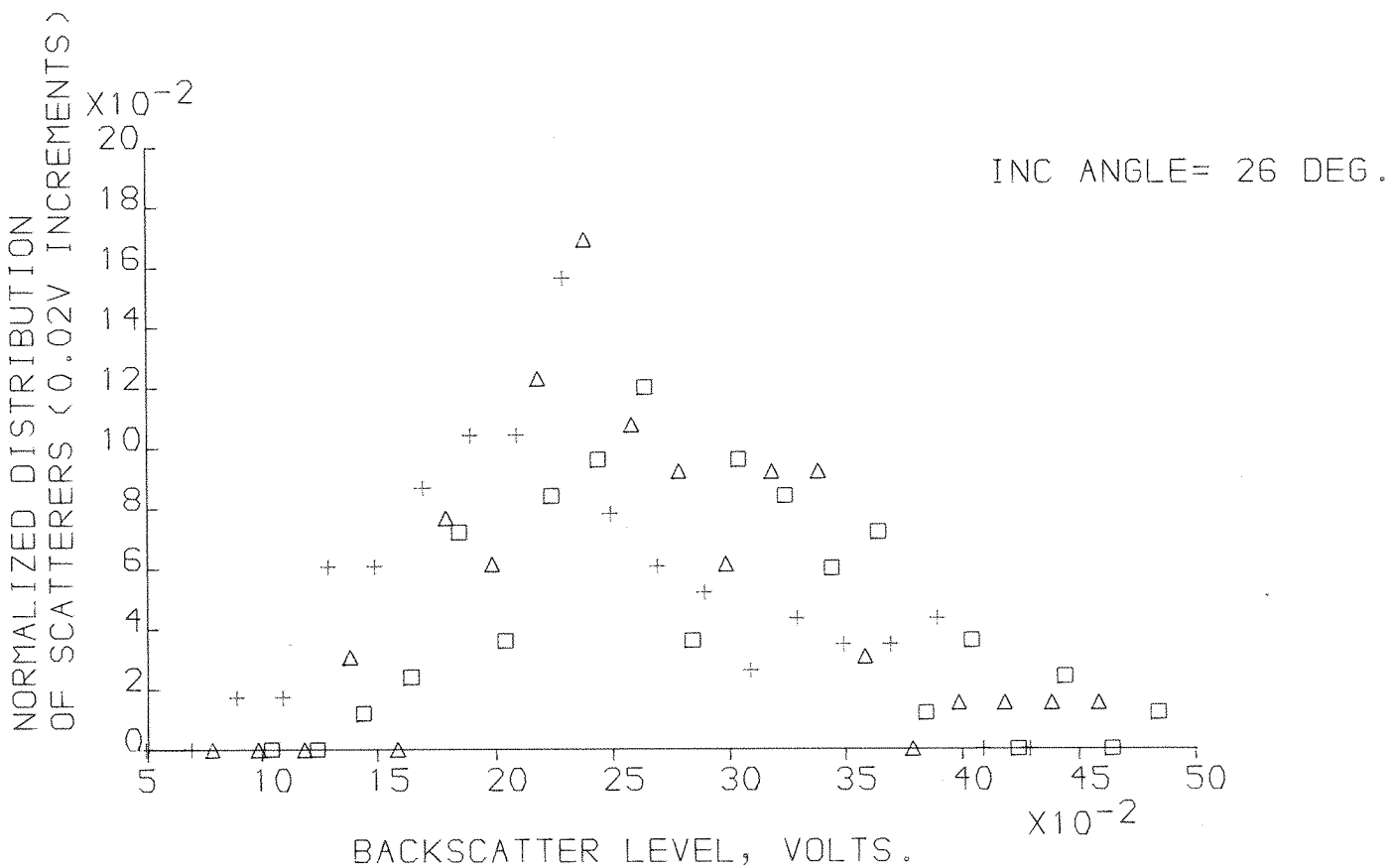

Fig A3 Distribution of sea surface scatterers derived from the sonar signal before entering the slick (Δ), in the slick (+) and after exiting the slick (□) at 26° incidence. Each data point is averaged over an area of 15.1m^2 of the surface.

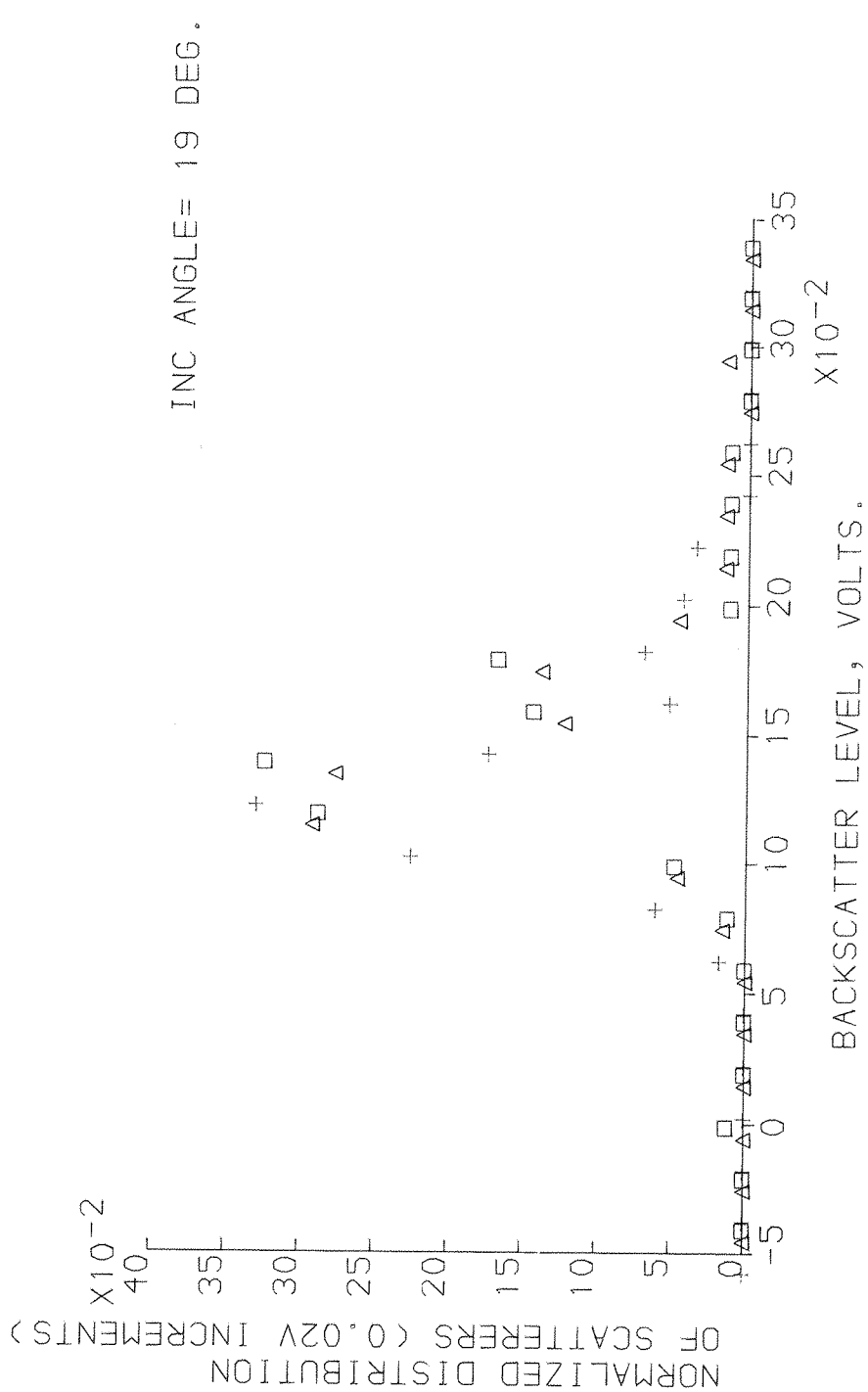

Fig A4 Distribution of sea surface scatterers derived from the sonar signal before entering the slick (▲), in the slick (+) and after exiting the slick (□) at 19° incidence. Each data point is averaged over an area of 15.1m^2 of the surface.

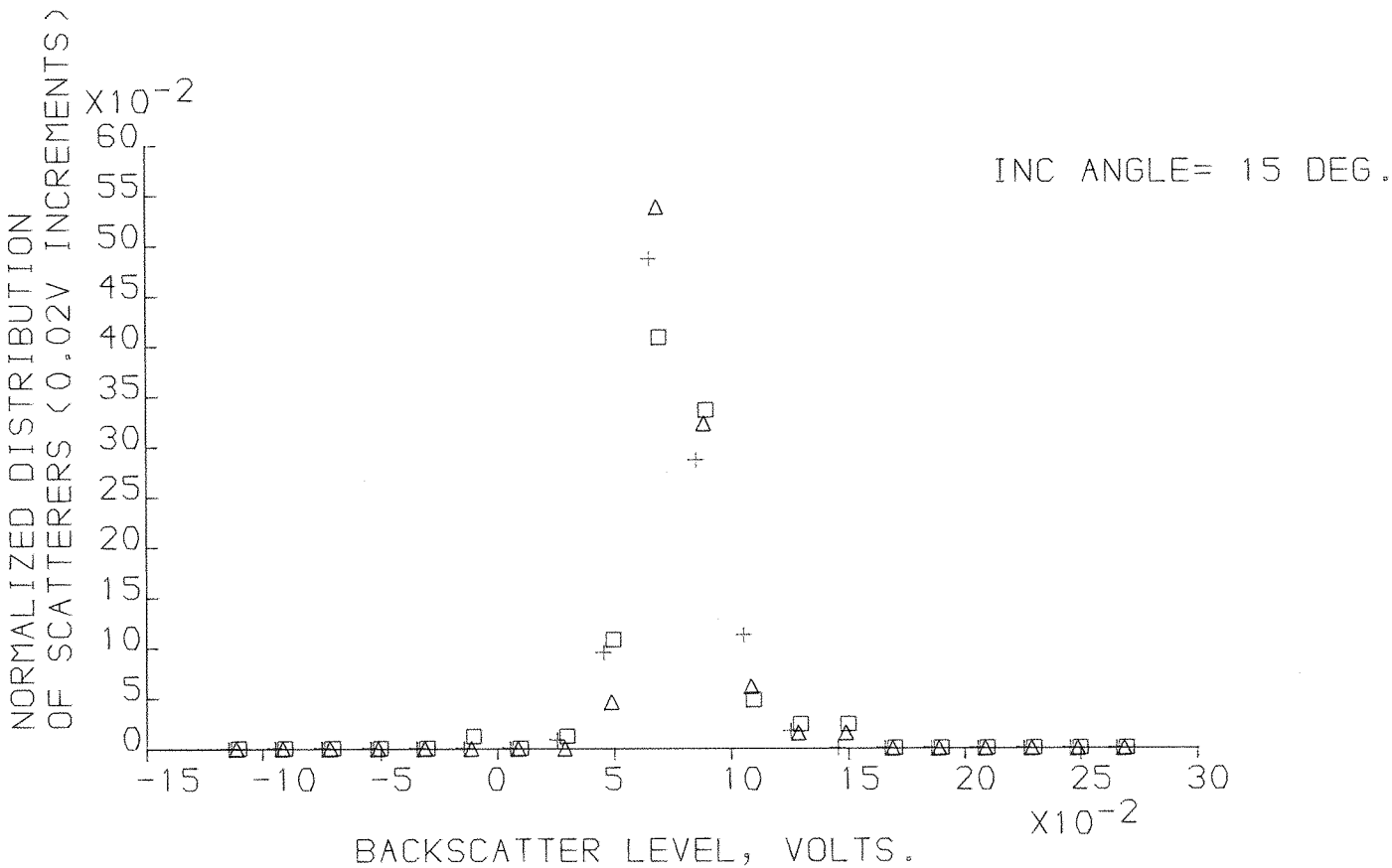

Fig A5 Distribution of sea surface scatterers derived from the sonar signal before entering the slick (△), in the slick (+) and after exiting the slick (□) at 15° incidence. Each data point is averaged over an area of 15.1m^2 of the surface.

Appendix B

EVOLUTION OF THE OIL SLICK ALONG ITS NARROW DIMENSION

On 07.07.87, the survey ship crossed the slick along its narrow dimension four times in succession. The edges of the slick were estimated from the deck in order to correlate the observations with the acoustic backscatter. The dimensions derived from these observations are reported in Table B.1. The slick width Y is determined from

$$Y(t) = V_s (t_{out} - t_{in})$$

and represents an approximate dimension as this dimension is not estimated instantaneously but during the period $(t_{out} - t_{in})$ it takes the ship to sail from one edge to the other. At $t = t_{out}$ the slick had extended a little more than at time $t = t_{in}$.

Run No	t_{in} h:min	t_{out} h:min	$\lvert t_{out} - t_{in} \rvert$ sec.	Elapsed time (h)	V_s m/s	Y m
1	13:44	13:49	300	0.9	1.85	555
2	14:32	14:39	420	1.7	1.58	663
3	15:17	15:23	360	2.45	1.60	576
4	17:14	17:22	480	4.4	1.90	912

Table B1

[1]Note: The oil discharge was completed at 12:50, and the dimension of the slick was estimated as about 250m at that time. The elapsed time is estimated from the time the first edge was crossed by the ship (t=0 at 12:50).

Error calculations

i/Spacial axis

$Y = V_s (t_{out} - t_{in})$

$dY/Y = dV_s/V_s + d(t_{out} - t_{in})/(t_{out} - t_{in})$

$\Delta Y/Y = \Delta V_s/V_s + 2 \Delta t/(t_{out} - t_{in})$

where $\Delta t = \Delta t_{out} = \Delta t_{in}$ and is estimated at 15s and ΔV_s is estimated at 0.2m/s, which yields to

$\Delta Y = \Delta V_s (t_{out} - t_{in}) + 2V_s \Delta t$

ii/ Temporal axis

The error bars on the axis represent the time it took the slick to grow from dimension it had at $t = t_{in}$ to that at time $t = t_{out}$. Suppose that at t_{in} the width of the slick is Y_{in}, at $t = t_{out}$ the slick width would be Y_{out} and the error of estimating both edges at $t = t_{in}$ will be a function of $Y_{out} - Y_{in}$ which is itself a function of $t_{out} - t_{in}$. To estimate this time error we therefore need to know the growth rate of the slick (which is the objective of this section). We will take an arbitrary rate.

The data from Table B.1 has been plotted versus the square root of time (Figure B1). The best fit (least mean square) across the data set is a line of slope equal to around 5.3 $m.s^{-1/2}$.

This result is consistent with Elliot's numerical model suggesting a $t^{1/2}$ growth of the width of a slick. His model was based on the horizontal and vertical shear diffusion associated respectively with the tidal stream and Stoke's drift of the oil particles and wind effects.

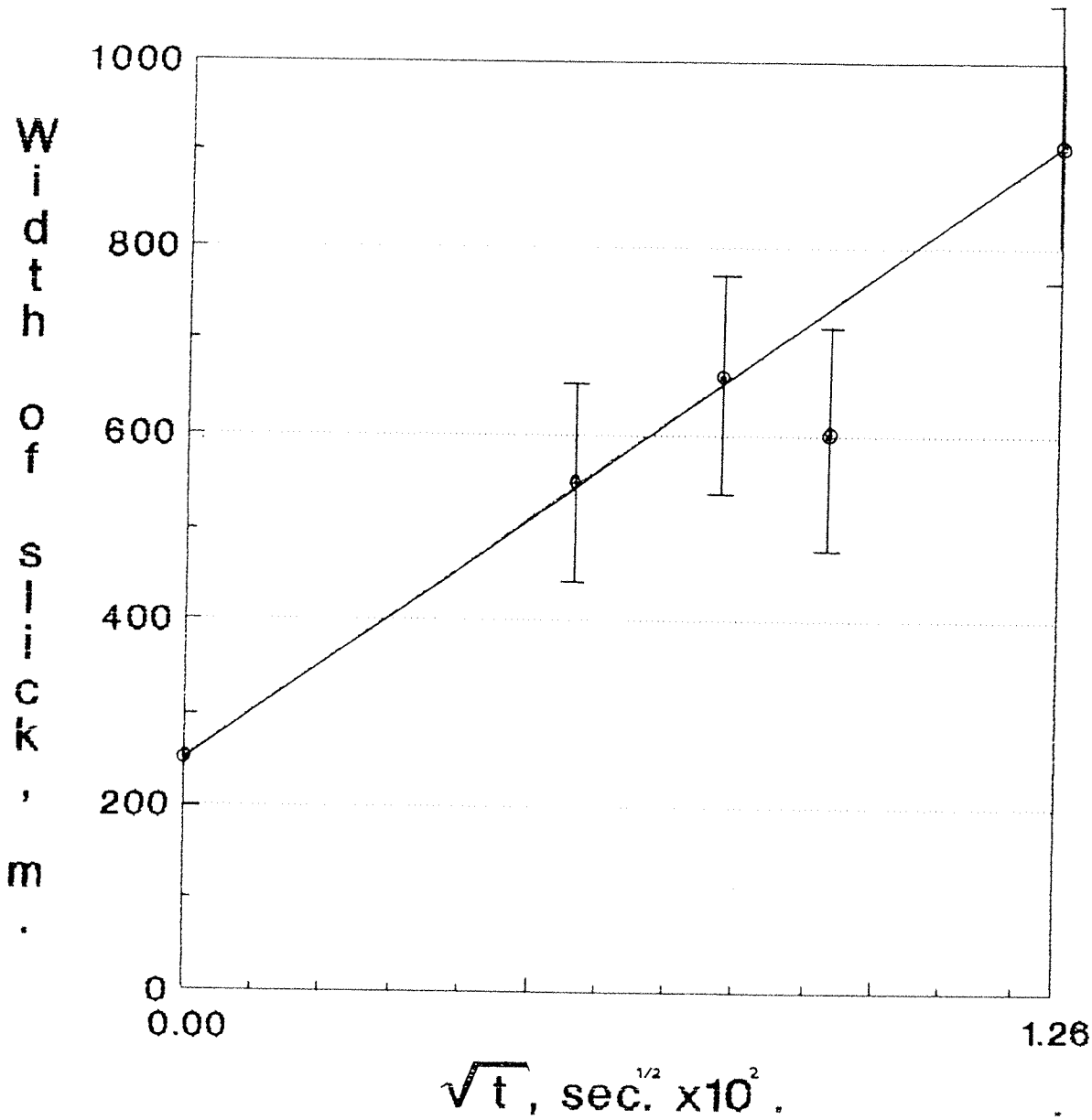

Fig B1 Evolution of the slick along its narrow dimension.

BIBLIOGRAPHY

Chapter one

Shaw P.T., Watts R.D.,and Rossby H.T., (1978): On the Estimation Of Oceanic Wind Speed and Stress from Ambiant Noise Measurements, *Deep Sea Res.*, Vol 25, 1225-1233.

Thorpe S.A. (1982): On the Clouds of Bubbles Formed by Breaking Wind-Waves in Deep Water, and Their Role in the Air-Sea Gas Transfer, *Phil.Trans.R.Soc. Lond.*, Vol A 304, 155-210.

Thorpe S.A. and Hall A.J. (1983): The Characteristics of Breaking Waves, Bubble Clouds and Near Surface Currents Observed Using Side Scan Sonar, *Continental Shelf Research*, Vol 1, 353-384.

Thorpe S.A., Hall A.J., Packwood A.R.,and Stubbs A.R. (1985): The Use of a Towed Side Scan Sonar to Investigate Processes Near the Sea Surface, *Continental Shelf Research*, Vol 4, 597-607.

Chapter two

Aleksandrov A.P. and Vaindruk E.S. (1974): The Investigation of the Variability of Hydrophysical Fields in the Ocean, ed. R. Osmidov, 122-128, Nauka Publishing Office, Moscow.

Chesterman W.D., Clynick P.R., and Stride A.H. (1958): An Acoustic Aid to Sea Bed Survey, *Acustica*, Vol 8, 285-290.

Clay C.S. and Medwin C.S. (1977): *Acoustical Oceanography*, Wiley, New York.

Colladon J.D. and Sturm J.K.F. (1827): Memoire sur la Compression des Liquides et la Vitesse du Son dans l'Eau, *Ann. Chim. Phys.*, Vol 36, 113-125.

Crawford G.B. and Farmer D.M. (1987): On the Spacial Distribution of Ocean Bubbles, *J. Geophys. Res.*, Vol 92(C8), 8231-8243.

Ewing M. and Worzel J. (1948): Propagation of Sound in The Ocean, *Geol. Soc. Am. Mem.*

Hall M.V. (1989): A Comprehensive Model of Wind-Generated Bubbles in the Ocean and Predictions of the Effects on Sound Propagation at Frequencies up to 40kHz, *J. Acoust. Soc. A.*,Vol 86(3), 1103-1117.

Kanwisher J. (1963): On the Exchange of Gases Between the Atmosphere and the Sea, *Deep Sea Res.*, Vol 10, 195-207.

Klein M. (1967): Side Scan Sonar, *Undersea Technol.*, Vol 8, 24-26.

Kunze W. (1957): General Aspects of Application of Horizontal Echo Sounding Method to Shipping, *Int. Hydrogr. Rev.*, Vol 34, 63-72.

Laughton A.S. (1981): The First Decade of Gloria, *J. Geophys. Res.*, Vol 86 (B12), 11511-11534.

Leonard R.W., Combs P.C. and Skidmore L.R. (1949): Attenuation of Sound in Synthetic Sea Water, *J. Acoust. Soc. A.*, Vol 21, p63.

Rayleigh Lord (1945): *The Theory of Sound*, Vol II, 2nd ed.,Dover Publications Inc., New York.

Rusby J.S.M. (1970): A Long Range Side Scan Sonar for Use in the Deep Sea, *Int. Hydrogr. Rev.*, Vol 47, 25-39.

Shulkin M. and Marsh H.W. (1962): Sound Absorption in Sea Water, *J. Acoust. Soc. A.*, Vol 34, p864.

Thorpe S.A. (1982): On the Clouds of Bubbles Formed by Breaking Wind-Waves in Deep Water, and Their Role in the Air-Sea Gas Transfer, *Phil.Trans.R.Soc. Lond.*, Vol A 304, 155-210.

Thorpe S.A. and Brubaker J.M. (1983): Observations of Sound Reflection by Temperature Microstructure, *Limnol. Oceanogr.*, Vol 28(4), 601-613.

Thorpe S.A. and Hall A.J. (1983): The Characteristics of Breaking Waves, Bubble Clouds and Near Surface Currents Observed Using Side Scan Sonar, *Continental Shelf Research*, Vol 1, 353-384.

Thorpe S.A., Hall A.J., Packwood A.R.,and Stubbs A.R. (1985): The Use of a Towed Side Scan Sonar to Investigate Processes Near the Sea Surface, *Continental Shelf Research*, Vol 4, 597-607.

Thorpe S.A. (1986): Measurements with an Automatically Recording Inverted Echo Sounder; ARIES and the Bubble Clouds, *J. Phys. Oceanogr.*, Vol 16(8), 1462-1478.

Thorpe S.A., Belloul M.B. and Hall A.J. (1987): Internal Waves and Whitecaps, *Nature*, Vol 330, p740.

Urick R.J. (1975): *Principles of Underwater Sound*, 2nd edn, Mc Graw Hill, New York.

Wood A.B. (1941): *A Textbook of Sound*, The Macmillan Company, New York.

Chapter three

Appell G.F., Mero T.N., Sprenke J.J. and Scmidt D.R. (1985): An Intercomparison of Two Acoustic Doppler Current Profilers, *Oceans 85*, Ocean Engineering and the Environment Conference Record, Vol2, p723.

Brekhovskikh L. and Lysanov Yu. (1982): *Fundamentals of Ocean Acoustics*, Springer-Verlag ed., Berlin Heidelberg.

Clay C.S. and Medwin C.S. (1977): *Acoustical Oceanography*, Wiley, New York.

Donelan M., Longuet-Higgins M.S. and Turner J.S. (1974): Periodicity in Whitecaps, *Nature*, Vol 239, 449-451.

Johnson B.D. and Cooke R.C. (1979): Bubble Population and Spectra in Coastal Waters: A Photographic Approach., *J. Geophys. Res.*, Vol 84 (C7),3761-3766.

Thorpe S.A. (1983): Bubble Clouds: A Review of Their Detection by Sonar, of Related Models and of How K_v May Be Determined, *Ocean Whitecaps*, ed. E.C.Moynehan and G. Mac Niocaill, D. Reidel Publishing Co.

Thorpe S.A. and Hall A.J. (1983): The Characteristics of Breaking Waves, Bubble Clouds and Near Surface Currents Observed Using Side Scan Sonar, *Continental Shelf Research*, Vol 1, 353-384.

Thorpe S.A., Belloul M.B. and Hall A.J. (1987): Internal Waves and Whitecaps, *Nature*, Vol 330, p740.

Chapter four

Aitken, J. (1883): On the Effect of Oil on Stormy Sea, *Proc. R. Soc. Edinburgh* , Vol 12, 56-75.

Alpers, W. and Huhnnerfuss H. (1989): The Damping of Ocean Waves by Surface Films: A Newlook at an Old Problem , *J. Geophy. Res.*, Vol 94(C5), 6251-6265.

Apel J.R. (1987): *Principles of Ocean Physics*, Academic Pr., New York.

Barger, W. R., W. D. Garrett, E. L. Mollo-Christensen, and K. W. Ruggles (1970): Effects of an Artificial Sea Slick Upon the Atmosphere and the Ocean , *J. Appl. Meteorol.*, Vol 9, 396-400.

Barrick D.E. and Peak W.H. (1968): A Review of Scattering from Surfaces with Different Roughness Scales, *Radio Science*, Vol 3, 865-868.

Bass F.G., Fuks I.M., Kalmykov A.I., Ostrovsky I.E. and Rosenberg A.D. (1968): VHF Radiowave Scattering by a Disturbed Sea Surface, *IEEE Trans.*, AP-16, 554-568.

Bortkoskii R. S. (1988): *Air Sea Exchanges of Heat and Moisture During Storms*, Atmospheric Science Library, D. Reidel Publishing Company.

Cini R. and Lombardini P.P. (1981): Experimental Evidence of a Maximum in the Frequency Domaine of the Ratio of Ripple Attenuation in Monolayered Water to that in Pure Water, *J. Colloid Interface Sci.*, Vol 81, 125-131.

Cini R., Lombardini P.P.,and Huhnerfuss H. (1983): Remote Sensing of Marine Slicks Utilizing their Influence on Wave Spectra, *Int. J. Remote Sens.*, Vol 4, 101-110.

Cox, C., and W. Munk, (1954): The Measurements of the Roughness of the Sea Surface from Photographs of the Sun's Glitter, *J. of the Opt. Soc. of A.*, Vol 44, 838-850.

Crombie D.D. (1955): Doppler Spectrum of Sea Echo at 13.56 Mc/s, *Nature*, Vol 175, 681-682.

Davies J.T. (1962): Some Effects of Surface-Active Agents on Waves and Ripples, *Chemistry and Industry*, May 26, 906-910.

Davies, J. T. and R. W. Vose, (1965): "On the Damping of Capillary Waves by Surface Films, *Proc. R. Soc. London*, Ser. 286, 218-234.

Elliott, A. J. (1986): Shear Diffusion and the Spread of Oil in the Surface Layers of the North Sea, *Dt.hydrogr. Z.* 39, 113-137.

Garrett W.D. (1974): The Surface Activity of Petroleum and Its Influence on the Spreading and Weathering of Oil Films at Sea, *J. Rech. Atm.*, 555-562.

Guinard N.W., Ransone J.T. and Daley J.C. (1971): Variation in the NRCS of the Sea with Increasing Roughness, *J. Geophys. Res.*, Vol 76, 1525-1538.

Hollinger J. P. and Mennella R.A. (1973): Oils spills : Measurements of their Distributions and Volumes by Multifrequency Microwave Radiometry, *Science*, Vol 181, 54-56.

Huhnerfuss, H., W. Alpers, and W. L. Jones, (1978): Measurements at 13.9 GHz of the radar backscattering cross section of the north sea covered with an artificial surface film, *Radio Sci.*, Vol 13, 979-983.

Huhnerfuss, H., W. Alpers, W. L. Jones, P. A. Lange, and K. Richter, (1981): The damping of ocean surface waves by a monomolecular film measured by wave staffs and microwave radar, *J. of Geophys. Res.*, Vol 86, 429-438.

Huhnerfuss H., Alpers W., Garrett W.D., Lange P.A. and Stolte S. (1983): Attenuation of Capillary and Gravity Waves by Monomolecular Organic Surface Films, *J. Geophys. Res.*, Vol 88, 9808-9816.

Johnson, J. W. and W. F. Croswell, (1982): Characteristics of 13.9 GHz Radar Scattering from Oil Films on the Sea Surface, *Radio Sci.* Vol. 17, no. 3, 611-617.

Krishen, K. (1973): Detection of Oil Spills Using a 13.3 GHz Radar Scatterometer, *J. Geophys. Res.*, Vol 78 (12), 1952-1963.

Lamb H. (1932): *Hydrodynamics*, 6th edn., Cambridge Univ. Press.

Linde, B., S. Pogorzelski, and A. Sliwinski, (1984): Attenuation Measurements of Waves on a Water Surface in the Frequency Range 20-50 Hz by the Ultrasonic Pulse Reflection Method, *Acustics Lett.*, Vol 7, 347-395.

Lucassen J. (1968): Longitudinal Capillary Waves, 1, Theory, *Trans. Faraday Soc.*, vol 64, 2221-2229.

Lucassen-Reynders E. H., and J. Lucassen, (1969): Properties of Capillary Waves, *Adv. Colloid Interface Sci.*, Vol 2, 396-400.

Mallinger, W. D., and T. P. Mickelson, (1973): Experiments with Monomolecular Films on the Surface of the Open Sea, *J. Phys. Oceanogr.*, Vol 3, 328-336.

Rayleigh Lord (1945): *The Theory of Sound*, Vol II, 2nd ed.,Dover Publications Inc., New York.

Rice S.O. (1951): Reflection of Electromagnetic Waves from Slightly Rough Surfaces, *Comm. Pure & Applied Math.*, Vol 4, 351-378.

Scott, J. C., (1978): The Historical Development of Theories of Wave-Calming Using Oil, *History of Technology*, Vol 3, 163-186.

Singh K.P.,Gray A.L.,Hawkins R.K. and O'Neil R.A. (1986): The Influence of Surface Oil on C- and Ku-band Ocean Backscatter, *IEEE Trans. Geosc. Rem. Sens.*, Vol GE-24(5), 738-743.

Tailby S.R. and Portalski S. (1970): *Trans. Inst. Chem. Eng. Lond.*, Vol 39, p328.

Thorpe S.A. (1982): On the Clouds of Bubbles Formed by Breaking Wind-Waves in Deep Water, and their Role in Air-Sea Gas Transfer, *Philos. Trans. R. Soc. London*, Vol A 304, 155-210.

Thorpe S.A. (1983): Bubble Clouds: A Review of Their Detection by Sonar, of Related Models and of How K_v may be Determined, *Ocean Whitecaps*, ed. E.C.Monehan and G. Mac Niocaill, D. Reidel Publishing Co.

Ulaby F.T., Moore R.K. and Fung A.K. *Microwave Remote Sensing : Active and Passive*. Vol.1. Microwave Remote Sensing Fundamentals and Radiometry, Reading, MA,USA: Addison-Wesley (1981).

Urick R.J. (1956): The Processes of Sound Scattering at the Ocean Surface and Bottom, *J. Mar. Res.*, Vol 15, p134.

Urick R.J. (1975): *Principles of Underwater Sound*, 2nd edn, Mc Graw Hill, New York.

Valenzuela G. (1978): Theories of the Interaction of Electromagnetic and Oceanic Waves- A Review, *Boundary Layer Met.*, Vol 13, 61-85.

Wright, J. W. (1968): A New Model for Sea Clutter, *IEEE Trans. Antennas Propag.*, AP 16, 217-223.

Yermakov, S. A., A. R. Panchenko, and T. G. Talipova, (1985): Damping of High Frequency Wind Waves by Artificial Surfactant Films, *Izvestiya Atmospheric and Oceanic Physics*, Vol 21, 54-63.

Chapter five

Huhnerfuss H., Garrett W.D., Hoge (1986): The Discrimination Between Crude Oil Spills and Monomolecular Sea Slicks by an Airborne Lidar, *Int. J. Remote Sens.*, Vol 7, 137-150.

Chapter six

Farmer D.M. and Vagle S. (1988): On the Determination of Breaking Surface Wave Distributions Using Ambiant Noise, *J. Geophys. Res.*, Vol 93 (C4), 3591-3600.

Guinard N.W., Ransone J.T. and Daley J.C. (1971): Variation in the NRCS of the Sea with Increasing Roughness, *J. Geophys. Res.*, Vol 76, 1525-1538.

Johnson, J. W. and W. F. Croswell, (1982): Characteristics of 13.9 GHz Radar Scattering from Oil Films on the Sea Surface, *Radio Sci.* Vol. 17, no. 3, 611-617.

Melville W.K., Loewen M.R., Felizardo F.C., Jessup A.T. and Buckingham M.J. (1988): Acoustic and Microwave Signatures of Breaking Waves, *Nature*, Vol 336(3), 54-56.

Phillips O.M. (1988): Radar Returns from the Sea Surface - Bragg Scattering and Breaking Waves, *J. Phys. Oceanogr.*, Vol 18, 1065-1074.

Singh K.P.,Gray A.L.,Hawkins R.K. and O'Neil R.A. (1986): The Influence of Surface Oil on C- and Ku-band Ocean Backscatter, *IEEE Trans. Geosc. Rem. Sens.*, Vol GE-24(5), 738-743.

Urick R.J. (1975): *Principles of Underwater Sound*, 2nd edn, Mc Graw Hill, New York.